Investigation of Integrated Energy Systems with Carbon Capturing and Chemical Looping Units for Hydrogen, Methane and Methanol Production

by

Mitra Ghannadi

A Thesis Submitted to the
School of Graduate and Postdoctoral Studies in partial
fulfillment of the requirements for the degree of

Master of Applied Science in Mechanical Engineering

Faculty of Engineering and Applied Science

University of Ontario Institute of Technology (Ontario Tech University)

Oshawa, Ontario, Canada

November 2023

THESIS EXAMINATION INFORMATION

Submitted by: **Mitra Ghannadi**

Master of Applied Science in Mechanical Engineering

Thesis title: Investigation of Integrated Energy Systems with Carbon Capturing and Chemical Looping Units for Hydrogen, Methane and Methanol Production

An oral defense of this thesis took place on November 29, 2023, in front of the following examining committee:

Examining Committee:

Chair of Examining Committee	Dr. Amirkianoosh Kiani
Research Supervisor	Dr. Ibrahim Dincer
Examining Committee Member	Dr. Martin Agelin-Chaab
Examining Committee Member	Dr. Atef Mohany
Thesis Examiner	Dr. Sayyed Ali Hosseini

The above committee determined that the thesis is acceptable in form and content and that a satisfactory knowledge of the field covered by the thesis was demonstrated by the candidate during an oral examination. A signed copy of the Certificate of Approval is available from the School of Graduate and Postdoctoral Studies.

ABSTRACT

This study investigates three multigeneration systems designed for hydrogen generation through chemical looping, incorporating an amine-based carbon dioxide capture subsystem. These systems consist of a solar tower heating subsystem and a power generation unit to fulfill electrical and heating requirements. Additionally, steam methane reforming or electrolysis is employed in each system to enhance its efficiency. The uniqueness of these systems lies in their innovative designs and significant contributions to addressing the global challenge of rising greenhouse gas emissions. This research generates and stores valuable products like hydrogen, fresh water, and electricity, and also effectively stores and converts carbon dioxide emissions into useful energy sources such as methanol or methane. All the products are finally stored to be used in future applications. The exergy efficiencies of systems 1, 2, and 3 are 25%, 32%, and 35.6%, respectively, and their energy efficiencies are 27%, 48%, and 48.6%.

Keywords: Hydrogen Production, Carbon Capturing, Efficiency, Chemical looping, Sustainability

AUTHOR'S DECLARATION

I hereby declare that this thesis consists of the original work that I have authored. This is a true copy of the thesis, including any required final revisions, as accepted by my examiners.

I authorize the University of Ontario Institute of Technology (Ontario Tech University) to lend this thesis to other institutions or individuals for the purpose of scholarly research. I further authorize the University of Ontario Institute of Technology (Ontario Tech University) to reproduce this thesis by photocopying or by other means, in total or in part, at the request of other institutions or individuals for the purpose of scholarly research. I understand that my thesis will be made electronically available to the public.

MITRA GHANNADI

ACKNOWLEDGEMENTS

I want to express my greatest appreciation to Professor Dr. Ibrahim Dincer, my supervisor, mentor, and instructor, for all his help, encouragement, and inspiration to complete my degree. He was the first to believe in me, allowing me to continue my education under his supervision. I am utterly honoured to have worked with such a perfect, knowledgeable professor who consistently offered me unconditional guidance, valuable knowledge, experiences and advice, and motivation and inspiration during this journey. I will forever be grateful for him changing my life.

My deepest gratitude goes to Andre Bolt for his exceptional support and guidance. I also want to thank all my kind colleagues at the Clean Energy Research Laboratory: Aysegul Kara, Ayse Meke, Ahmet Kilicaslan, Dogan Erdemir, Hilal Akci, Khalid Altayib, Mehmet Gursoy, Mert Temiz, Mohamed Ismail, Muarij Khalil, Murat Cankenez, Muhammad Ishaq, Sibel Uygun, and Sulenur Asal. Their kindness and assistance have been priceless.

Primarily, I extend my most tremendous gratefulness to my precious family: my impressive, devoted mother, my reliable, encouraging father, and my role model best sister, Mina Ghanadi. Their unwavering trust, hope, energy, and infinite support have always been my passion. Their help, prayers, and encouragement have been ceaseless, allowing me to build my future and become the person I aspire to be. I could not have come this far without their infinite support and assistance. I am also grateful for my cheerful close friends, Bahar Bagheri, Dorsa Ghahremani, Negar Nasibi, Pantea Paidar, Parya Ramezanzadeh, and Rasta Sepehriyan, who stood by my side and didn’t let me go. I was always blessed with their warm presence and thoughtful support. Thank God that I have found all of you in my life.

STATEMENT OF CONTRIBUTIONS

The content covered in this thesis has partially taken from the following papers of mine, which are published or under review:

M. Ghannadi and I. Dincer, “Evaluation of iron-based chemical looping for hydrogen production from biomass using combined power cycle with carbon capturing and storage,” Sustainable Energy Technologies and Assessments, vol. 59, p. 103418, Oct. 2023, doi: 10.1016/j.seta.2023.103418.

M. Ghannadi and I. Dincer, “A New System for Hydrogen and Methane Production with Post-combustion Amine-based Carbon Capturing Option for Better Sustainability,” Energy Conversion and Management (revised and submitted)

TABLE OF CONTENTS

LIST OF TABLES

LIST OF FIGURES

LIST OF ABBREVIATIONS AND SYMBOLS

Abbreviations

CCS	Carbon Capture and Storage
CLHP	Chemical Looping Hydrogen Production
EES	Engineering Equation Solver
EBE	Energy Balance Equation
EnBE	Entropy Balance Equation
ExBE	Exergy Balance Equation
GT	Gas Turbine
GHG	Green House Gas
HE	Heat Exchanger
LHV	Lower Heating Value (kW)
MBE	Mass Balance Equation
ORC	Organic Rankine Cycle
ST	Steam Turbine

Symbols

Chem	Chemical
Comp	Compressor
$\dot{E}x$	Exergy rate (kW)
$\dot{E}x_{\dot{Q}}$	Exergy rate associated with heat transfer rate (kW)
$\dot{S}$	Entropy rate (kW/K)
$\dot{Q}$	Heat rate (kW)
$\dot{m}$	Mass flow rate (kg/s)
M	Molar mass (kmol/kg)
$\dot{n}$	Mole flow rate (kmol/s)
Phys	Physical
P	Pressure (kPa)
I	Solar Energy Intensity
$\underline{h}$	Specific enthalpy (kW)
$\overline{h_f^o}$	Specific enthalpy of formation (kJ/kmol)
$\underline{s}$	Specific entropy (kW/K)
$\overline{s_f^o}$	Specific entropy of formation (kJ/kmol)
$\underline{ex}$	Specific exergy (kW)
$\overline{ex_f^o}$	Specific exergy of formation (kJ/kmol)
ν	Specific Volume (m^3/kg)
i,j	State number
T	Temperature (^oC or K)
V	Volume
W	Work (J)
$\dot{W}$	Work rate (kW)

Greek letters

μ	Chemical Potential
η	Energy efficiency (%)
ψ	Exergy efficiency (%)

Subscripts

a	Actual
o	Ambient
b	Boundary
comp	Compressor
d	Destruction
gen	Generation
in	Inlet
is	Isentropic
net	Network
N	Number
out	Outlet
s	Source
Tot	Total

Superscripts

*	Hypothetical term
0	Standard state value

Chapter 1. Introduction

Energy is a fundamental need for the sustainability and ongoing progress of humanity. The global population is experiencing substantial growth, leading to a corresponding increase in energy consumption. The significance of renewable energy sources and their prospective contribution to forthcoming sustainable energy solutions is underscored. This chapter delves into the global reliance on fossil fuels and the increasing rate at which they are used. Also, it provides an overview of the significance of hydrogen generation and carbon capture in energy storage systems. Eventually, the advantages of the chemical looping technique in the context of hydrogen generation, as well as its significance in using renewable energy sources, are explained.

1.1 Environmental Concerns

Worldwide warming refers to the rise in average worldwide temperatures, which has reverse consequences for ecosystems. The results include higher-than-normal temperatures, rising sea levels, and arid conditions [1]. The influence of global warming on climate and ecosystems presents substantial hazards, such as heatwaves, droughts, and storms. This will result in significant and far-reaching impacts on the environment, public health, and the economy [1]. Significantly, this increase in temperature poses a severe risk of initiating crucial tipping points in the climate system, such as the thawing of polar ice caps and permafrost, leading to permanent alterations such as rising sea levels and the emission of more greenhouse gases [1]. These modifications emphasize the urgent need to tackle climate change in order to prevent beyond these dangerous thresholds. The depletion of fossil fuel supplies and the resulting climate change make it imperative that we learn more about and implement alternatives to traditional forms of energy generation [2]. In Figure 1.1, the carbon dioxide emissions in various sectors of Canada for 2022 are shown. As illustrated, fuel combustion produces the most CO2 emissions in the country. Therefore, finding a way to reduce greenhouse gas emissions and replace fossil fuels with renewable energy sources has become one of the world's primary concerns. In response, a concerted international effort backed by thorough research is making strides toward widespread use of renewable energy sources. Carbon capture and storage (CCS) and hydrogen generation are essential techniques in this field because of their promising ability to lower GHG

emissions [3]. Addressing this challenge requires innovative strategies to achieve balanced stability between fluctuating energy production and demand variability. As a result, many researchers are actively paving the way for innovative new methods. Rising temperatures, the greenhouse effect, and changes in climate patterns are only a few examples of environmental problems for which many experts are working to discover practical solutions [4].

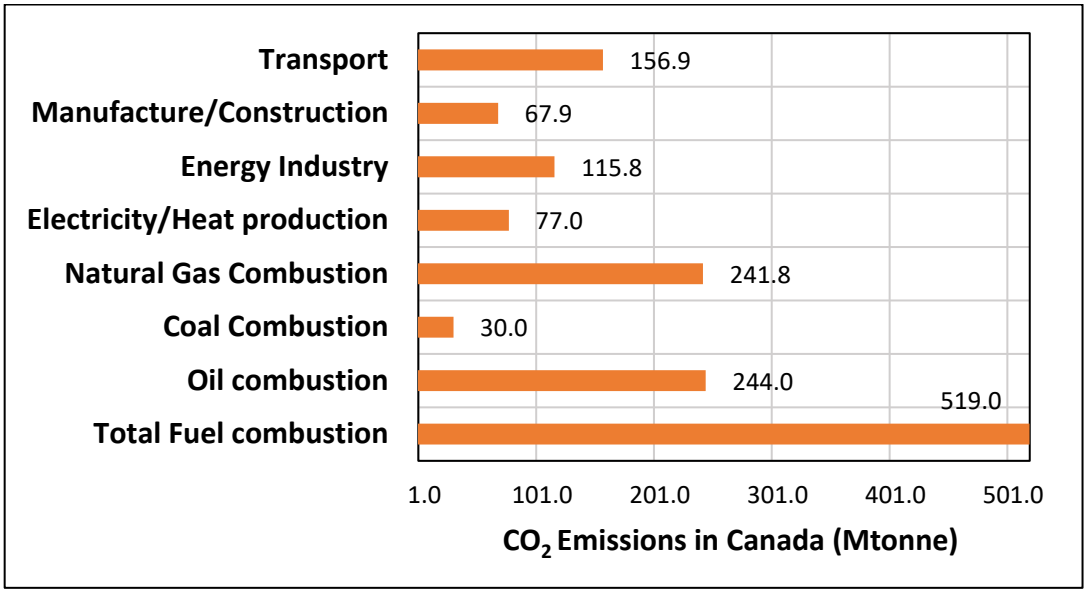

Figure 1.1 CO_2 emissions in different sectors of Canada in 2022 (data from [5])

Hydrogen, which can supplant traditional fossil fuels, is a pivotal component of efforts aimed at amplifying energy dependability and streamlining financial outlays [6]. Given the escalating global energy demands and climbing temperatures, adopting renewable energy measures has gained momentum in the past few years [7]. Research has substantiated that technologies like carbon capture and storage coupled with hydrogen production can markedly diminish the release of greenhouse gases [8].

1.2 Renewable Energy Sources

The use of renewable energy sources is widely regarded as a crucial strategy to mitigate the escalating levels of greenhouse gas emissions and mitigate the adverse consequences of climate change [9]. The adoption of renewable energy solutions has surged in recent years, propelled by the widening global energy demands and temperature escalations [10]. A primary barrier to shifting entirely to renewable energy sources is their inconsistent and

fluctuating nature [11]. This issue necessitates technological advancements, particularly in handling the delicate equilibrium between variable energy output and constantly shifting consumption.

Given these circumstances, many researchers have devoted their energies to developing innovative strategies through thorough studies. The rise in sustainable energy alternatives has been notable, spurred by growing energy demands and increasing global temperatures. [10]. A significant challenge in transitioning to a wholly renewable energy infrastructure lies in the intrinsic variability and intermittence of these sources [11].

Modern scholarly publications emphasize hydrogen's emerging promise as an eco-friendly and versatile energy method, essential for addressing the intricacies of energy carbon removal and broader sustainability goals [12]. Its diverse uses range from fueling hydrogen-driven transport to acting as an energy stabilizer in various renewable energy amalgamations [13]. Owing to its emission-free combustion and flexibility in industrial contexts, hydrogen generation plays a pivotal role in guiding the globe toward a green, carbon-neutral energy framework [14].

Initiatives are underway to develop mechanisms for capturing and storing carbon dioxide discharges. The generation of green hydrogen through electrolysis or alternative eco-friendly energy methods necessitates an equilibrium between the cost of input energy and the attainable capacity factor, in addition to considering the expenses associated with supplementary machinery to address the variability in hydrogen output. A feasible and economically viable shift mandates an unbiased approach to hydrogen technology [15].

1.3 Hydrogen Production

Researchers have redirected their attention towards hydrogen generation as a potential solution to tackle the issues associated with climate change, environmental deterioration, and unanticipated social consequences [16]. If the production framework for hydrogen is carefully developed and implemented, it has the potential to provide energy benefits and address environmental concerns. At the beginning of 2020, the Hydrogen Council published research [17], which said that hydrogen energy is projected to increase substantially, possibly by 8% of the worldwide energy demand (GED) by 2030, for 2.50

USD per kilogram of production. According to projections, the use of hydrogen energy is expected to increase every year, with the potential to meet at least 18% of global energy demand by the year 2050 [17]. By 2030, hydrogen energy, benefitting from reduced costs and increasing economic viability, is poised to revolutionize multiple sectors [17]. Hydrogen is likely to emerge as a critical low-carbon alternative in transportation, encompassing commercial vehicles and trains, due to lower equipment and refuelling costs [17]. It also shows promise in building heating, especially for natural gas-reliant structures, offering a competitive, eco-friendly solution [17]. In industrial heating, hydrogen could become the primary option for carbon emission reduction, and its role in power system stabilization is set to grow with decreasing production costs and increasing demand [17]. The shift in the economic field, marked by falling costs and rising carbon prices, positions low-carbon and renewable hydrogen to challenge conventional hydrogen in industrial applications, underlining its pivotal role in sustainable energy transition [17]. Therefore, Hydrogen is prominent in energy-centric industries due to its advantageous characteristics, such as high energy density, cost-effective manufacturing, and low carbon content [18].

Hydrogen can be generated from various sources, encompassing natural gas, coal, biomass, and water. As a flexible and clean-combustion fuel, hydrogen can supplant fossil fuels in diverse settings. This makes it an attractive candidate for endeavours aimed at reducing carbon emissions. As a minimal-emission fuel, hydrogen is applicable in transportation, energy generation, and industrial operations, playing a role in climate change mitigation. Nevertheless, the derivation of hydrogen from fossil fuels results in the release of carbon dioxide, a robust greenhouse gas. Consequently, to enhance the sustainability of hydrogen production, renewable methodologies such as biomass are preferred over fossil fuels [19].

Hydrogen can be sourced from biomass through biological methods like biophotolysis or thermochemical techniques such as electrolysis and thermolysis. Thermochemical methods often outperform biological ones in efficiency and cost-effectiveness [20]. The iron-centric chemical looping technique is an emerging method that utilizes metallic oxygen carriers for oxygen shuttling between dual chemical reactions. This facilitates the generation of hydrogen or syngas (a combination of hydrogen and carbon monoxide) while concurrently capturing and sequestering carbon dioxide [21].

The innovative notion of using hydrogen as a medium for storing renewable energy, due to its advantageous properties such as storability, transportability, and usefulness, emerges as a very promising strategy [22]. Furthermore, integrating carbon capture technology with hydrogen generation emerges as a crucial approach to mitigating the release of GHG emissions [23]. Hydrogen, renowned for its notable energy density, cost-effective production techniques, minimal carbon emissions, and versatile applicability, possesses the capacity to provide energy advantages and address environmental concerns. Consequently, it emerges as a leading contender among prospective fuel sources and energy carriers in the future [24]. As a result, the idea of a hydrogen-centric energy storage system is swiftly evolving into a cost-effective solution for large-scale renewable energy storage, simplifying its conveyance and export [25]

1.4 Motivation

Both global energy output and consumption have increased dramatically over the last several decades, and these increases are expected to continue. The increased use of fossil fuels has negatively influenced the environment [26]. On a global scale, the dependence on these fuel sources has caused significant environmental damage due to the subsequent increase in carbon dioxide emissions. Hydrogen is emerging as a promising energy carrier with significant promise and little environmental hazards. Moreover, the method by which hydrogen is used is essential for optimizing its performance in many systems, such as power generation. The integration of iron-based chemical looping technology with a carbon capture system result in the reduction of carbon emissions and the efficient generation of hydrogen. This work presents the development of three innovative integrated multigeneration systems aimed at concurrently producing hydrogen and capturing carbon. This is achieved using an absorber and stripper system based on amine technology.

Moreover, solar energy is poised to provide the necessary heat inside the system. The electricity provided by the combined Brayton-Rankine-ORC cycle serves several uses. Three distinct approaches for iron-based chemical looping, electrolysis, and steam methane reforming have been combined to generate and store hydrogen simultaneously. Following the acquisition of sufficient thermal energy and electrical power via combining and heating carbon dioxide and hydrogen, the resultant methane or methanol is generated, subsequently

stored, or used for various applications within the system. Two systems typically use solar energy as the primary source to provide the necessary heat for the system. It is advisable to use this product in areas with enough sunlight. The governing and balancing equations are used in order to calculate the energy and exergy efficiencies, as well as the production rates of methane or methanol and hydrogen and the percentage of carbon capture.

1.5 Objectives

The primary purpose of this study is to develop and assess multigenerational energy storage systems that improve sustainability and their energy and exergy efficiencies by including hydrogen production units, carbon capturing methods, or other efficient renewable energy subsystems that help to build a new system that can simultaneously capture the carbon dioxide and produces new energy resources such as methane, methanol, and hydrogen.

The objectives of this thesis are articulated with a view to advancing the field of sustainable energy. The primary aim is to develop multi-generational energy storage systems that not only yield hydrogen, methane, or methanol but also seamlessly integrate carbon capture from various facilities. This innovative approach is designed to mitigate environmental impact while enhancing energy storage capabilities. Further, this research endeavours to investigate and identify potential enhancements in the performance of energy storage systems. This includes thoroughly examining the production rates and efficiencies of energy sources. By scrutinizing these variables, the study seeks to uncover insights that could lead to significant advancements in energy storage technology. In addition to these practical objectives, the thesis will conduct a meticulous analysis of the thermodynamic parameters of all individual components and subsystems within each energy system. This analysis will be grounded in their respective chemical and physical balance equations and reactions, providing a comprehensive understanding of the operational dynamics of these systems. Lastly, the thesis will evaluate the performance of hydrogen, methane, and methanol production when these processes are combined with iron-based chemical looping. By comparing different methodologies, the research aims to ascertain the most effective techniques for producing these fuels, thus contributing to the broader quest for efficient and sustainable energy solutions.

1.6 Novelties

The unique nature of these systems arises from their inventive design and the integration of diverse processes. In this thesis, three proposed multigeneration systems are designed to produce hydrogen and other products, such as methane or methanol and capture carbon simultaneously. The carbon dioxide is aimed to be captured from two different sources, which are coal power plant and steel production facility. The hot flue gas of these sources is entered into an amine-based carbon capturing subsystem, including a stripper and absorber, to capture the carbon dioxide for further use. The necessary thermal and power energies need to be provided to these systems to produce the required heat and electricity. The power generation of these systems consists of three different cycles named Brayton, Rankine, and Organic Rankine cycle. In terms of the heating system, the two systems have the integration of a solar tower subsystem that has allowed for the use of a significant proportion of the thermal energy intake from a renewable source. The energy will be used to operate secondary components. Hydrogen synthesis uses methods other than chemical looping to reach maximum productivity. Hydrogen is produced via iron-based chemical looping, steam methane reformation and electrolysis. The main aim of this study is to conduct a comprehensive assessment of the energy and exergy of these particular systems and examine their sustainable characteristics.

Chapter 2. Literature Review

The present chapter initiates an analysis of the existing approaches to carbon capture, which are classified into several strategies and technologies. The subsequent section of the paper focuses on an examination of modern hydrogen generation systems that include carbon capture capabilities, as shown by recent scholarly publications. Following this, a comprehensive examination is presented, comparing several iron-based chemical looping systems in terms of their effectiveness in hydrogen generation and carbon capture. Hydrogen generation and carbon capture are closely interconnected in the broader context of sustainable energy and environmental management. Integrating carbon capture and storage technology with hydrogen that is produced by using renewable energy sources, particularly avoiding the use of fossil fuels, effectively reduces carbon emissions and finds practical uses for the captured carbon. This technique not only supports decarbonization efforts across different industries but also improves the efficiency of renewable energy systems by effectively handling the intermittent nature of sources such as solar power through efficient energy storage. Subsequently, the identification of prospective prospects and the proposal of future research directions within this field are emphasized. The following section presents the conclusions drawn from the comprehensive examination and assessment of hydrogen generation and carbon capture technologies. In conclusion, the chapter highlights and delimits the gaps in current information within literature.

2.1 Utilization of Hydrogen Production

In recent years, hydrogen energy has emerged as a notable alternative to traditional fossil fuels, serving as a pivotal element in pursuing a diverse and sustainable energy future [27]. Hydrogen can be derived from various natural resources, including water, natural gas, and biomass. Its production involves complex chemical reactions and significant energy input [28]. These complexities categorize hydrogen production into three primary domains based on their distinct chemical processes and energy utilization: thermochemical, electrochemical, and biological methodologies [29]. These methods employ advanced techniques like water electrolysis, steam methane reforming, methane pyrolysis, coal gasification, and chemical looping, further emphasizing hydrogen's flexibility as an energy source [30]. SMR dominates as a prevalent industrial technique for hydrogen production.

This endothermic process requires added heat, typically sourced from burning excess methane or off-gas from hydrogen purification units, which mainly consists of unreacted methane and some hydrogen [31]. Regrettably, this combustion results in less than optimal fuel efficiency and significant CO_2 emissions, exacerbating global warming [32]. Efforts to address environmental concerns in traditional SMR include carbon capture from combustion exhaust using chemical or physical absorbents [33]. Notably, the most significant energy losses in the SMR process transpire during combustion, highlighting the limitations of prevailing hydrogen production practices [34]. Research suggests that nickel-based catalysts can yield syngas with a higher H_2-to-CO ratio when applied in steam reforming of bio-oil. Coupling this with the water-gas shift reaction can boost hydrogen production [35]. Conversely, biochar gasification stands out for its ability to produce high-purity and efficient syngas, marking a cleaner alternative in syngas production techniques [36]. CL offers a promising method for hydrogen production, especially with solid fuels like coal, biomass, and biochar [37]. This innovative process uses the reducing potential of carbon-based materials, initiating a dynamic redox cycle wherein metal oxides act as oxygen carriers. Concurrently, steam serves as both the oxidizer and hydrogen source [38]. Despite its advantages, challenges remain, chiefly the low reactivity between solid fuels and oxygen carriers due to inefficient solid-solid contact in the reactor and the complex selection of a suitable oxygen carrier [39]. Anaya et al. [40] assessed the economic and environmental facets of CL in hydrogen production, revealing its potential as a more sustainable option than traditional SMR [40]. Research indicates that utilizing biomass as the carbon source in iron-based chemical looping can bolster the process's sustainability [41]. Furthermore, the carbon molar mass in the biomass appears to influence hydrogen production efficiency positively; a greater molar mass results in heightened efficiency [42]. Incorporating a solar-assisted mechanism enhances the system's performance and diminishes its environmental footprint. Elevated temperatures tend to yield more biomass with a reduced carbon molar mass, and the integration of solar energy can further amplify the efficiency and sustainability of the process [43]. From these findings, it can be deduced that combining iron-based chemical looping with Brayton and Rankine cycles and integrating solar systems can significantly elevate the efficiency of hydrogen production with carbon capture derived from biomass. Iron-based materials undergo a recycling

process between reactors. These reactors produce hydrogen by facilitating a reaction between the fuel and the iron-based material while simultaneously capturing carbon dioxide emissions through the reaction of the reduced iron-based material with these emissions [44]. This approach presents multiple benefits compared to conventional carbon capture and storage techniques, including reduced energy consumption, decreased capital expenses, and enhanced efficiency [45]. Oruc and Dincer [46] evaluated the exergy and energy efficiencies of a chemical looping facility powered by varying biomasses for hydrogen production, utilizing iron as the core component. Ishaq and Dincer [47] introduced a novel multigenerational system powered by biomass and solar energy, equipped with Brayton and Rankine cycles, an electrolyzer, a CuCl chemical looping cycle for hydrogen synthesis, and an absorption cooling mechanism. Their system achieves an electrical production of 8.3 MW and a hydrogen output of 59.45 mol/s. Siddiqui and Dincer [48] conducted an efficiency analysis on a distinctive integrated system for hydrogen and power generation, drawing power from solar energy. This system comprises an ammonia fuel cell, an absorption chiller, and a solid oxide fuel cell. A comprehensive thermodynamic assessment of the modelled system was executed to gauge its performance. Their innovative approach showcased an enhancement in energy efficiency by 19.3% and exergy efficiency by 17.8% when juxtaposed with a standard single-generation system's electrical yield.

Kathe et al. [49] delved into the chemical looping process via thermodynamic modelling. Their research indicated that the achieved thermal efficiency surpassed the steam methane reforming benchmark by 6%. Fanhe et al. [50] explored the heat integration and exergy analysis of hydrogen production from natural gas, leveraging iron-based chemical looping technology. Their findings suggest that adopting iron-based chemical looping for hydrogen synthesis from natural gas can elevate exergy efficiency by 4.3%.

Jiang et al. [51] undertook the development and comparative analysis of biomass gasification and chemical looping-based methods for cogenerating hydrogen and power, assessing both from thermodynamic and techno-economic perspectives. In their study, they examined three separate hydrogen production strategies and juxtaposed their outcomes. Among the methods tested, which included calcium looping and hydrogen generation from biomass gasification, the iron-based looping cycles emerged as the most superior in energy

and exergy efficiency. Similarly, Cao et al. [52] employed biomass gasification-solid oxide fuel cell technology and a solar energy system to optimize hydrogen production, analyzing the process from both exergy and thermo-economic angles. Their findings revealed that integrating biomass gasification with solar energy systems led to a reduction in carbon dioxide emissions by 12.9% while concurrently boosting the total system output by 8.7%.

2.2 Utilization of Carbon Capturing

Carbon capture methodologies, pivotal in contemporary environmental engineering discourses, encompass a spectrum of strategies and technologies to sequester carbon dioxide emissions at their source, notably power plants and industrial facilities [53]. These strategies are primarily segmented into three categories: post-combustion capture, where CO_2 is isolated after fossil fuels have been combusted [54]. Pre-combustion capture involves transforming fossil fuels into a gaseous mixture of hydrogen and CO_2 before combustion, subsequently isolating the CO_2 [55]. Furthermore, oxy-fuel combustion is a process in which fossil fuels are combusted in oxygen, resulting in a concentrated CO_2 stream more readily captured [56]. Technological advancements in this domain have facilitated the development of diverse carbon capture tools [57]. Absorption techniques utilize solvents, often amine-based, to chemically bind and subsequently release CO_2, enabling its capture [58]. Physical adsorption, on the other hand, employs solid materials known as adsorbents, which temporarily adhere CO_2 molecules to their surface [59]. Membrane-based systems, gaining traction in recent years, leverage semi-permeable membranes that selectively permit the passage of CO_2, segregating it from other gases [60]. These multifaceted approaches, in concert, strive to mitigate the environmental ramifications of escalating anthropogenic CO_2 emissions [61]. Addressing the environmental challenges associated with coal power plants necessitates the implementation of Carbon Capture and Storage (CCS) methodologies [62]. As pivotal infrastructures in the global energy matrix, these plants are underscored as primary culprits in the emission of greenhouse gases [63]. Within the realm of coal energy, CCS presents an innovative approach, facilitating the interception and secure containment of CO_2 emissions, thereby substantially diminishing their ecological impact [64].

In a comprehensive study, Jiang et al. [65] explored the implications of Monoethanolamine (MEA)-centred technologies within coal-fueled power infrastructures. Their research accentuates the feasibility of synergizing amine-driven CCS processes with biomass combustion, paving the way for a more environmentally sustainable coal energy paradigm [65].

2.3 Methane and Methanol Production

Methane's potential as an energy vector is receiving augmented attention due to its lesser carbon implications [66]. Central to this is the Sabatier reaction, which transforms CO_2 and hydrogen into methane and water, presenting a promising avenue for storing renewable energy and counteracting greenhouse gas emissions [66]. This methodology not only acts as a buffer for surplus renewable energy but also alleviates the challenges of energy intermittency inherent to renewables, subsequently contributing to a reduction in greenhouse emissions [67]. In an insightful study, Bassano et al. [68] delved into the Power-to-Gas paradigm, wherein renewable energy is harnessed to generate hydrogen that, when amalgamated with CO_2 via the Sabatier reaction, yields methane. Their findings accentuate the kinetic enhancements realized under elevated pressure conditions [68]. The allure of methanol as an energy carrier is intensifying, largely attributed to its multifunctional attributes and its alignment with sustainability benchmarks. Methanol's appeal is twofold: its potential as a green energy vector, capitalizing on captured CO_2 and generated hydrogen, and its esteemed status as a versatile industrial feedstock, particularly in sectors like transport [69]. Its dual utility renders methanol an eco-conscious energy alternative and a coveted commodity for diverse applications [70]. Complementing the sustainable energy discourse is the emergent technology of seawater desalination. This technique taps into the vast reservoirs of the oceans to yield freshwater, positioning it as a robust solution to global freshwater deficits, augmenting water security in drought-prone zones, and moderating freshwater costs across various geographies [71].

Chapter 3. System Description

In this section, we elucidate three energy systems and their corresponding sub-structures formulated in the scope of this research. We explore the distinct inputs and outputs for each subsystem in detail. The principal sources of renewable energy, combined with carbon capture mechanisms, independently furnish the system's heat and electricity. In conjunction with alternative methods, these systems employ a chemical looping procedure to generate and accumulate hydrogen.

This research introduces three innovative frameworks to exploit renewable energy sources, facilitating the generation and storage of hydrogen, methane, and methanol for subsequent applications. Traditional techniques for producing these essential resources rely on fossil fuels, leading to considerable ecological repercussions. The systems produce hydrogen, methanol, and methane by capturing carbon from diverse facilities, leveraging a range of electrical and heating modalities, and capitalizing on renewable energy sources.

Systems 1 and 2 use solar energy as an input, but system 1 additionally employs pyrolysis of plastic trash. In these systems, H_2 and CH_4 are created. However, system 3 is linked to a steel manufacturing facility, which mainly produces H_2 and CH_3OH. When constructing and modelling the proposed multigeneration systems, several considerations were considered. A prospective need and purpose were initially determined before building all three solutions.

As global warming and climate change become more widely researched, there is a growing need to reduce their effects. This might be a solution if countries integrate dependable carbon capture technology into their existing systems and convert to more clean energy alternatives. All planned systems incorporated aspects of carbon capture technologies and procedures for producing more benign hydrocarbons (i.e. CH_4) and alternative fuel sources (H_2).

By identifying gaps in literature, a novel multigeneration system may be built based on the literature research. The system's state point values were calculated after a preliminary design for the system was produced. The derived mass, energy, entropy, and exergy balance equations may be used to validate the system state point values. Exergy and exergy

degradation rates of various components aid in identifying potential problems. Furthermore, the system was confirmed by comparing various state point values and system work/heat transfer rates to those of comparable systems.

After calculating the system's usable outputs, it may be decided whether the system satisfies the minimum requirements to meet the demands of its target demography. If the system fails to satisfy the minimal standard, it is redesigned and changed.

3.1 System 1

System 1 showcases a comprehensive schematic representation, illustrating the intricate processes of hydrogen generation and carbon capture and storage. Figure 3.1 presents an overview of system 1 in a flowchart, illustrating the sequential execution of the system's distinct operations. Figure 3.2 illustrates a comprehensive depiction of the system, including all its components and the associated work processes in detail.

This system is achieved through iron-based chemical looping, integrated with the combined Brayton-Rankine power generation cycle and a solar energy system for thermal energy utilization. It employs a sustainable approach by harnessing plastic waste, predominantly polypropylene. After undergoing a meticulous granulation process, this plastic waste is systematically channelled into a specialized pyrolytic reactor, where it transforms to extract methane. Also, the system has four reactors, each meticulously designed for iron-based chemical looping, ensuring optimal performance and efficiency. Table 3.1 delineates the chemical reactions happening in each chemical looping reactor during hydrogen production.

Table 3.1 System 1 chemical reactions with their temperature level and enthalpy of reaction of related components

Component	Reaction	Enthalpy of Reaction (kJ/mol)	Temperature (˚C)
Reactor 1	$H_2O + CH_4 \rightarrow 3H_2 + CO$	ΔH = - 41.2	600
Reactor 2	$8CO + 2Fe_3O_4 \rightarrow 8CO_2 + 6Fe$	ΔH = - 524.8	700
Reactor 3	$4H_2O + 3Fe \rightarrow Fe_3O_4 + 4H_2$	ΔH = 536.8	700
Reactor 4	$2O_2 + 3Fe \rightarrow Fe_3O_4$	ΔH = - 1117.6	750

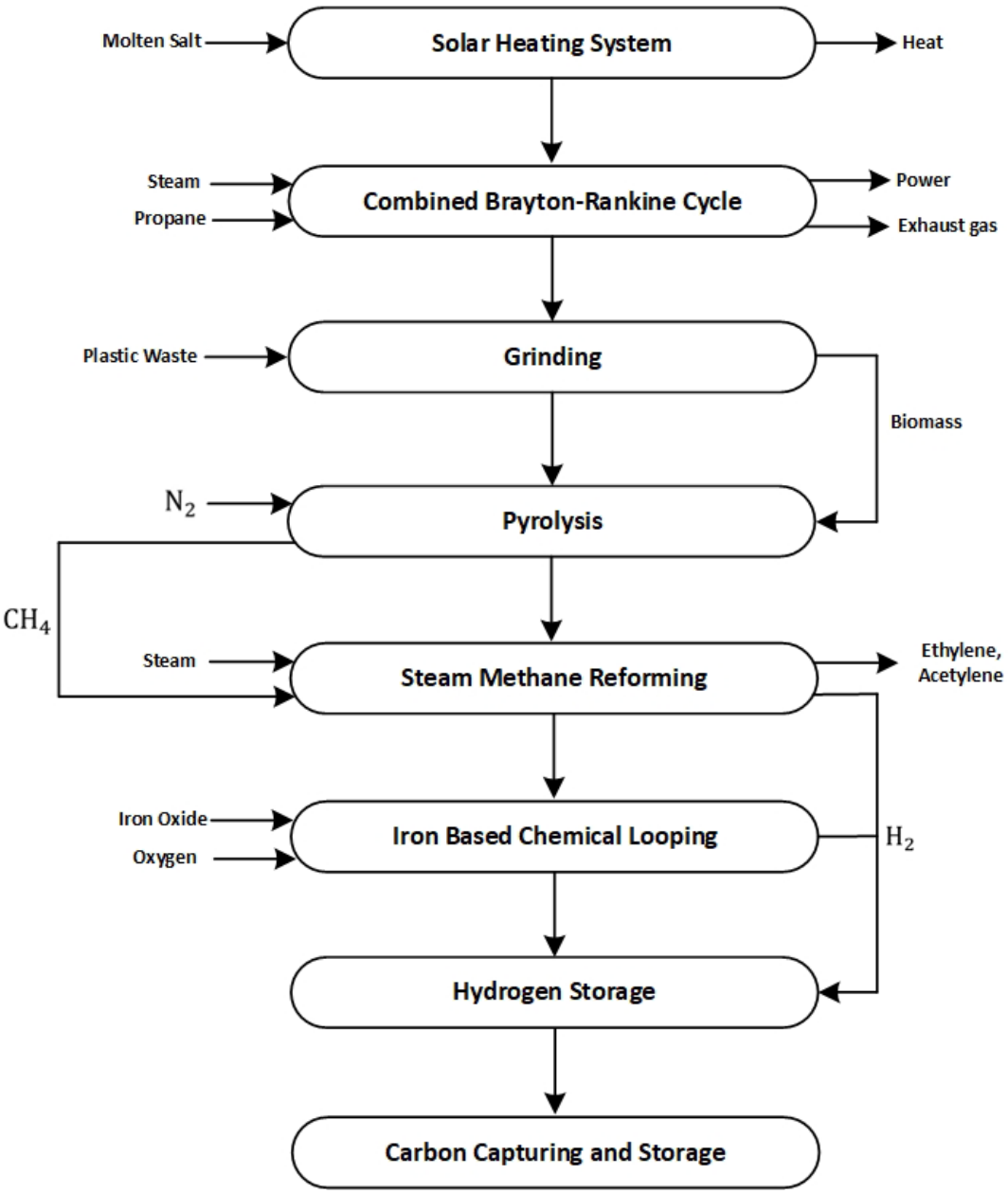

Figure 3.1 A step-by-step algorithm of system 1 subsystems

It is paramount to note that the first and third reactors are specifically tailored to facilitate hydrogen extraction. Conversely, the secondary reactor has been optimized for the pivotal role of CCS. Solar heliostats have been strategically incorporated to bolster the system's energy efficiency and sustainability.

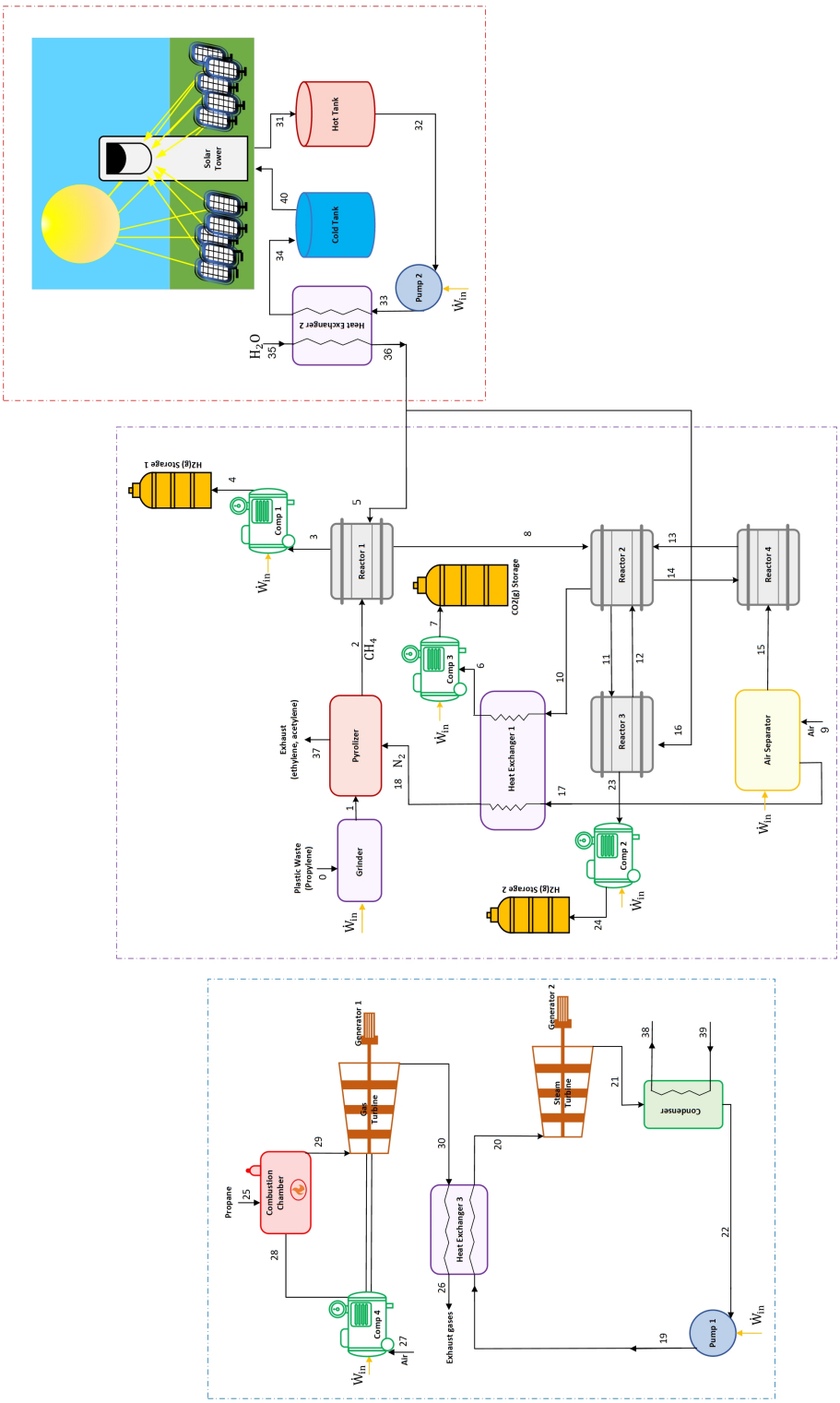

Figure 3.2 Schematic of system 1 for chemical looping and SMR hydrogen production and CCS from plastic waste with power generation and solar energy subsystems

These heliostats capture and harness solar radiation, furnishing the requisite thermal energy to the entire system. The captured solar energy by heliostats undergoes a systematic conversion process to functional heat and is distributed throughout the system [48].

Furthermore, the amalgamated Brayton-Rankine cycle, an integral system component, is envisioned and calibrated to generate the essential power, ensuring operational continuity and reliability. Anchoring the research on conceptually robust assumptions is imperative for scholarly analysis and evaluation. These assumptions not only set the foundation for the study but also ensure its validity and reliability. This is especially true for intricate systems that require a clear operational framework. At the core of this analysis, the system is presumed to function within the parameters of a steady state and consistent flow mode. This denotes a constant, unvarying operational state, ensuring that temporal changes do not influence the system's behaviour or outcomes. A foundational assumption pertains to the environmental conditions in which the system is determined. It is posited that the ambient temperature within which the system operates is a moderate 25℃. Simultaneously, the prevailing atmospheric pressure is standardized at 101 kPa, mirroring common terrestrial conditions.

The feedstock, which plays a pivotal role in the system, comprises polypropylene plastic waste weighing 1000 grams. This waste has been meticulously crushed and amalgamated with 100 grams of the ZSM-5 catalyst, facilitating the desired chemical reactions. Then, this plastic waste goes through a pyrolizer. Pyrolysis is executed within a reactor set at a temperature of 450℃. Notably, this procedure unfolds in an oxygen-deprived environment. The heating rate adopted for this process is 10℃/min, and the entire pyrolytic phase spans 75 minutes, as evidenced by reference [72]. As for the solar components, the solar tower, a crucial energy source, boasts a direct normal irradiance of 1.82 kW/m^2. Its efficiency is marked at a commendable 75%. Complementing the tower are the 20 solar heliostats, each with an area of 11×11 m^2 [46]. The system's design is such that heat losses are minimal, if not absent, across pivotal components like heat exchangers, turbines, compressors, and pumps. This ensures maximum energy conservation and efficiency. The choice of fuel for the combustion chamber is propane, a hydrocarbon with a significantly lower heating value (LHV) of 46.5 MJ/kg. This ensures optimal energy release during combustion.

In simplifying the analysis, all products emanating from the combustion chamber and the incoming air are treated as ideal gases. This approximation aids in streamlining calculations. Furthermore, any pressure losses in the heat exchangers, combustion

chamber, and associated piping are negligible in pressure dynamics. This ensures consistency in flow and operational stability. Within the iron-based chemical looping subsystem, the initial processing of plastic waste commences with a meticulous granulation process facilitated by a specialized grinding apparatus. After this, the granulated waste is directed to a pyrolytic chamber. In an oxygen-deprived environment, propylene undergoes a transformative chemical interaction within this chamber, yielding products such as methane, ethylene, and acetylene. Post-pyrolysis, a purification step ensues, wherein a specialized polyethylene membrane material facilitates the selective extraction of methane at an ambient temperature of 25°C and under a pressure setting of 200 kPa. This purified methane is introduced into the primary reactor, which undergoes a catalytic conversion, producing hydrogen and carbon monoxide.

The ensuing hydrogen is subjected to a pressurization phase, facilitated by the initial compressor, and is subsequently stored in a dedicated reservoir designed to withstand pressures up to 35,000 kilopascals. Concurrently, the carbon monoxide generated is channelled to the secondary reactor, engaging in a chemical interaction with iron oxide, yielding iron and carbon dioxide. This carbon dioxide undergoes a thermal regulation process in a heat exchanger, after which it is pressurized and directed underground via specialized conduits for enhanced oil recovery applications. The iron, a byproduct of the process, is systematically routed to tertiary and quaternary reactors. Iron interacts with water vapour in the third reactor, producing hydrogen and iron oxide. The hydrogen from this phase is pressurized and stored, with the storage facility calibrated for pressures of 35,000 kilopascals. The resulting iron oxide is recycled and reintroduced to the secondary reactor, ensuring the continuity of the chemical loop. In the fourth reactor, the iron undergoes an oxidative reaction, yielding iron oxide, which is subsequently redirected to the secondary reactor to sustain its operational cycle. The requisite oxygen for this phase is sourced from ambient air after separating.

Additionally, the pyrolytic chamber requires nitrogen, which, after separation, is thermally conditioned via a heat exchanger before its introduction to the pyrolytic chamber. The thermal energy is essential for the reactors and is derived from a solar infrastructure. Solar panels harness sunlight, reflect it onto a solar tower, and convert it into heat for the system's

operations. Machinery efficiency is crucial for system performance. The gas and steam turbines and the compressors are hypothesized to possess an isentropic efficiency of 80%. In tandem, the pumps, vital for fluid movement, are considered to operate in an isentropic fashion. Lastly, the integrated Brayton-Rankine cycle, a cornerstone of the system's thermodynamic operations, has a pressure ratio of 9. This parameter is instrumental in determining the cycle's performance and output.

3.2 System 2

System 2, as illustrated in Fig. 3.3, presents a detailed depiction of the currently developed integrated energy framework, highlighting the sequential processes undertaken during its operation. Such a methodical representation ensures a step-by-step understanding of each segment, allowing the reader to navigate the complexities and grasp the interconnected nature of the various subsystems.

The system can be deconstructed into several discernible cycles and subcomponents within this elaborate energy framework. Each of these has been meticulously designed to fulfill a particular role, ensuring the seamless functioning of the entire system. The system's functional architecture is grounded in a series of pivotal presumptions integral to its scholarly evaluation.

At the outset, the system is designed to operate consistently within steady-state and uniform flow dynamics parameters. This ensures predictable and uninterrupted functionality. Environmental conditions have been standardized with the system operating at a consistent ambient temperature of 25°C and an atmospheric pressure benchmarked at 101 kPa. From a thermal perspective, one of the standout assumptions is the system's ability to retain heat, so there is no heat loss accruing throughout the system with minimum thermal dissipation, ensuring that the energy within the system boundaries is optimally conserved.

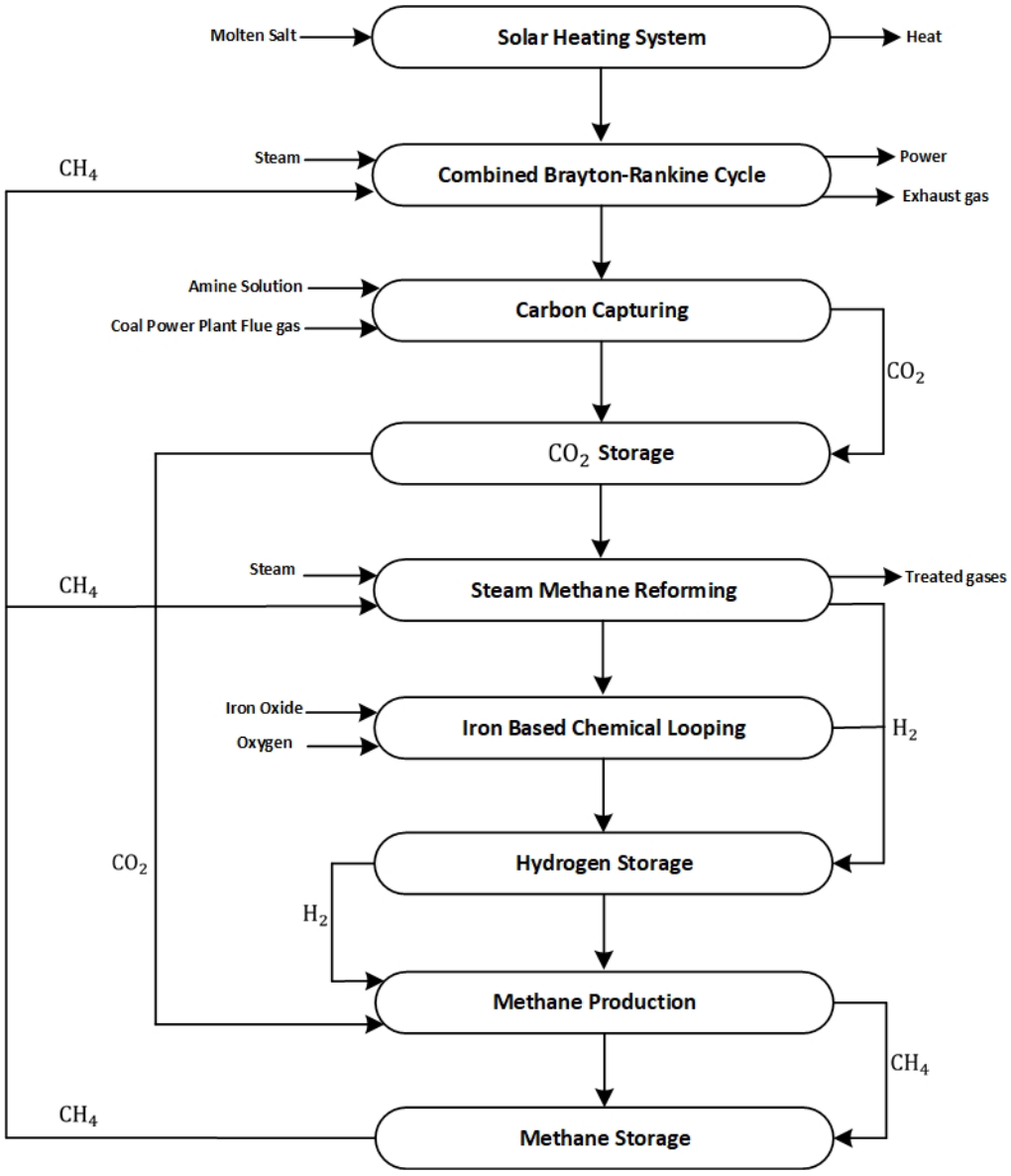

Figure 3.3 A step-by-step algorithm of system 2 subsystems

To further elucidate the complexities of the model, Fig. 3.4 offers a comprehensive visualization of the unique multigeneration system, specifically tailored for the simultaneous production of hydrogen and methane, complemented with carbon capture capabilities. Through this representation, one gains an encompassing perspective of the intricate methodologies and the synergistic interactions between the diverse components of the system.

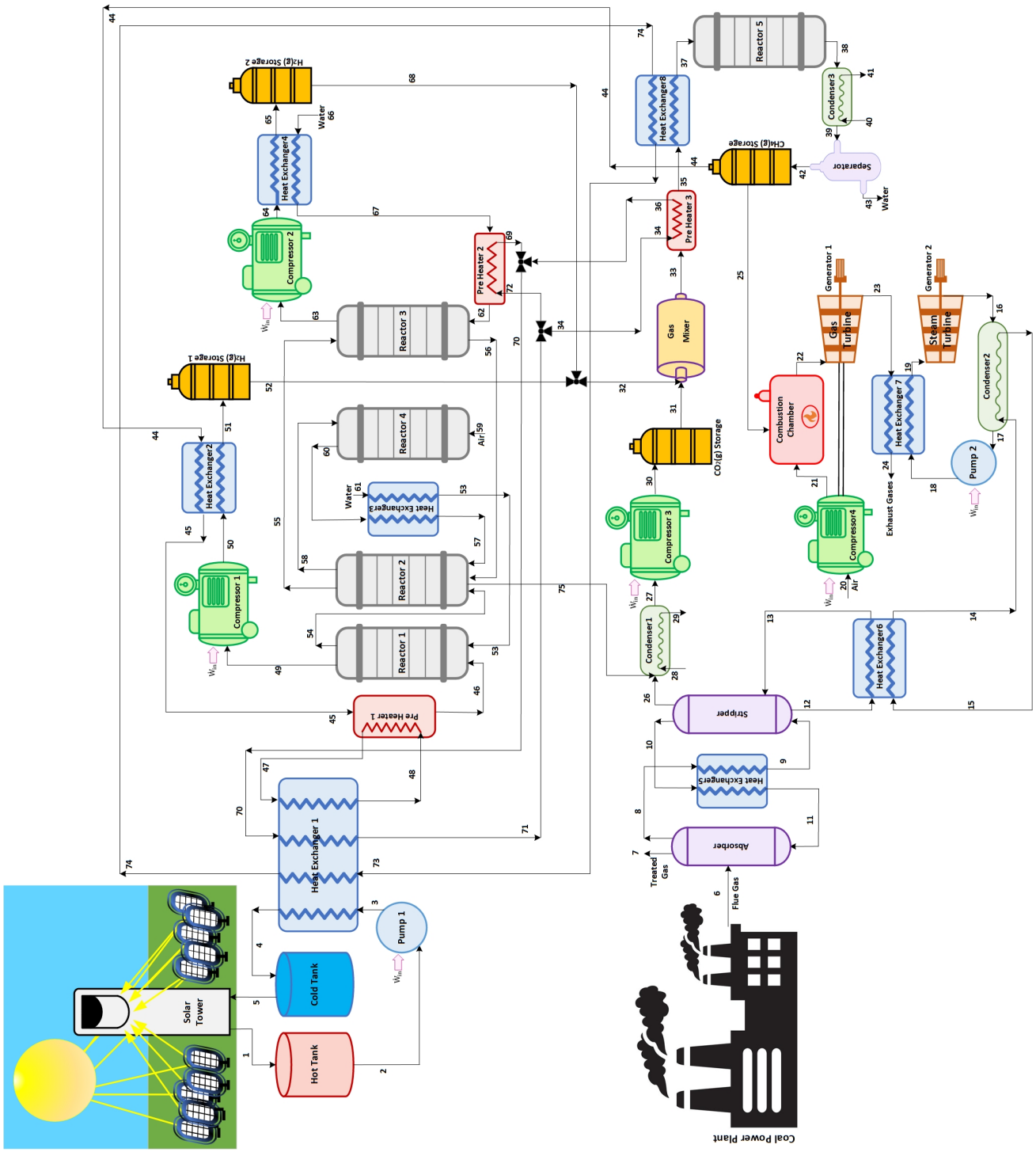

Figure 3.4 Schematic of system 2 for chemical looping and SMR hydrogen production and Carbon capture from coal-fired power plant and methane production with separated power generation and solar energy subsystems

To reach the maximum productivity of the system's operation, some identifiable components, such as condensers, pumps, and compressors, should work in an isentropic manner. Nevertheless, the turbines of the system are ascribed with an isentropic efficiency of 80 percent. In order to simplify the analysis, it is assumed that all gases involved in burning follow ideal gas behaviour. It is worth mentioning that some elements, such as preheater pumps, condensers, and heat exchangers, function with minimal changes in heat and pressure. A central aspect of this system is the production of hydrogen. This is realized by applying two diverse techniques: Fe-based Chemical Looping and Steam Methane Reforming. The primary material or feedstock essential for this hydrogen production phase is derived from methane, generated in a separate, dedicated model subsystem. Parallelly, another subsystem is carbon capturing from a coal-fired power plant. It is operationalized, leveraging an amine-based solution. This subsystem is tasked with extracting carbon dioxide from the flue gases emitted by a coal-fired power station. Once extracted, both hydrogen and carbon dioxide are methodically channelled into their respective storage facilities, ensuring their preservation for prospective applications. The third subsystem is defined as the methane production section, explicitly designed to use a part of the generated hydrogen and extracted carbon dioxide to produce another energy source for further utilization. In the methane production facet of the system, a definite amount of hydrogen and carbon dioxide is subjected to a preheating process. After this preparatory phase, the mixture is introduced into a specialized reactor, where the conditions are optimized for methane synthesis.

Methane is spotlighted as the primary agent in fueling the combustion processes. Its role is not only central but also critical to the energy dynamics of the system. Apart from these 3 multigenerational subsystems, the power and the heat needed for several system components are obtained from two different subsystems. One of them is the combination of the Brayton cycle and the Rankine cycle. This integrated cycle has been calibrated as the system's electricity generation unit. This cycle operates with a distinct pressure ratio, precisely set at 9, which significantly shapes the cycle's energy conversion and overall efficiency. Therefore, to ensure a steady power output, this cycle is the most suitable option for the system's sustainable operation. Then, a solar energy module has been incorporated, tasked with providing the requisite thermal input, thereby bolstering the system's overall

energy efficiency and sustainability. Multiple chemical reactions take place at different points in the system. Four reactors using two technologies work cyclically to produce hydrogen inside this system. The first step in this process involves preheating methane from the methane storage tank, which the system generates. Reactor 1 responds to reaction (3.1), where methane interacts with water vapour. The process of steam methane reforming results in the production of hydrogen gas by thermal means, occurring at a temperature of 600℃ and a pressure of 0.5 MPa.

$$H_2O(g) + CH_4(g) \rightarrow CO(g) + 3H_2(g) \qquad \Delta H = -41.2 \text{ kJ/mol} \qquad (3.1)$$

The hydrogen gas produced as a byproduct of this chemical reaction is subjected to compression by compressor 1 to a pressure of 35 MPa, and then it moves on to the cooling phase, aided by heat exchanger 2. Subsequently, the hydrogen will be kept inside the first hydrogen storage tank. An additional consequence of this chemical reaction is the formation of carbon monoxide, which is then sent to the second reactor to facilitate the subsequent stage of hydrogen generation's chemical looping technique with Fe, as the catalyst has four reactors. The primary goal of reactor 1 in this methodology is to produce carbon monoxide for use in the subsequent reactor. In the second reactor, a chemical reaction occurs between carbon monoxide and iron (II, III) oxide powder obtained from reactors 3 and 4. This reaction results in iron and carbon dioxide forming at a temperature of 700℃. This process is represented by reaction (3.2). The created iron will then be split into two equally sized portions and sent back to reactors 3 and 4 to complete the remaining steps of the CL process. The CO_2 generated is then combined with the CO_2 captured from a coal-fired power plant inside the carbon capture subsystem to store it in a storage tank for additional application. In the third reactor, hydrogen is produced using reaction (3.3), which combines superheated steam and iron powder at 700℃.

$$8CO(g) + 2Fe_3O_4(s) \rightarrow 8CO_2(g) + 6Fe(s) \qquad \Delta H = -524.8 \text{ kJ/mol} \qquad (3.2)$$

$$4H_2O(g) + 3Fe(s) \rightarrow Fe_3O_4(s) + 4H_2(g) \qquad \Delta H = 536.8 \text{ kJ/mol} \qquad (3.3)$$

The hydrogen produced by the reactor undergoes pressurization via compressor 2, cooled via heat exchanger 4, and then transported to an H_2 storage 2 at a pressure of 35 MPa. The byproduct, Fe_3O_4, is then reintroduced into reactor 2 for recycling. In order to conclude the

reaction that was initiated in the second reactor, the iron is transferred to reactor 4, where it reacts with the oxygen in the air at 750 degrees Celsius, as illustrated in the reaction (3.4).

$$2O_2(g) + 3Fe(s) \rightarrow Fe_3O_4(s) \qquad \Delta H = -1117.6 \text{ kJ/mol} \qquad (3.4)$$

This generates Fe_3O_4, which is then sent back into reactor 2, where it was initially used. Coal-fired power facilities primarily emit CO_2, SO_2, and NO_x as flue gas. A monoethanolamine (MEA) solution is brought into contact with flue gas via an absorber as part of the carbon capture process. The CO_2 molecules inside the absorber react with the MEA, forming a chemical bond following the reaction (3.5). This technique alone sequesters CO_2 while releasing other processed gases.

$$CO_2 + 2MEA \rightarrow MEAHCOO^- + MEAH^+ \qquad \Delta H = -88 \text{ kJ/mol} \qquad (3.5)$$

The amine solution, enriched with CO_2, is then transported to a stripper unit, which is subjected to heat to release the accumulated CO_2. The stripper uses heat exchanger 5 to transfer heat to the amine solution via reactions (3.6) and (3.7), liberating a concentrated CO_2 stream. The amine solution that has undergone regeneration, resulting in a significant reduction in CO_2 content, is reintroduced into the absorber to continue capturing CO_2. After the separation, the concentrated CO_2 will be combined with the CO_2 emitted from reactor 2. Subsequently, it will undergo pressurization via compressor 3 and be stored in a designated tank for future application.

$$MEACOO^- \rightarrow MEA + CO_2 \qquad \Delta H = +75 \text{ kJ/mol} \qquad (3.6)$$

$$MEAH^+ + H_2O \rightarrow MEA + H_3O^+ \qquad \Delta H = +25 \text{ kJ/mol} \qquad (3.7)$$

$$CO_2(g) + 4H_2(g) \rightarrow CH_4(g) + 2H_2O(g) \qquad \Delta H = -165 \text{ kJ/mol} \qquad (3.8)$$

The first phase in the methane generation process combines a part of stored hydrogen with a proportion of collected carbon dioxide using a gas mixer. Following this, the carefully prepared mixture is then sent to Reactor 5, where a transformational reaction takes place at a temperature of 400℃, in accordance with the principles outlined in the reaction (3.8). The principal products of this reaction are methane and water. The subsequent products are sent into a condenser and separator to separate the aqueous solution from the methane gas. After completing this process of separation, the methane gas that has been purified is then

stored in a specifically designated tank for further use. This explanation exemplifies the coordination in the methane and hydrogen generation process along with carbon capturing and storage, illustrating the system's pursuit of efficiency and optimal resource use.

3.3 System 3

In this part, a third intricate and distinctive system has been devised and introduced alongside the two systems that were previously delineated. This system encompasses two distinct methods for hydrogen generation, including chemical looping and electrolysis. Furthermore, it facilitates the production of electricity and heat and the capture of carbon emissions from a steel production facility. Using methanol as a catalyst in producing freshwater via the reaction of carbon dioxide and hydrogen is very efficient. Figure 3.5 comprehensively depicts the whole system through a step-by-step flowchart. The input and output parameters for each specific subset of the system are shown. Within each of the parts, as mentioned earlier, several components and distinct processes are involved in the production of hydrogen, methanol, electricity, water, and heat. As depicted in Figure 3.6, the schematic presents a comprehensive overview of the envisioned multigenerational system. All the assumptions for this system are similar to the two previous systems, such as the percentage of component efficiencies and neglecting the heat loss of all the components during the system to be able to compare the three systems to each other and reach the utmost efficiency.

Within this intricate framework, the initial process involves the capture of carbon dioxide emanating from a steel production facility. This is adeptly achieved by utilizing a solution of monoethanolamine. The subsystem designed for this purpose is equipped with a series of components, including an absorber, stripper, heat exchanger 1, a boiler, and a condenser after going through two heat exchangers to get the extra heat from the flue gas. This heat will then be used in other parts of the system. In system 3 under consideration, the steel

production facility is the primary target for CO_2 capture. The flue gas from this facility exhibits a notably high temperature.

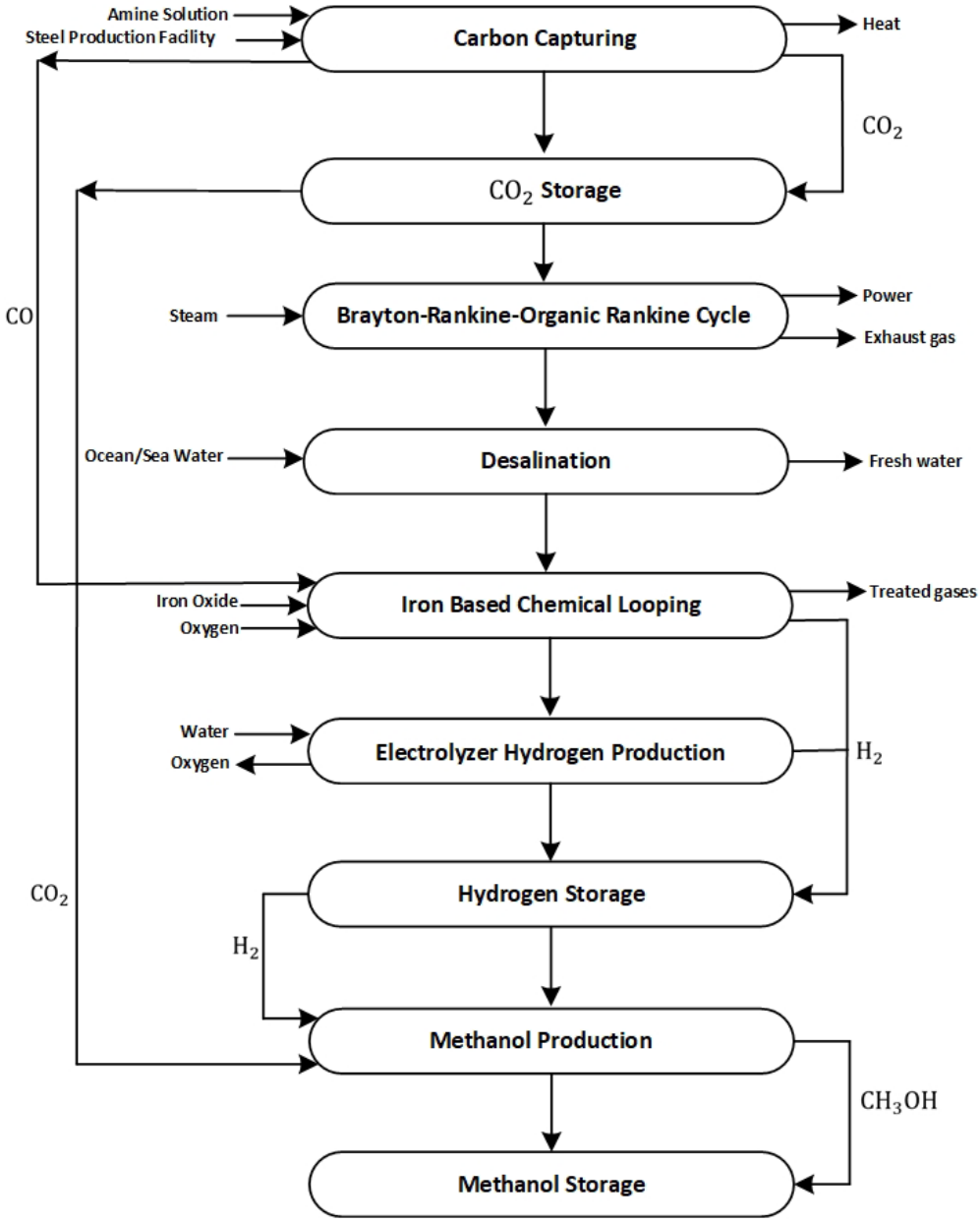

Figure 3.5 A step-by-step algorithm of system 3 subsystems

Consequently, two heat exchangers are used to receive the heat from the flue gas and provide the required heat for the other components to function efficiently. Upon crossing through these heat exchangers, the flue gas proceeds to the absorber, where it undergoes a reaction with lean MEA. This interaction facilitates the absorption of CO_2 into the solution. Subsequently, this mixture is directed through Heat Exchanger 1 before reaching the

stripper. Within the stripper, the CO_2 is heated via the boiler, allowing it to separate from the rich amine mixture.

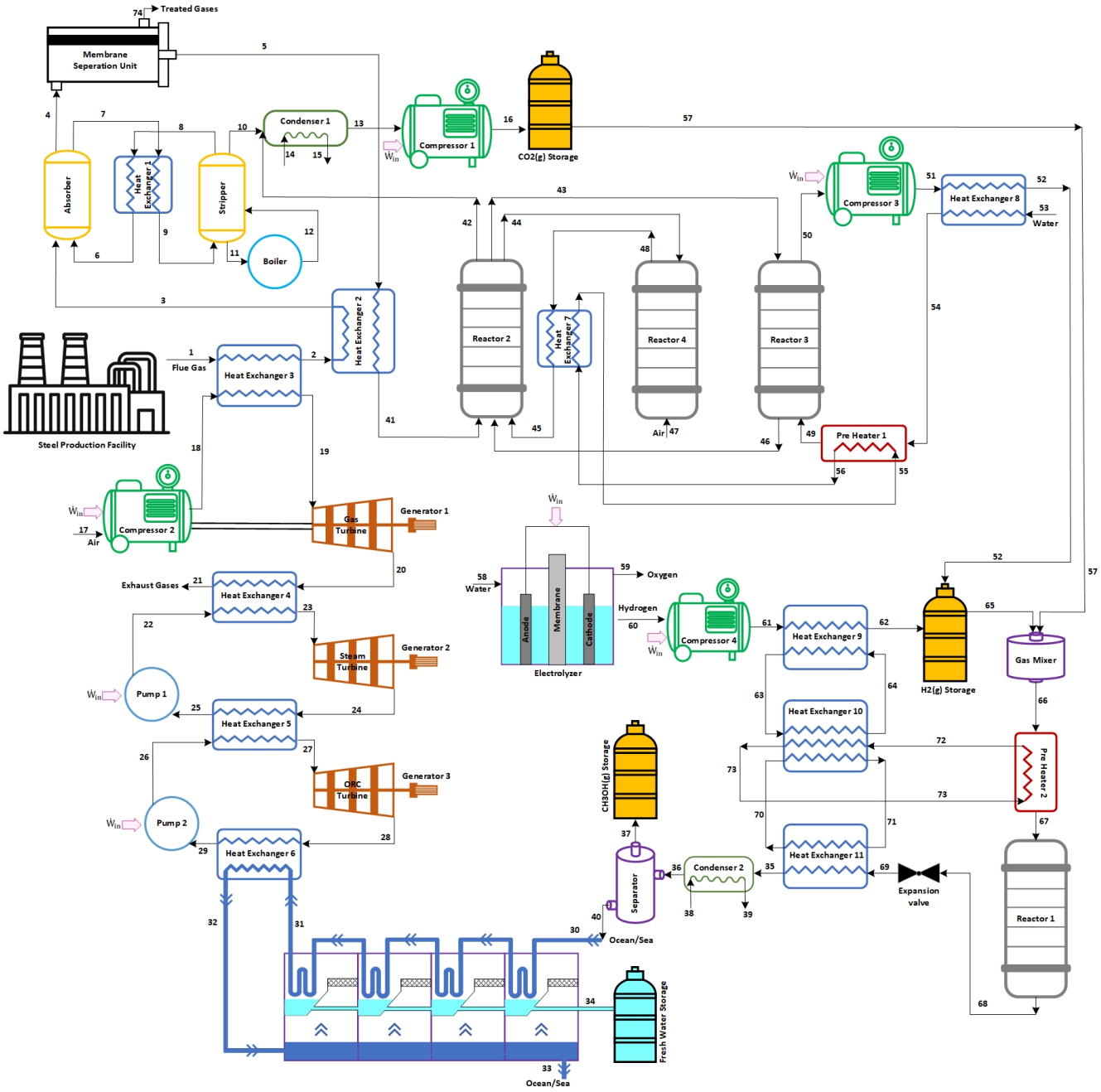

Figure 3.6 Schematic of system 3 for chemical looping and electrolysis hydrogen production and Carbon capture from steel production facility and methanol and freshwater production with separated power generation

The resultant CO_2 and water vapour then pass into Condenser 1 to separate the liquid water from carbon dioxide. The chemical reactions that happen inside the absorber and the

stripper are already introduced in equations (3.6), (3.7), and (3.8). Finally, the CO_2 is channelled into Compressor 1 and stored appropriately earmarked for future applications. Parallel to this process, the treated gases post their interaction with the absorber, undergoing a filtration process. Carbon monoxide is selectively extracted using a membrane separator, positioning it for subsequent utilization in the chemical looping process for hydrogen production.

In the preliminary phase of the carbon capture procedure, it is imperative to note the role of the thermal dynamics associated with the flue gas emanating from steel production operations. Specifically, this residual heat is adeptly harnessed by heat exchangers 2 and 3. These exchangers play a pivotal role in ensuring that the acquired thermal energy is subsequently utilized to elevate the air temperature intended for the combustion sequence within the Brayton cycle. This heat is also instrumental in pre-conditioning the carbon monoxide before introducing it to reactor 2.

The system's core objective revolves around producing hydrogen, a vital energy carrier. This production is realized through the synergistic deployment of two distinct methodologies: Fe-based chemical looping and the process of electrolysis. Delving into the nuances of the former technique, reactor 2 becomes a focal point. Within this reactor, the pre-heated carbon monoxide undergoes a reaction with iron (II, III) oxide. This reaction is meticulously calibrated to occur at an optimal temperature of T=700 ℃. The ensuing chemical transformation can be elucidated through the (3.2) reaction.

Subsequently, as delineated in reactions (3.3) and (3.4), the system embodies a cyclical operational design. Within this cycle, reactor 3 plays a central role where a portion of the iron synthesized undergoes a reaction with water vapour. This reaction, meticulously maintained at an ambient temperature of 700 ℃, culminates in the generation of hydrogen gas and iron (II, III) oxide. The emergent hydrogen gas is subsequently subjected to a compression phase and methodically stored in a dedicated hydrogen reservoir. Concurrently, the residual iron synthesized in reactor 2 is channelled to reactor 4. Here, it undergoes a reaction with ambient air oxygen. This reaction, optimized at a temperature setting of 750 ℃, forms iron (II, III) oxide. It is noteworthy that the iron (II, III) oxide synthesized in reactors 3 and 4 is subsequently routed back to reactor 2. This strategic

reallocation ensures the perpetuation of the hydrogen production cycle, with each phase mirroring its predecessor in terms of operational methodology.

Another avenue for hydrogen production within the system involves leveraging a polymer electrolyte membrane (PEM) electrolyzer. This advanced apparatus employs electrical energy to facilitate the hydrogen generation process. Post-production, a specialized compressor is deployed to elevate the pressure of the newly formed hydrogen, optimizing it for storage. This compressed hydrogen is then systematically reserved in designated storage units, ensuring its availability for future applications. After these processes, a calibrated blend of the stored hydrogen and previously captured carbon dioxide is prepared. This amalgamation undergoes a preheating phase to achieve optimal reaction conditions. The pre-conditioned mixture is then introduced into reactor 1, maintained at a temperature of T= 260 °C. Under these specific conditions, the resultant chemical transformation within this reactor leads to methanol synthesis. This process can be further elucidated as follows:

$$3H_2 + CO_2 \rightarrow CH_3OH + H_2O \qquad \Delta H = -49.3 \text{ kJ/mol} \qquad (3.9)$$

Within the energy framework of this system, the requisite electrical power is derived from an intricate integration of three distinct cycles: the Brayton, Rankine, and Organic Rankine cycles. Each cycle contributes synergistically, ensuring a seamless and efficient power generation mechanism. Central to the Organic Rankine cycle is the role of heat exchanger 6. This component has been meticulously designed to transfer its thermal energy to seawater, initiating desalination. Based on this, the system further capitalizes on a sophisticated multi-stage thermal desalination methodology. This process, utilizing oceanic or marine water as its primary input, culminates in the production of potable freshwater, enhancing the system's sustainability and utility.

Chapter 4. Analysis and Modelling

This chapter provides a comprehensive examination and modelling of the systems that have been constructed, as well as their corresponding subsystems. The approach used for analyzing each component is detailed, along with the simulation settings that were taken into consideration.

All system components' thermodynamic modelling and analysis are elucidated through implementing balance equations, EES software, and Aspen Plus. In order to evaluate the optimization of the system, an analysis is conducted to determine the energy and exergy efficiency, as well as the exergy destruction and sustainability of all three systems.

4.1 System 1

This section is dedicated to the examination and modelling of System 1. A comprehensive description of the thermodynamic analysis of each component inside the system is provided, along with the relevant modelling parameters.

This part examines the thermodynamic balancing equations for all components inside the system using Aspen Plus modelling and EES software. Additionally, it investigates the features of each state point and evaluates the overall system performance, including its connected subsystems.

4.1.1 Solar Energy Heating Subsystem

The entire system's heat is generated by solar heliostats, condensers, and reactor 3, as well as the hydrogen production chemical looping system.

$$\dot{Q}_{in,total} = \dot{Q}_{solar} + \dot{Q}_{cond} - \dot{Q}_{reactor\,3} \tag{4.1}$$

In the designated cold tank, a eutectic mixture of 60% LiCl and 40% KCl exists in a molten state. The mass, energy, entropy, and exergy balance equations of the cold tank are as follows:

$$\dot{m}_{34} = \dot{m}_{40} \tag{4.2}$$

$$\dot{m}_{34} h_{34} = \dot{m}_{40} h_{40} \tag{4.3}$$

$$\dot{S}_{gen} + \dot{m}_{34}s_{34} = \dot{m}_{40}s_{40} \tag{4.4}$$

$$\dot{m}_{34}ex_{34} = \dot{m}_{40}ex_{40} + \dot{E}x_{d} \tag{4.5}$$

Figure 4.1 presents an illustrative overview of the solar energy heating system. In order to conduct a comprehensive analysis of the system, it is crucial to ascertain the thermodynamic balance equations for each individual component.

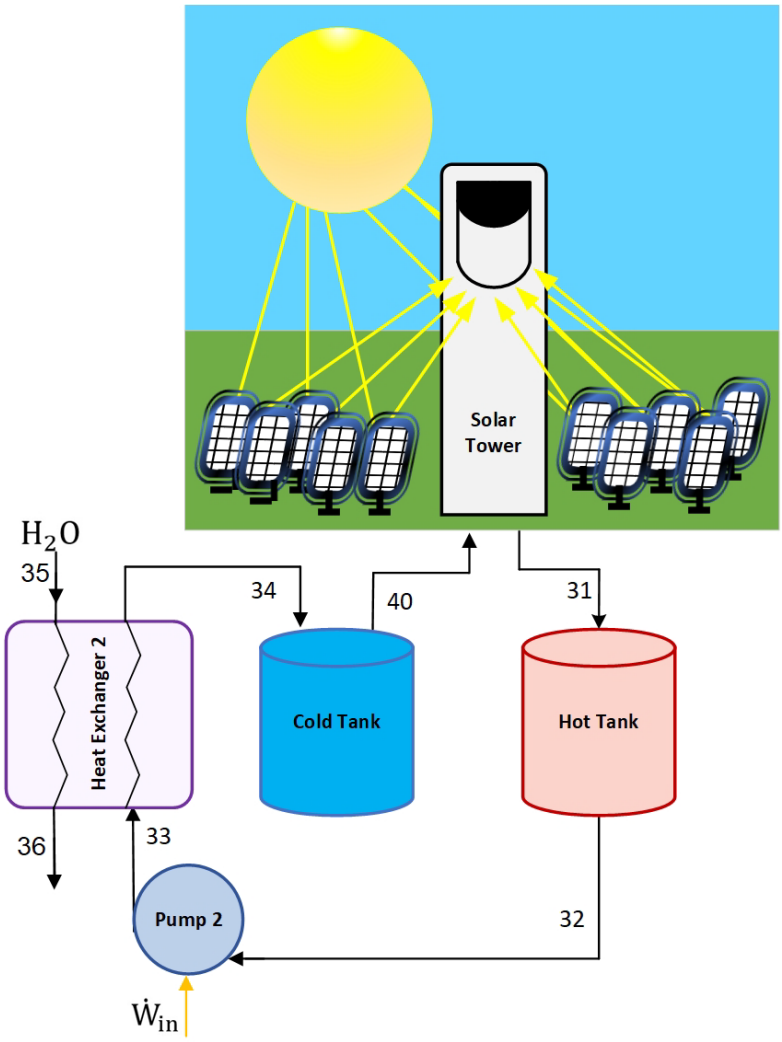

Figure 4.1 Schematic of solar heating subsystem of system 1

This liquid mixture is then subjected to thermal energy harvested from the solar tower heliostats, elevating its temperature before its subsequent relocation to the hot storage reservoir. In essence, the solar tower's radiant energy is harnessed to induce thermal elevation in water.

For the solar tower of system 1, the balance equations are as follows:

$$\dot{m}_{40} = \dot{m}_{31} \tag{4.6}$$

$$\dot{Q}_{solar} + \dot{m}_{40}h_{40} = \dot{m}_{31}h_{31} \tag{4.7}$$

$$\dot{S}_{gen} + \frac{\dot{Q}_{solar}}{T_s} + \dot{m}_{40}s_{40} = \dot{m}_{31}s_{31} \tag{4.8}$$

$$\dot{Q}_{solar}\left(1 - \frac{T_0}{T_s}\right) + \dot{m}_{40}ex_{40} = \dot{m}_{31}ex_{31} + \dot{E}x_d \tag{4.9}$$

Therefore, the heated mixture went into the hot tank after coming out of the solar tower. To have a better understanding of the component operation, the balance equations of this hot tank are derived as follows:

$$\dot{m}_{31} = \dot{m}_{32} \tag{4.10}$$

$$\dot{m}_{31}h_{31} = \dot{m}_{32}h_{32} \tag{4.11}$$

$$\dot{S}_{gen} + \dot{m}_{31}s_{31} = \dot{m}_{32}s_{32} \tag{4.12}$$

$$\dot{m}_{31}ex_{31} = \dot{m}_{32}ex_{32} + \dot{E}x_d \tag{4.13}$$

The thermally enriched molten salt mixture is propelled via pump 2 through a secondary heat exchanger. Here, it relinquishes its acquired heat and is cycled back to the cold reservoir. The balance equations of the pump 2 for the solar heating system are shown as follows:

$$\dot{m}_{32} = \dot{m}_{33} \tag{4.14}$$

$$\dot{m}_{32}h_{32} + \dot{W}_{in} = \dot{m}_{33}h_{33} \tag{4.15}$$

$$\dot{S}_{gen} + \dot{m}_{32}s_{32} = \dot{m}_{33}s_{33} \tag{4.16}$$

$$\dot{m}_{32}ex_{32} + \dot{W}_{in} = \dot{E}x_d + \dot{m}_{33}ex_{33} \tag{4.17}$$

Concurrently, water introduced into this system assimilates the heat from the secondary heat exchanger, transitioning into water vapour, channelling to both the primary and

tertiary reactors. The second heat exchanger in this subsystem has the below balance equations:

$$\dot{m}_{33} = \dot{m}_{34} \, , \dot{m}_{35} = \dot{m}_{36} \tag{4.18}$$

$$\dot{m}_{33}h_{33} + \dot{m}_{35}h_{35} = \dot{m}_{34}h_{34} + \dot{m}_{36}h_{36} \tag{4.19}$$

$$\dot{S}_{gen} + \dot{m}_{33}s_{33} + \dot{m}_{35}s_{35} = \dot{m}_{34}s_{34} + \dot{m}_{36}s_{36} \tag{4.20}$$

$$\dot{m}_{33}ex_{33} + \dot{m}_{35}ex_{35} = \dot{m}_{34}ex_{34} + \dot{m}_{36}ex_{36} + \dot{E}x_{d} \tag{4.21}$$

Considering the capacity of the solar direct normal irradiance as 1.82 kW/m^2 and the solar tower's thermal output rate calculated as 3303.3 kW, the rate of heat influx from the solar tower can be ascertained utilizing the subsequent mathematical expression, as referenced in [73]:

$$\dot{Q}_{Heliostat} = A_{Heliostat\,field} \times I \times N_{Heliostat} \tag{4.22}$$

Given an anticipated solar tower efficiency of 75%, the estimation of the heat rate generated from the solar tower and provided to the system functions as described below:

$$\dot{Q}_{solar} = \dot{Q}_{Heliostat} \times \eta_{solar} \tag{4.23}$$

4.1.2 Power Generation Subsystem

Figure 4.2 provides a visual representation of the overall structure and functioning of the power generation subsystem for system 1.

To facilitate a thorough examination of the system, it is important to establish the thermodynamic equilibrium equations for every component. All balance equations from (4.24) to (4.55) are the mass, energy, entropy, and exergy balance equations of all power generation subsystem components of system 1.

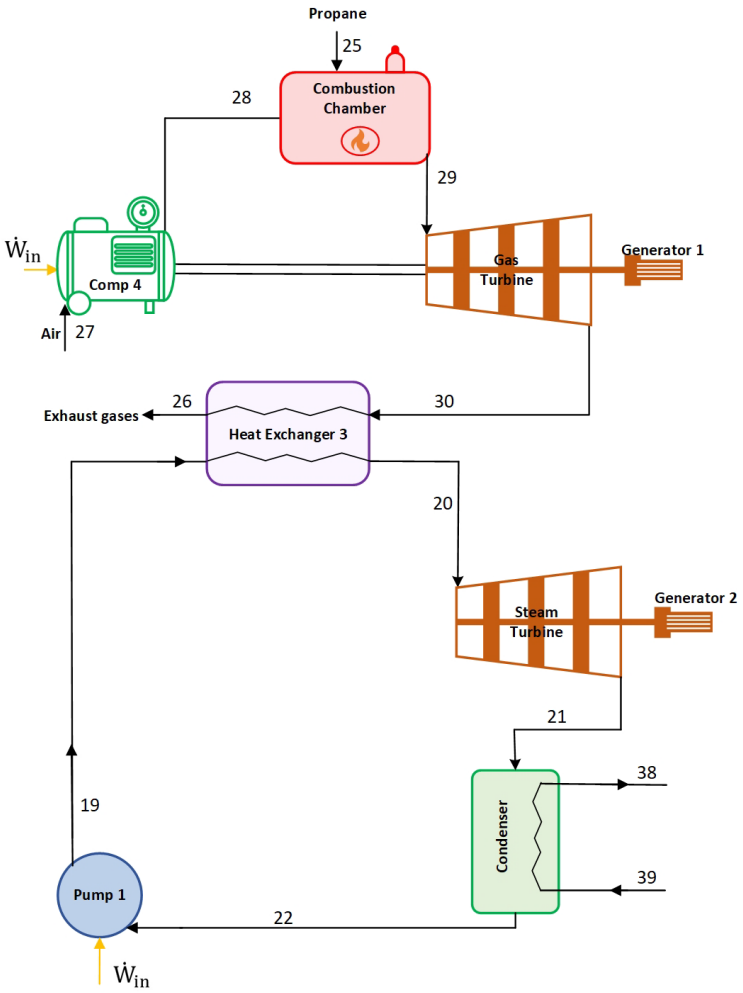

Figure 4.2 Schematic of power generation subsystem of system 1

For pump 1:

$$\dot{m}_{22} = \dot{m}_{19} \tag{4.24}$$

$$\dot{m}_{22}h_{22} + \dot{W}_{in} = \dot{m}_{19}h_{19} \tag{4.25}$$

$$\dot{S}_{gen} + \dot{m}_{22}s_{22} = \dot{m}_{19}s_{19} \tag{4.26}$$

$$\dot{m}_{22}ex_{22} + \dot{W}_{in} = \dot{E}x_{d} + \dot{m}_{19}ex_{19} \tag{4.27}$$

For condenser:

$$\dot{m}_{21} = \dot{m}_{22}\,,\ \dot{m}_{39} = \dot{m}_{38} \tag{4.28}$$

$$\dot{m}_{39}h_{39} + \dot{m}_{21}h_{21} = \dot{m}_{22}h_{22} + \dot{m}_{38}h_{38} + \dot{Q}_{out} \tag{4.29}$$

$$\dot{m}_{39}s_{39} + \dot{m}_{21}s_{21} = \dot{m}_{22}s_{22} + \dot{m}_{38}s_{38} + \frac{\dot{Q}_{out}}{T_b} \quad (4.30)$$

$$\dot{m}_{39}ex_{39} + \dot{m}_{21}ex_{21} = \dot{m}_{22}ex_{22} + \dot{m}_{38}ex_{38} + \dot{Q}_{out}(1 - \frac{T_0}{T_b}) + \dot{E}x_d \quad (4.31)$$

For steam turbine:

$$\dot{m}_{20} = \dot{m}_{21} \quad (4.32)$$

$$\dot{m}_{20}h_{20} = \dot{m}_{21}h_{21} + \dot{W}_{out} \quad (4.33)$$

$$\dot{S}_{gen} + \dot{m}_{20}s_{20} = \dot{m}_{21}s_{21} \quad (4.34)$$

$$\dot{m}_{20}ex_{20} = \dot{E}x_d + \dot{m}_{21}ex_{21} + \dot{W}_{out} \quad (4.35)$$

For gas turbine:

$$\dot{m}_{29} = \dot{m}_{30} \quad (4.36)$$

$$\dot{m}_{29}h_{29} = \dot{m}_{30}h_{30} + \dot{W}_{out} \quad (4.37)$$

$$\dot{S}_{gen} + \dot{m}_{29}s_{29} = \dot{m}_{30}s_{30} \quad (4.38)$$

$$\dot{m}_{29}ex_{29} = \dot{E}x_d + \dot{m}_{30}ex_{30} + \dot{W}_{out} \quad (4.39)$$

For heat exchanger 3:

$$\dot{m}_{30} = \dot{m}_{26}\,,\, \dot{m}_{19} = \dot{m}_{20} \quad (4.40)$$

$$\dot{m}_{30}h_{30} + \dot{m}_{19}h_{19} = \dot{m}_{20}h_{20} + \dot{m}_{26}h_{26} \quad (4.41)$$

$$\dot{S}_{gen} + \dot{m}_{30}s_{30} + \dot{m}_{19}s_{19} = \dot{m}_{20}s_{20} + \dot{m}_{26}s_{26} \quad (4.42)$$

$$\dot{m}_{30}ex_{30} + \dot{m}_{19}ex_{19} = \dot{m}_{20}ex_{20} + \dot{m}_{26}ex_{26} + \dot{E}x_d \quad (4.43)$$

For compressor 4:

$$\dot{m}_{27} = \dot{m}_{28} \quad (4.44)$$

$$\dot{W}_{in} + \dot{m}_{27}h_{27} = \dot{m}_{28}h_{28} \quad (4.45)$$

$$\dot{S}_{gen} + \dot{m}_{27}s_{27} = \dot{m}_{28}s_{28} \tag{4.46}$$

$$\dot{W}_{in} + \dot{m}_{27}ex_{27} = \dot{E}x_{d} + \dot{m}_{28}ex_{28} \tag{4.47}$$

For the combustion chamber, the physical balance equations are as follows:

$$\dot{m}_{28} + \dot{m}_{25} = \dot{m}_{29} \tag{4.48}$$

$$\dot{m}_{28}h_{28} + \dot{Q}_{in} + \dot{m}_{25}h_{25} = \dot{m}_{29}h_{29} \tag{4.49}$$

$$\dot{S}_{gen,} + \dot{m}_{28}s_{28} + \dot{m}_{25}s_{25} + \frac{\dot{Q}_{in}}{T_s} = \dot{m}_{29}s_{29} \tag{4.50}$$

$$\dot{m}_{28}ex_{28} + \dot{E}x_{\dot{Q}_{in}} + \dot{m}_{25}ex_{25} = \dot{E}x_{d} + \dot{m}_{29}ex_{29} \tag{4.51}$$

For the combustion chamber, the chemical balance equations are as follows:

$$\dot{n}_{C3H8} = \dot{n}_{CO2} + \dot{n}_{CO} + \dot{n}_{H2O} \tag{4.52}$$

$$\dot{n}_{C3H8}(\overline{h_f^0} + \bar{h} - \overline{h^0} - P\bar{v})_{C3H8} + \dot{n}_{O2}(\overline{h_f^0} + \bar{h} - \overline{h^0} - P\bar{v})_{O2} + \dot{Q}_{in} = \dot{n}_{CO}(\overline{h_f^0} + \bar{h} - \overline{h^0} - P\bar{v})_{CO} + \dot{n}_{CO2}(\overline{h_f^0} + \bar{h} - \overline{h^0} - P\bar{v})_{CO2} + \dot{n}_{H2O}(\overline{h_f^0} + \bar{h} - \overline{h^0} - P\bar{v})_{H2O} \tag{4.53}$$

$$\dot{S}_{gen} + \dot{n}_{C3H8}(\overline{s_f^0} + \bar{s} - \overline{s^0})_{C3H8} + \dot{n}_{O2}(\overline{s_f^0} + \bar{s} - \overline{s^0})_{O2} + \frac{\dot{Q}_{in}}{T_s} = \dot{n}_{CO2}(\overline{s_f^0} + \bar{s} - \overline{s^0})_{CO2} + \dot{n}_{CO}(\overline{s_f^0} + \bar{s} - \overline{s^0})_{CO} + \dot{n}_{H2O}(\overline{s_f^0} + \bar{s} - \overline{s^0})_{H2O} \tag{4.54}$$

$$\dot{n}_{C3H8}(\overline{ex_f^0} + \overline{ex} - \overline{ex^0} - P\bar{v})_{C3H8} + \dot{n}_{O2}(\overline{ex_f^0} + \overline{ex} - \overline{ex^0} - P\bar{v})_{O2} + \dot{Q}_{in}\left(1 - \frac{T_0}{T_s}\right) = \dot{n}_{CO}\left(\overline{ex_f^0} + \overline{ex} - \overline{ex^0} - P\bar{v}\right)_{CO} + \dot{n}_{CO2}(\overline{ex_f^0} + \overline{ex} - \overline{ex^0} - P\bar{v})_{CO2} + \dot{n}_{H2O}(\overline{ex_f^0} + \overline{ex} - \overline{ex^0} - P\bar{v})_{H2O} + \dot{E}x_{d} \tag{4.55}$$

The system's requisite energy output is catered to by the integrated power cycle, a mechanism designed for enhanced efficiency. Before the operation within the Brayton cycle turbine, there is a transfer of thermal energy from the exiting water of said turbine to the outflow from the pump associated with the Rankine cycle. A graphical representation detailing the T-s diagram of these intertwined cycles can be found illustrated in Figure 4.3.

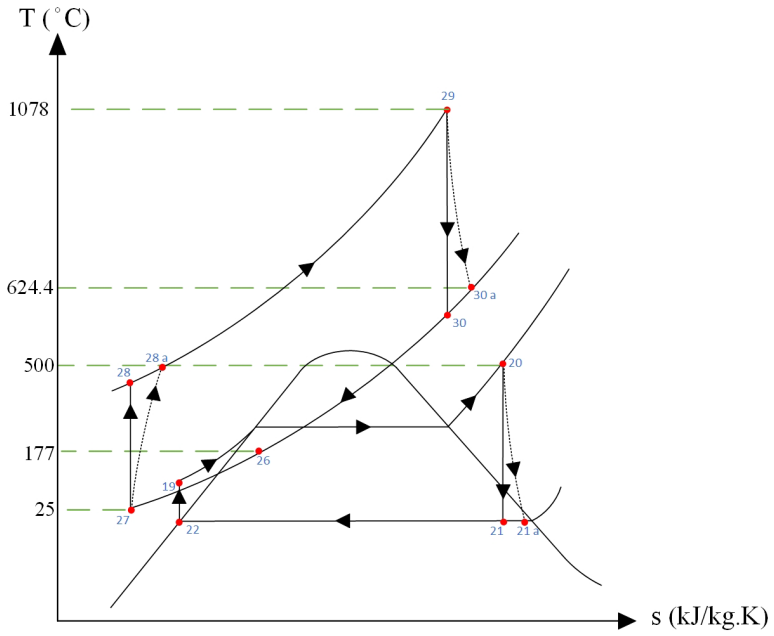

Figure 4.3 The T-s diagram of the power generation subsystem of system 1

From Figure 4.3, it's evident that the Rankine cycle functions at relatively subdued temperatures compared to the Brayton cycle. Owing to its elevated temperature intake, the gas turbine showcases superior energy efficiency in contrast to the steam turbine. Yet, a notable challenge arises as the gaseous output from the gas turbine registers temperatures around 500℃, implying substantial thermal losses. Given the pronounced thermal nature of the gas post its turbine traversal, the integration of the Rankine cycle as a supplementary bottoming cycle presents an opportunity. This integration facilitates the harnessing of residual heat to generate steam, further optimizing the Rankine cycle's operation. The following equation describes the system's cumulative network output:

$$\dot{W}_{tot,net} = \dot{W}_{GT} + \dot{W}_{ST} - \sum \dot{W}_{comp,i} - \sum \dot{W}_{pump,i} \tag{4.56}$$

The isentropic efficiency of 80% should be taken into account when calculating the performance of the gas turbine, steam turbine, and all four compressors. Hence, the quantification of the work rate for each of these components is determined in the following manner:

$$\dot{W}_a = \dot{W}_i \times \eta_{is,i} \tag{4.57}$$

4.1.3 Hydrogen Production and Carbon Capturing Subsystem

As shown in Figure 4.4, the hydrogen generation subsystem within System 1 has two distinct components, which include steam methane reforming and chemical looping.

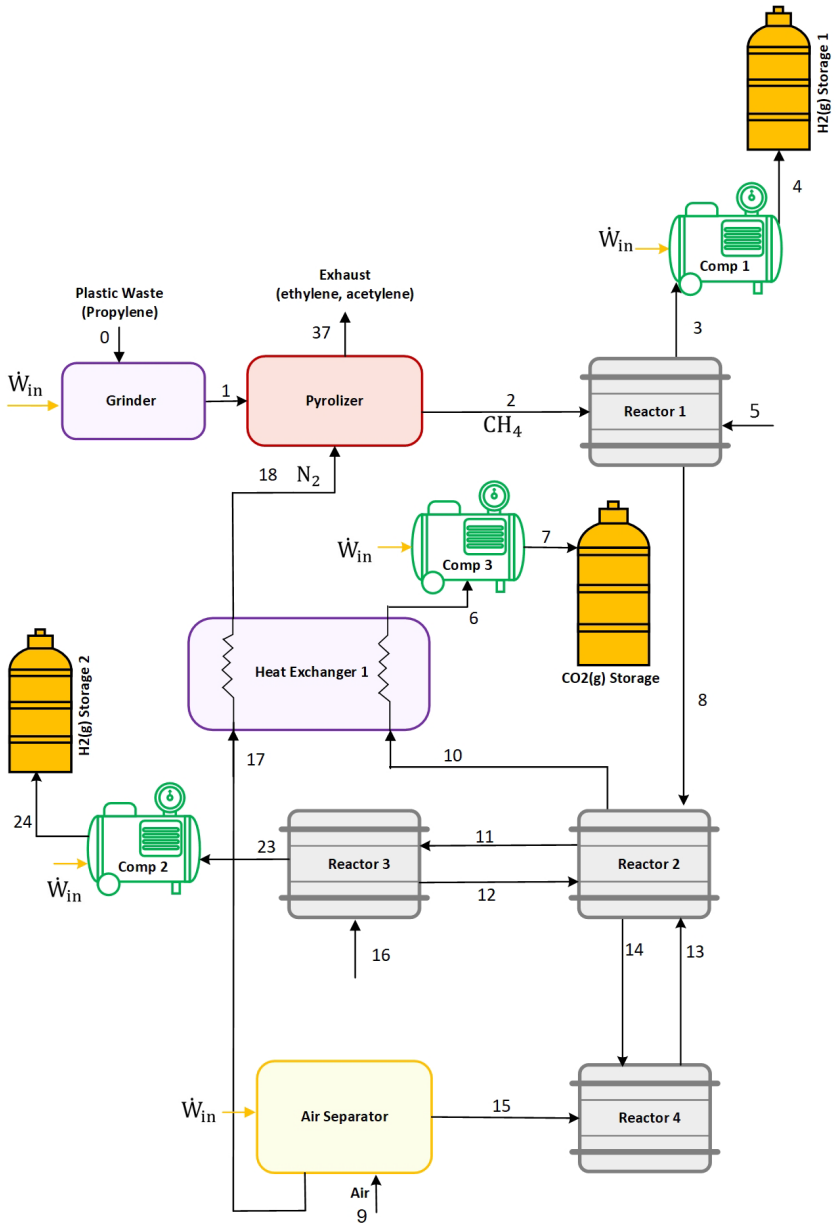

Figure 4.4 Schematic of hydrogen production and carbon capturing of system 1

This subcategory encompasses a total of four reactors, whereby various chemical processes take place, eventually resulting in the creation of hydrogen. The chemical and physical mass, energy, entropy, and exergy balance equations of these four reactors are written as follows:

For reactor 1, the physical balance equations are as follows:

$$\dot{m}_2 + \dot{m}_5 = \dot{m}_3 + \dot{m}_8 \tag{4.58}$$

$$\dot{m}_2 h_2 + \dot{m}_5 h_5 + \dot{Q}_{in} = \dot{m}_3 h_3 + \dot{m}_8 h_8 \tag{4.59}$$

$$\dot{S}_{gen} + \dot{m}_2 s_2 + \dot{m}_5 s_5 + \frac{\dot{Q}_{in}}{T_s} = \dot{m}_3 s_3 + \dot{m}_8 s_8 \tag{4.60}$$

$$\dot{m}_2 ex_2 + \dot{m}_5 ex_5 + \dot{Q}_{in}(1 - \frac{T_0}{T_s}) = \dot{m}_3 ex_3 + \dot{m}_8 ex_8 + \dot{E}x_d \tag{4.61}$$

For reactor 1, the chemical balance equations are as follows:

$$\dot{n}_{CH4} + \dot{n}_{H2O} = \dot{n}_{CO} + \dot{n}_{H2} \tag{4.62}$$

$$\dot{n}_{H2O}(\overline{h_f^0} + \bar{h} - \overline{h^0} - P\bar{v})_{H2O} + \dot{n}_{CH4}(\overline{h_f^0} + \bar{h} - \overline{h^0} - P\bar{v})_{CH4} + \dot{Q}_{in} = \dot{n}_{CO}(\overline{h_f^0} + \bar{h} - \overline{h^0} - P\bar{v})_{CO} + \dot{n}_{H2}(\overline{h_f^0} + \bar{h} - \overline{h^0} - P\bar{v})_{H2} \tag{4.63}$$

$$\dot{S}_{gen} + \dot{n}_{H2O}(\overline{s_f^0} + \bar{s} - \overline{s^0})_{H2O} + \dot{n}_{CH4}(\overline{s_f^0} + \bar{s} - \overline{s^0})_{CH4} + \frac{\dot{Q}_{in}}{T_s} = \dot{n}_{CO}(\overline{s_f^0} + \bar{s} - \overline{s^0})_{CO} + \dot{n}_{H2}(\overline{s_f^0} + \bar{s} - \overline{s^0})_{H2} \tag{4.64}$$

$$\dot{n}_{H2O}(\overline{ex_f^0} + \overline{ex} - \overline{ex^0} - P\bar{v})_{H2O} + \dot{n}_{CH4}(\overline{ex_f^0} + \overline{ex} - \overline{ex^0} - P\bar{v})_{CH4} + \dot{Q}_{in}(1 - \frac{T_0}{T_s}) = \dot{n}_{CO}(\overline{ex_f^0} + \overline{ex} - \overline{ex^0} - P\bar{v})_{CO} + \dot{n}_{H2}(\overline{ex_f^0} + \overline{ex} - \overline{ex^0} - P\bar{v})_{H2} + \dot{E}x_d \tag{4.65}$$

For reactor 2, the physical balance equations are as follows:

$$\dot{m}_8 + \dot{m}_{12} + \dot{m}_{13} = \dot{m}_{10} + \dot{m}_{11} + \dot{m}_{14} \tag{4.66}$$

$$\dot{m}_8 h_8 + \dot{m}_{12} h_{12} + \dot{m}_{13} h_{13} + \dot{Q}_{in} = \dot{m}_{10} h_{10} + \dot{m}_{11} h_{11} + \dot{m}_{14} h_{14} \tag{4.67}$$

$$\dot{S}_{gen} + \dot{m}_8 s_8 + \dot{m}_{12} s_{12} + \dot{m}_{13} s_{13} + \frac{\dot{Q}_{in}}{T_s} = \dot{m}_{10} s_{10} + \dot{m}_{11} s_{11} + \dot{m}_{14} s_{14} \tag{4.68}$$

$$\dot{m}_8 ex_8 + \dot{m}_{12} ex_{12} + \dot{m}_{13} ex_{13} + \dot{Q}_{in}(1 - \frac{T_0}{T_s}) = \dot{m}_{10} ex_{10} + \dot{m}_{11} ex_{11} + \dot{m}_{14} ex_{14} + \dot{E}x_d \tag{4.69}$$

For reactor 2, the chemical balance equations are as follows:

$$\dot{n}_{Fe3O4} + \dot{n}_{CO} = \dot{n}_{CO2} + \dot{n}_{Fe} \tag{4.70}$$

$$\dot{n}_{CO}(\overline{h_f^0} + \bar{h} - \overline{h^0} - P\bar{v})_{CO} + \dot{n}_{Fe3O4}(\overline{h_f^0} + \bar{h} - \overline{h^0} - P\bar{v})_{Fe3O4} + \dot{Q}_{in} = \dot{n}_{CO2}(\overline{h_f^0} + \bar{h} - \overline{h^0} - P\bar{v})_{CO2} + \dot{n}_{Fe}(\overline{h_f^0} + \bar{h} - \overline{h^0} - P\bar{v})_{Fe} \tag{4.71}$$

$$\dot{S}_{gen} + \dot{n}_{CO}(\overline{s_f^0} + \bar{s} - \overline{s^0})_{CO} + \dot{n}_{Fe3O4}(\overline{s_f^0} + \bar{s} - \overline{s^0})_{Fe3O4} + \frac{\dot{Q}_{in}}{T_s} = \dot{n}_{CO2}(\overline{s_f^0} + \bar{s} - \overline{s^0})_{CO2} + \dot{n}_{Fe}(\overline{s_f^0} + \bar{s} - \overline{s^0})_{Fe} \tag{4.72}$$

$$\dot{n}_{CO}(\overline{ex_f^0} + \overline{ex} - \overline{ex^0} - P\bar{v})_{CO} + \dot{n}_{Fe3O4}(\overline{ex_f^0} + \overline{ex} - \overline{ex^0} - P\bar{v})_{Fe3O4} + \dot{Q}_{in}(1 - \frac{T_0}{T_s}) = \dot{n}_{CO2}(\overline{ex_f^0} + \overline{ex} - \overline{ex^0} - P\bar{v})_{CO2} + \dot{n}_{Fe}(\overline{ex_f^0} + \overline{ex} - \overline{ex^0} - P\bar{v})_{Fe} + \dot{E}x_d \tag{4.73}$$

For reactor 3, the physical balance equations are as follows:

$$\dot{m}_{11} + \dot{m}_{16} = \dot{m}_{23} + \dot{m}_{12} \tag{4.74}$$

$$\dot{m}_{11}h_{11} + \dot{m}_{16}h_{16} = \dot{m}_{12}h_{12} + \dot{m}_{23}h_{23} + \dot{Q}_{out} \tag{4.75}$$

$$\dot{S}_{gen} + \dot{m}_{11}s_{11} + \dot{m}_{16}s_{16} = \dot{m}_{12}s_{12} + \dot{m}_{23}s_{23} + \frac{\dot{Q}_{out}}{T_b} \tag{4.76}$$

$$\dot{m}_{16}ex_{16} + \dot{m}_{11}ex_{11} = \dot{m}_{12}ex_{12} + \dot{m}_{23}ex_{23} + \dot{Q}_{out}(1 - \frac{T_0}{T_s}) + \dot{E}x_d \tag{4.77}$$

For reactor 3, the physical balance equations are as follows:

$$\dot{n}_{Fe} + \dot{n}_{O2} = \dot{n}_{Fe3O4} + \dot{n}_{H2} \tag{4.78}$$

$$\dot{n}_{H2O}(\overline{h_f^0} + \bar{h} - \overline{h^0} - P\bar{v})_{H2O} + \dot{n}_{Fe}(\overline{h_f^0} + \bar{h} - \overline{h^0} - P\bar{v})_{Fe} = \dot{n}_{H2}(\overline{h_f^0} + \bar{h} - \overline{h^0} - P\bar{v})_{H2} + \dot{n}_{Fe3O4}(\overline{h_f^0} + \bar{h} - \overline{h^0} - P\bar{v})_{Fe3O4} + \dot{Q}_{out} \tag{4.79}$$

$$\dot{S}_{gen} + \dot{n}_{Fe}(\overline{s_f^0} + \bar{s} - \overline{s^0})_{Fe} + \dot{n}_{H2O}(\overline{s_f^0} + \bar{s} - \overline{s^0})_{H2O} = \dot{n}_{Fe3O4}(\overline{s_f^0} + \bar{s} - \overline{s^0})_{Fe3O4} + \dot{n}_{H2}(\overline{s_f^0} + \bar{s} - \overline{s^0})_{H2} + \frac{\dot{Q}_{out}}{T_b} \tag{4.80}$$

$$\dot{n}_{H2O}(\overline{ex_f^0} + \overline{ex} - \overline{ex^0} - P\bar{v})_{H2O} + \dot{n}_{Fe}(\overline{ex_f^0} + \overline{ex} - \overline{ex^0} - P\bar{v})_{Fe} = \dot{n}_{Fe3O4}(\overline{ex_f^0} + \overline{ex} - \overline{ex^0} - P\bar{v})_{Fe3O4} + \dot{n}_{H2}(\overline{ex_f^0} + \overline{ex} - \overline{ex^0} - P\bar{v})_{H2} + \dot{E}x_d + \dot{Q}_{out}(1 - \frac{T_0}{T_b}) \tag{4.81}$$

For reactor 4, the physical balance equations are as follows:

$$\dot{m}_{15} + \dot{m}_{14} = \dot{m}_{13} \tag{4.82}$$

$$\dot{m}_{15}h_{15} + \dot{Q}_{in} + \dot{m}_{14}h_{14} = \dot{m}_{13}h_{13} \tag{4.83}$$

$$\dot{S}_{gen} + \dot{m}_{15}s_{15} + \dot{m}_{14}s_{14} + \frac{\dot{Q}_{in}}{T_s} = \dot{m}_{13}s_{13} \tag{4.84}$$

$$\dot{m}_{14}ex_{14} + \dot{m}_{15}ex_{15} + \dot{Q}_{in}(1 - \frac{T_0}{T_s}) = \dot{m}_{13}ex_{13} + \dot{E}x_d \tag{4.85}$$

For reactor 4, the physical balance equations are as follows:

$$\dot{n}_{O_2} + \dot{n}_{Fe} = \dot{n}_{Fe_3O_4} \tag{4.86}$$

$$\dot{n}_{O_2}\left(\overline{h_f^0} + \bar{h} - \overline{h^0} - P\bar{v}\right)_{O_2} + \dot{n}_{Fe}\left(\overline{h_f^0} + \bar{h} - \overline{h^0} - P\bar{v}\right)_{Fe} + \dot{Q}_{in} = \dot{n}_{Fe3O4}\left(\overline{h_f^0} + \bar{h} - \overline{h^0} - P\bar{v}\right)_{Fe3O4} \tag{4.87}$$

$$\dot{S}_{gen} + \dot{n}_{O_2}(\overline{s_f^0} + \bar{s} - \overline{s^0})_{O_2} + \dot{n}_{Fe}(\overline{s_f^0} + \bar{s} - \overline{s^0})_{Fe} + \frac{\dot{Q}_{in}}{T_s} = \dot{n}_{Fe3O4}(\overline{s_f^0} + \bar{s} - \overline{s^0})_{Fe3O4} \tag{4.88}$$

$$\dot{n}_{O_2}(\overline{ex_f^0} + \overline{ex} - \overline{ex^0} - P\bar{v})_{O_2} + \dot{n}_{Fe}(\overline{ex_f^0} + \overline{ex} - \overline{ex^0} - P\bar{v})_{Fe} + \dot{Q}_{in}(1 - \frac{T_0}{T_s}) = \dot{n}_{Fe3O4}(\overline{ex_f^0} + \overline{ex} - \overline{ex^0} - P\bar{v})_{Fe3O4} + \dot{E}x_d \tag{4.89}$$

After the hydrogen and carbon capture process is created, three compressors are strategically positioned to compress the gases effectively before their storage. Their related mass, energy, entropy, and exergy balance equations are as follows:

For compressor 1,

$$\dot{m}_3 = \dot{m}_4 \tag{4.90}$$

$$\dot{m}_3 h_3 + \dot{W}_{in} = \dot{m}_4 h_4 \tag{4.91}$$

$$\dot{S}_{gen} + \dot{m}_3 s_3 = \dot{m}_4 s_4 \tag{4.92}$$

$$\dot{m}_3 ex_3 + \dot{W}_{in} = \dot{E}x_d + \dot{m}_4 ex_4 \tag{4.93}$$

For compressor 2,

$$\dot{m}_{23} = \dot{m}_{24} \tag{4.94}$$

$$\dot{m}_{23}h_{23} + \dot{W}_{in} = \dot{m}_{24}h_{24} \quad (4.95)$$

$$\dot{S}_{gen} + \dot{m}_{23}s_{23} = \dot{m}_{24}s_{24} \quad (4.96)$$

$$\dot{m}_{23}ex_{23} + \dot{W}_{in} = \dot{E}x_{d} + \dot{m}_{24}ex_{24} \quad (4.97)$$

For compressor 3,

$$\dot{m}_{6} = \dot{m}_{7} \quad (4.98)$$

$$\dot{W}_{in} + \dot{m}_{6}h_{6} = \dot{m}_{7}h_{7} \quad (4.99)$$

$$\dot{S}_{gen} + \dot{m}_{6}s_{6} = \dot{m}_{7}s_{7} \quad (4.100)$$

$$\dot{W}_{in} + \dot{m}_{6}ex_{6} = \dot{E}x_{d} + \dot{m}_{7}ex_{7} \quad (4.101)$$

The methane production for the first reactor is achieved by pyrolysis, wherein ground plastic, mainly composed of polypropylene, is subjected to thermal decomposition. Hence, it is essential to equip this particular subcategory with a grinder and a pyrolizer. Their related mass, energy, entropy, and exergy balance equations are as follows:

For the grinder:

$$\dot{m}_{0} = \dot{m}_{1} \quad (4.102)$$

$$\dot{m}_{0}h_{0} + \dot{W}_{in} = \dot{m}_{1}h_{1} \quad (4.103)$$

$$\dot{S}_{gen} + \dot{m}_{0}s_{0} = \dot{m}_{1}s_{1} \quad (4.104)$$

$$\dot{m}_{0}ex_{0} + \dot{W}_{in} = \dot{E}x_{d} + \dot{m}_{1}ex_{1} \quad (4.105)$$

For the pyrolizer, the physical balance equations are as follows:

$$\dot{m}_{1} + \dot{m}_{18} = \dot{m}_{2} + \dot{m}_{37} \quad (4.106)$$

$$\dot{m}_{1}h_{1} + \dot{m}_{18}h_{18} + \dot{Q}_{in} = \dot{m}_{2}h_{2} + \dot{m}_{37}h_{37} \quad (4.107)$$

$$\dot{S}_{gen} + \dot{m}_{1}s_{1} + \dot{m}_{18}s_{18} + \frac{\dot{Q}_{in}}{T_{s}} = \dot{m}_{2}s_{2} + \dot{m}_{37}s_{37} \quad (4.108)$$

$$\dot{m}_{1}ex_{1} + \dot{m}_{18}ex_{18} + \dot{Q}_{in}(1 - \frac{T_{0}}{T_{s}}) = \dot{m}_{2}ex_{2} + \dot{m}_{37}ex_{37} + \dot{E}x_{d} \quad (4.109)$$

For the pyrolizer, the chemical balance equations are as follows:

$$\dot{n}_{C3H6} + \dot{n}_{H2} = \dot{n}_{CH4} + \dot{n}_{C2H4} + \dot{n}_{C2H2} \quad (4.110)$$

$$\dot{n}_{C3H6}(\overline{h_f^0} + \bar{h} - \overline{h^0} - P\bar{v})_{C3H6} + \dot{Q}_{in} = \dot{n}_{C2H2}(\overline{h_f^0} + \bar{h} - \overline{h^0} - P\bar{v})_{C2H2} + \dot{n}_{CH4}(\overline{h_f^0} + \bar{h} - \overline{h^0} - P\bar{v})_{CH4} + \dot{n}_{C2H4}(\overline{h_f^0} + \bar{h} - \overline{h^0} - P\bar{v})_{C2H4} \quad (4.111)$$

$$\dot{S}_{gen} + \dot{n}_{C3H6}(\overline{s_f^0} + \bar{s} - \overline{s^0})_{C3H6} + \frac{\dot{Q}_{in}}{T_s} = \dot{n}_{CH4}(\overline{s_f^0} + \bar{s} - \overline{s^0})_{CH4} + \dot{n}_{C2H2}(\overline{s_f^0} + \bar{s} - \overline{s^0})_{C2H2} + \dot{n}_{C2H4}(\overline{s_f^0} + \bar{s} - \overline{s^0})_{C2H4} \quad (4.112)$$

$$\dot{n}_{C3H6}(\overline{ex_f^0} + \overline{ex} - \overline{ex^0} - P\bar{v})_{C3H6} + \dot{Q}_{in}\left(1 - \frac{T_0}{T_s}\right) = \dot{n}_{C2H2}\left(\overline{ex_f^0} + \overline{ex} - \overline{ex^0} - P\bar{v}\right)_{C2H2} + \dot{n}_{CH4}\left(\overline{ex_f^0} + \overline{ex} - \overline{ex^0} - P\bar{v}\right)_{CH4} + \dot{n}_{C2H4}\left(\overline{ex_f^0} + \overline{ex} - \overline{ex^0} - P\bar{v}\right)_{C2H4} + \dot{E}x_d \quad (4.113)$$

The cryogenic air separator supplies the necessary oxygen for the fourth reactor and nitrogen for the pyrolysis process, and heat exchanger 1 is responsible for heat transfer between the components during some processes. Their related mass, energy, entropy, and exergy balance equations are as follows:

For cryogenic air separator:

$$\dot{m}_9 = \dot{m}_{17} + \dot{m}_{15} \quad (4.114)$$

$$\dot{m}_9 h_9 + \dot{W}_{in} = \dot{m}_{17} h_{17} + \dot{m}_{15} h_{15} \quad (4.115)$$

$$\dot{m}_9 s_9 + \dot{S}_{gen} = \dot{m}_{17} s_{17} + \dot{m}_{15} s_{15} \quad (4.116)$$

$$\dot{m}_9 ex_9 = \dot{m}_{17} ex_{17} + \dot{m}_{15} ex_{15} + \dot{E}x_d \quad (4.117)$$

For heat exchanger 1:

$$\dot{m}_{10} = \dot{m}_6 \, , \dot{m}_{17} = \dot{m}_{18} \quad (4.118)$$

$$\dot{m}_{10} h_{10} + \dot{m}_{17} h_{17} = \dot{m}_6 h_6 + \dot{m}_{18} h_{18} \quad (4.119)$$

$$\dot{S}_{gen} + \dot{m}_{10} s_{10} + \dot{m}_{17} s_{17} = \dot{m}_6 s_6 + \dot{m}_{18} s_{18} \quad (4.120)$$

$$\dot{m}_{10} ex_{10} + \dot{m}_{17} ex_{17} = \dot{m}_6 ex_6 + \dot{m}_{18} ex_{18} + \dot{E}x_d \quad (4.121)$$

4.1.4 Modelling and Analysis

Following the preliminary design, system 1 underwent a comprehensive evaluation, including thermodynamic analysis, efficiency evaluation, and exergy destruction analysis. In this context, subsequent to formulating the balance equations for all component parts of the system, the system was modelled using EES and Aspen Plus software. This modelling process included the evaluation of the efficiency, exergy destruction, and other thermodynamic characteristics related to each individual component within the system, as well as the whole system. The data was calculated and then subjected to a comparative analysis. The Aspen Plus simulation of the power generation unit and the hydrogen production unit of the system can be seen in Figure 4.5.

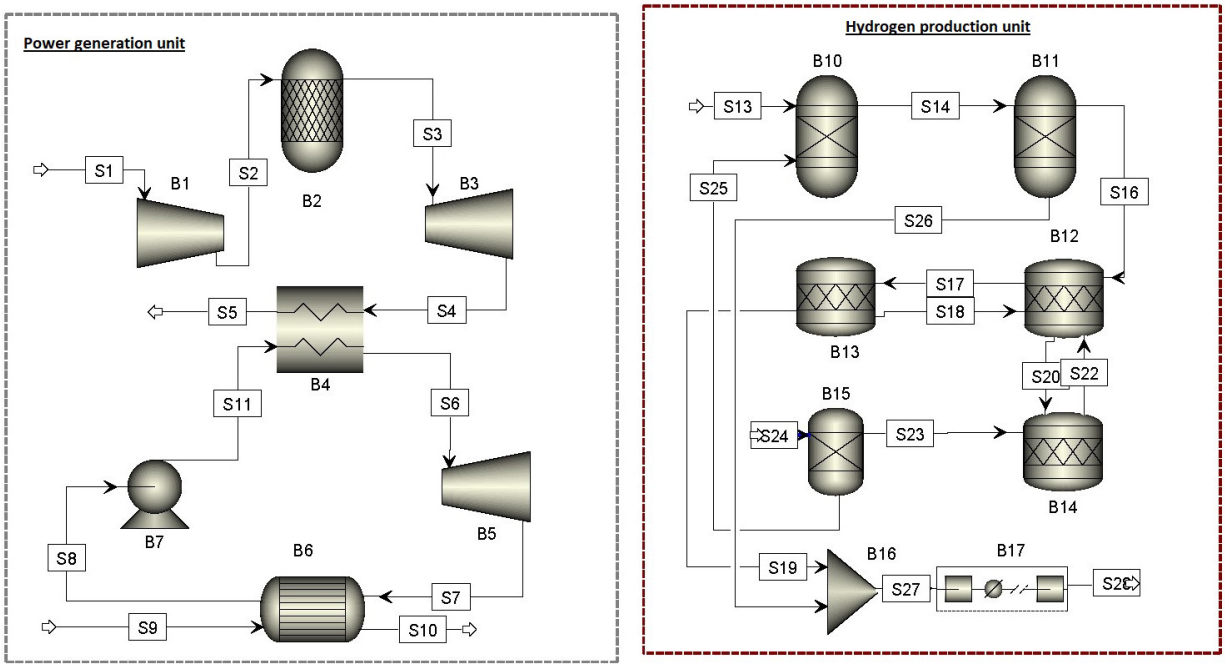

Figure 4.5 Aspen Plus simulation for the power generation and the hydrogen generation subsystems of system 1

According to the physical and chemical balance equations, interactions, Aspen Plus simulation and calculations and assumptions of system 1 components, the amount of mass flow rate, pressure, temperature, specific enthalpy, specific entropy and specific exergy of all state points of system 1 is calculated by using EES software which is shown in Table 4.1.

Table 4.1 Thermodynamic properties of all state points of system 1

State Point	Working Fluid	Mass flow Rate (kg/s)	Pressure (kPa)	Temperature (℃)	Specific Enthalpy (kJ/kg)	Specific Entropy (kJ/kg.K)	Specific exergy (kJ/kg)
0	Polypropylene	1	101	25	103.5	0.343	5.782
1	Polypropylene	1	101	25	103.5	0.343	5.782
2	Methane	128.3	90	300	734.4	1.773	210.6
3	Hydrogen (H_2 (g))	0.01	101	80	791.4	67.2	118045
4	Hydrogen (H_2 (g))	0.01	35000	80	4946	31.57	102514
5	Steam	90.08	1000	450	3371	7.62	1105
6	Carbon Dioxide (g)	352.1	101	25	-0.9353	0	4.033
7	Carbon Dioxide (g)	352.1	15000	35	-234.3	-1.535	227.5
8	Carbon Monoxide (g)	224	1000	50	419.9	5.074	392.4
9	Air	2	101	25	298.6	5.697	296.8
10	Carbon Dioxide (g)	352.1	101	500	487	0.9539	207.2
11	Iron(Fe)	167.5	101	500	7649	3.656	6564
12	Fe_3O_4	231.5	101	500	3721	3.818	2588
13	Fe_3O_4	231.5	701	919	3934	3.814	2802
14	Iron(Fe)	167.5	101	500	7649	3.656	6564
15	Oxygen (O_2(g))	2	700	22	154.2	0.6904	146.6
16	Steam	90.08	1000	450	3371	7.62	1105
17	Nitrogen (N_2 (g))	2	700	22	1615	4.376	1455
18	Nitrogen (N_2 (g))	2	101	30	247	0.7754	241.7
19	Water	3	8000	50	201.9	0.6556	11.04
20	Superheated steam	3	8000	500	3399	6.727	1399
21	Water	3	150	20	238.4	7.522	146.9
22	Saturated liquid water	3	10	20	191.8	0.649	2.894
23	Hydrogen (H_2 (g))	0.01	101	80	791.4	67.2	118045
24	Hydrogen (H_2 (g))	0.01	35000	80	4946	31.57	102514
25	Propane (C_3H_8)	10	101	25	-2374	6.128	104.3
26	Exhaust gases	10	101	177	452.3	6.113	182.3
27	Air	10	101	25	298.6	5.697	86.5
28	Air	10	909	500	625.2	5.808	201.8
29	Superheated air	10	909	1078	1457	6.689	862.4
30	Air	10	101	624.4	930.5	6.846	289.1
31	Molten salt	197	101	623	353.7	0.462	68197
32	Molten salt	197	101	619	351.1	0.459	57844
33	Molten salt	197	906	619	278.5	0.391	50234
34	Molten salt	197	906	345	206.51	0.145	28399
35	Water(l)	10	101	25	104.9	0.3672	0
36	Steam	180.2	1000	450	3371	7.62	1105
37	Ethylene, Acetylene (C_2H_2 , C_2H_4)	128.3	90	300	734.4	1.773	210.6
38	Steam	5	101	450	3383	8.69	797.7
39	Water(l)	5	101	25	104.9	0.3672	0
40	Molten salt	197	101	340	205.02	0.138	28240

To conduct a more comprehensive study, it was necessary to ascertain the exergy destruction of each individual component inside the system, as well as the overall system. The equation (4.122) finds out the exergy destruction rate for each component, and the amount of physical and chemical exergies can be determined by using the equations (4.123) and (4.124).

$$\dot{E}x_d = \sum \dot{E}x_{\dot{Q}_{net}} + \sum \dot{W}_{net} + \sum \dot{m}_i ex_i - \sum \dot{m}_j ex_j \tag{4.122}$$

$$ex_{Phys} = \sum_i [(h_i - h_o) - (s_i - s_o)] \tag{4.123}$$

$$\overline{ex}_{Chem} = \sum_i (\mu_i^* - \mu_{i,o}) \tag{4.124}$$

Therefore, the total exergy of each component according to its physical and chemical exergy balance equations is presented in equation (4.125), and the calculation of exergy of heat transfer for each component is shown in equation (4.126).

$$ex_i = ex_{phys,i} + ex_{chem,i} \tag{4.125}$$

$$\dot{E}x_{\dot{Q}_i} = \dot{Q}_i \left(1 - \frac{T_0}{T_{s,i}}\right) \tag{4.126}$$

Moreover, finding out the power generation cycle energy and exergy efficiencies was crucial to assess the power generated by the system. The equations for calculating the exergy and energy efficiencies of the power generation subsystem are shown as follows:

$$\eta_{Brayton} = \frac{\dot{W}_{net,Brayton}}{\dot{m}_{Propane} \times LHV_{Propane}} \tag{4.127}$$

$$\psi_{Brayton} = \frac{\dot{W}_{net,Brayton}}{\dot{m}_{Propane} \times ex_{Propane}} \tag{4.128}$$

$$\eta_{Rankine} = \frac{\dot{W}_{net,Rankine}}{\dot{Q}_{in,Rankine}} \tag{4.129}$$

$$\psi_{Rankine} = \frac{\dot{W}_{net,Rankine}}{\dot{E}x_{\dot{Q}_{in,Rankine}}} \tag{4.130}$$

Hydrogen production subsystem energy and exergy efficiencies were also intended to be determined. The equations for calculating the exergy and energy efficiencies of the hydrogen production subsystem are shown as follows:

$$\eta_{H_2} = \frac{\dot{n}_{H_2} \times M_{H_2}}{\dot{Q}_{in}} \tag{4.131}$$

$$\psi_{H_2} = \frac{\dot{n}_{H_2} \times \dot{E}x_{H_2}}{\dot{Q}_{in}} \tag{4.132}$$

Finally, it is vital to evaluate the exergy and energy efficiencies of the overall system. Therefore, the (4.133) and (4.134) equations are considered to calculate the desired efficiencies.

$$\eta_{Overall} = \frac{(\dot{W}_{tot,net}) + (\dot{m}_3 \times LHV_{H_2}) + (\dot{m}_{23} \times LHV_{H_2})}{\dot{Q}_{in,total}} \tag{4.133}$$

$$\psi_{Overall} = \frac{(\dot{W}_{tot,net}) + \dot{E}x_{H_2,total}}{\dot{E}x_{\dot{Q}_{in,total}}} \tag{4.134}$$

4.2 System 2

This part delves into the comprehensive analysis and representation of system 2. An exhaustive discourse is offered, encompassing the thermodynamic evaluation of each component embedded within the system, accompanied by the pertinent simulation metrics. This research scrutinizes the thermodynamic balance equations pertinent to all components encapsulated within the system, employing the Aspen Plus simulation and EES software. Moreover, the research probes into the attributes of distinct state junctions and appraises the cumulative efficacy of the system, considering its integrated sub-systemic structures.

4.2.1 Solar Energy Heating Subsystem

The solar thermal arrangement is composed of a central solar tower surrounded by an array of 100 heliostats, each spanning an area of 35×35 m^2 in a reflective surface. Accompanying these are two reservoirs, one designated as hot and the other as cold, containing a eutectic mixture of molten salts, predominantly 60% Lithium Chloride and 40% Potassium Chloride. This system also incorporates a heat exchanger and a circulation pump. The operational flow involves the molten salt being channelled from the cold reservoir to the

solar tower. As shown in Figure 4.6, it undergoes thermal augmentation due to the solar energy captured by the heliostats, after which it is directed to the hot reservoir. Subsequently, upon pressurization by the pump, the heated molten salt navigates through heat exchanger 1, transferring its acquired thermal energy to the water flowing through adjacent tubes within the exchanger before making its return to the cold reservoir.

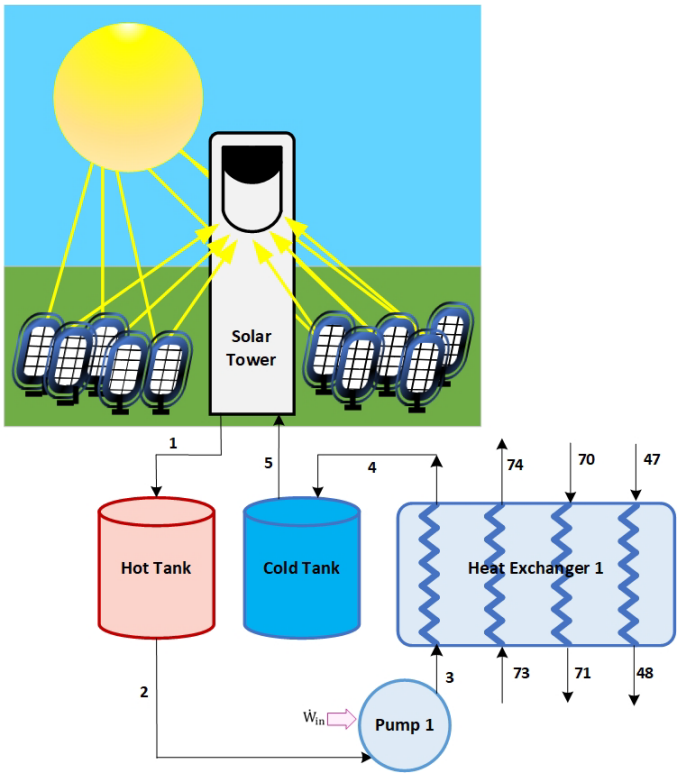

Figure 4.6 Schematic of solar heating subsystem of system 2

It is noteworthy that the heliostats are assumed to operate with an efficiency of 80%, and the solar tower's irradiance (Ib) is 1.5 kW/m^2. The equation (4.135) describes the way of calculating the solar system heating rate of the system.

$$\dot{Q}_{solar} = A_{Heliostat\,field} \times I_b \times \eta_{Heliostat} \tag{4.135}$$

For a better understanding of the solar thermal subsystem, thermodynamic balance equations of all the components are determined. The following equations display the mass, energy, entropy, and exergy balance equations of each component for system 2, respectively.

For solar tower:

$$\dot{m}_5 = \dot{m}_1 \tag{4.136}$$

$$\dot{Q}_{solar} + \dot{m}_5 h_5 = \dot{m}_1 h_1 \tag{4.137}$$

$$\dot{S}_{gen} + \frac{\dot{Q}_{solar}}{T_s} + \dot{m}_5 s_5 = \dot{m}_1 s_1 \tag{4.138}$$

$$\dot{Q}_{solar}\left(1 - \frac{T_0}{T_s}\right) + \dot{m}_5 ex_5 = \dot{m}_1 ex_1 + \dot{E}x_d \tag{4.139}$$

For hot tank:

$$\dot{m}_1 = \dot{m}_2 \tag{4.140}$$

$$\dot{m}_1 h_1 = \dot{m}_2 h_2 \tag{4.141}$$

$$\dot{S}_{gen} + \dot{m}_1 s_1 = \dot{m}_2 s_2 \tag{4.142}$$

$$\dot{m}_1 ex_1 = \dot{E}x_d + \dot{m}_2 ex_2 \tag{4.143}$$

For cold tank:

$$\dot{m}_4 = \dot{m}_5 \tag{4.144}$$

$$\dot{m}_4 h_4 = \dot{m}_5 h_5 \tag{4.145}$$

$$\dot{S}_{gen} + \dot{m}_4 s_4 = \dot{m}_5 s_5 \tag{4.146}$$

$$\dot{m}_4 ex_4 = \dot{E}x_d + \dot{m}_5 ex_5 \tag{4.147}$$

For pump 1:

$$\dot{m}_2 = \dot{m}_3 \tag{4.148}$$

$$\dot{m}_2 h_2 + \dot{W}_{in} = \dot{m}_3 h_3 \tag{4.149}$$

$$\dot{S}_{gen} + \dot{m}_2 s_2 = \dot{m}_3 s_3 \tag{4.150}$$

$$\dot{m}_2 ex_2 + \dot{W}_{in} = \dot{E}x_d + \dot{m}_3 ex_3 \tag{4.151}$$

For heat exchanger 1:

$$\dot{m}_3 + \dot{m}_{73} + \dot{m}_{70} + \dot{m}_{47} = \dot{m}_4 + \dot{m}_{74} + \dot{m}_{71} + \dot{m}_{48} \tag{4.152}$$

$$\dot{m}_3 h_3 + \dot{m}_{73} h_{73} + \dot{m}_{70} h_{70} + \dot{m}_{47} h_{47} = \dot{m}_4 h_4 + \dot{m}_{74} h_{74} + \dot{m}_{71} h_{71} + \dot{m}_{48} h_{48} \quad (4.153)$$

$$\dot{S}_{gen} + \dot{m}_3 s_3 + \dot{m}_{73} s_{73} + \dot{m}_{70} s_{70} + \dot{m}_{47} s_{47} = \dot{m}_4 s_4 + \dot{m}_{74} s_{74} + \dot{m}_{71} s_{71} + \dot{m}_{48} s_{48} \quad (4.154)$$

$$\dot{m}_3 ex_3 + \dot{m}_{73} ex_{73} + \dot{m}_{70} ex_{70} + \dot{m}_{47} ex_{47} = \dot{m}_4 ex_4 + \dot{m}_{74} ex_{74} + \dot{m}_{71} ex_{71} + \dot{m}_{48} ex_{48} + \dot{E}x_d \quad (4.155)$$

4.2.2 Power Generation Subsystem

Figure 4.7 offers a graphical depiction illustrating the operational dynamics of the power generation mechanism for system 2.

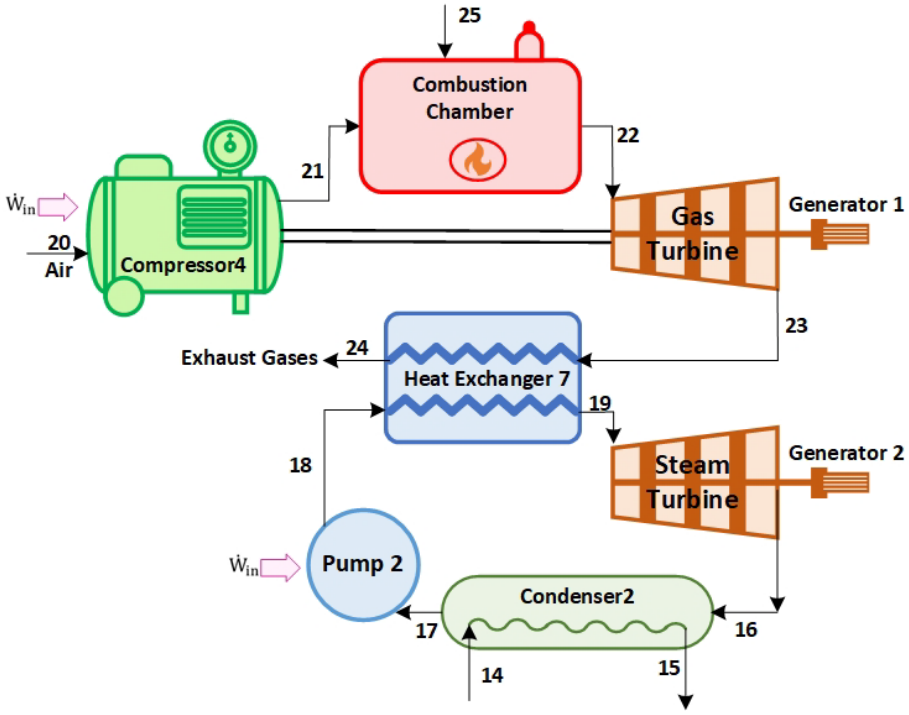

Figure 4.7 Schematic of power generation subsystem of system 2

For an in-depth system analysis, defining the thermodynamic balance equations for each constituent is crucial. Presented below are the balance equations pertaining to mass, energy, entropy, and exergy for all elements associated with the power generation subsystems of system 2.

For pump 2:

$$\dot{m}_{17} = \dot{m}_{18} \tag{4.156}$$

$$\dot{m}_{17}h_{17} + \dot{W}_{in} = \dot{m}_{18}h_{18} \tag{4.157}$$

$$\dot{S}_{gen} + \dot{m}_{17}s_{17} = \dot{m}_{18}s_{18} \tag{4.158}$$

$$\dot{m}_{17}ex_{17} + \dot{W}_{in} = \dot{E}x_{d} + \dot{m}_{18}ex_{18} \tag{4.159}$$

For condenser 2:

$$\dot{m}_{14} + \dot{m}_{16} = \dot{m}_{15} + \dot{m}_{17} \tag{4.160}$$

$$\dot{m}_{14}h_{14} + \dot{m}_{16}h_{16} = \dot{m}_{15}h_{15} + \dot{m}_{17}h_{17} + \dot{Q}_{out} \tag{4.161}$$

$$\dot{S}_{gen} + \dot{m}_{14}s_{14} + \dot{m}_{16}s_{16} = \dot{m}_{15}s_{15} + \dot{m}_{17}s_{17} + \frac{\dot{Q}_{out}}{T_b} \tag{4.162}$$

$$\dot{m}_{14}ex_{14} + \dot{m}_{16}ex_{16} = \dot{m}_{15}ex_{15} + \dot{m}_{17}ex_{17} + \dot{Q}_{out}(1 - \frac{T_0}{T_b}) + \dot{E}x_{d} \tag{4.163}$$

For steam turbine:

$$\dot{m}_{19} = \dot{m}_{16} \tag{4.164}$$

$$\dot{m}_{19}h_{19} = \dot{m}_{16}h_{16} + \dot{W}_{out} \tag{4.165}$$

$$\dot{S}_{gen} + \dot{m}_{19}s_{19} = \dot{m}_{16}s_{16} \tag{4.166}$$

$$\dot{m}_{19}ex_{19} = \dot{E}x_{d} + \dot{m}_{16}ex_{16} + \dot{W}_{out} \tag{4.167}$$

For gas turbine:

$$\dot{m}_{22} = \dot{m}_{23} \tag{4.168}$$

$$\dot{m}_{22}h_{22} = \dot{m}_{23}h_{23} + \dot{W}_{out} \tag{4.169}$$

$$\dot{S}_{gen} + \dot{m}_{22}s_{22} = \dot{m}_{23}s_{23} \tag{4.170}$$

$$\dot{m}_{22}ex_{22} = \dot{E}x_{d} + \dot{m}_{23}ex_{23} + \dot{W}_{out} \tag{4.171}$$

For heat exchanger 7:

$$\dot{m}_{18} + \dot{m}_{23} = \dot{m}_{19} + \dot{m}_{24} \tag{4.172}$$

$$\dot{m}_{18}h_{18} + \dot{m}_{23}h_{23} = \dot{m}_{19}h_{19} + \dot{m}_{24}h_{24} \tag{4.173}$$

$$\dot{S}_{gen} + \dot{m}_{18}s_{18} + \dot{m}_{23}s_{23} = \dot{m}_{19}s_{19} + \dot{m}_{24}s_{24} \tag{4.174}$$

$$\dot{m}_{18}ex_{18} + \dot{m}_{23}ex_{23} = \dot{m}_{19}ex_{19} + \dot{m}_{24}ex_{24} + \dot{E}x_{d} \tag{4.175}$$

For compressor 4:

$$\dot{m}_{20} = \dot{m}_{21} \tag{4.176}$$

$$\dot{W}_{in} + \dot{m}_{20}h_{20} = \dot{m}_{21}h_{21} \tag{4.177}$$

$$\dot{S}_{gen} + \dot{m}_{20}s_{20} = \dot{m}_{21}s_{21} \tag{4.178}$$

$$\dot{W}_{in} + \dot{m}_{20}ex_{20} = \dot{E}x_{d} + \dot{m}_{21}ex_{21} \tag{4.179}$$

For the combustion chamber, the chemical balance equations are the same as system 1, which are stated in the equations (4.52), (4.53), (4.54), and (4.55). The physical balance equations for the combustion chamber of this system are as follows:

$$\dot{m}_{21} + \dot{m}_{25} = \dot{m}_{22} \tag{4.180}$$

$$\dot{m}_{21}h_{21} + \dot{Q}_{in} + \dot{m}_{25}h_{25} = \dot{m}_{22}h_{22} \tag{4.181}$$

$$\dot{S}_{gen,} + \dot{m}_{21}s_{21} + \dot{m}_{25}s_{25} + \frac{\dot{Q}_{in}}{T_s} = \dot{m}_{22}s_{22} \tag{4.182}$$

$$\dot{m}_{21}ex_{21} + \dot{E}x_{\dot{Q}_{in}} + \dot{m}_{25}ex_{25} = \dot{E}x_{d} + \dot{m}_{22}ex_{22} \tag{4.183}$$

The system's essential electrical output is derived from an integrated power cycle, offering enhanced efficiency compared to standalone cycles. Presented subsequently is the definitive energy equation characterizing the cumulative network rate of the system:

$$\dot{W}_{total} = (\dot{W}_{\text{Gas Turbine}} \times \eta_{is}) + (\dot{W}_{\text{Steam Turbine}} \times \eta_{is}) - \sum_{i=1}^{2} \dot{W}_{pump,i} - \sum_{i=1}^{4} \dot{W}_{compressor,i} \tag{4.184}$$

After the power cycle operation, a heat exchanger facilitates the heat transfer from the turbine's residual emissions to the discharge from the pump within the Rankine cycle.

The gas turbine exhibits superior efficiency compared to the steam turbine due to its operation at higher input temperatures. However, this efficiency is counteracted by notable thermal losses, resulting in the gases released from the gas turbine having temperatures close to 880°C. Given the intense heat of these exiting gases, the Rankine cycle is integrated to capture this residual heat, converting it into steam.

For a holistic evaluation of the system's combined power segment and considering the tandem operation of the Brayton with the Rankine cycle, it is essential to determine the efficiencies of each cycle individually. These distinct values are then combined to deduce the comprehensive energy and exergy efficiencies. Subsequently, the energy and exergy balance equations for the power system are presented:

$$\eta_{\text{total power}} = \frac{\dot{W}_{\text{Brayton}}}{\dot{m}_{CH_4}(\text{LHV}_{CH_4})} \times \frac{\dot{W}_{\text{Rankine}}}{\dot{Q}_{\text{in,Rankine}}} \tag{4.185}$$

$$\psi_{\text{total power}} = \frac{\dot{W}_{\text{net,Brayton}}}{\dot{m}_{CH_4}(\text{ex}_{CH_4})} \times \frac{\dot{W}_{\text{Rankine}}}{\dot{E}x_{\dot{Q}_{\text{in,Rankine}}}} \tag{4.186}$$

4.2.3 Hydrogen Production Subsystem

Within system 2, the subsystem dedicated to hydrogen production encompasses two different methods: steam methane reforming and iron-based chemical looping.

The formation of hydrogen using both methods together in this system is represented in Figure 4.8. In order to conduct a comprehensive examination of the system, it is important to establish the thermodynamic balance equations for every component involved. For reactors 1,2,3 and 4, the chemical balance equations are already represented in (4.65), (4.73), (4.81) and (4.89), respectively.

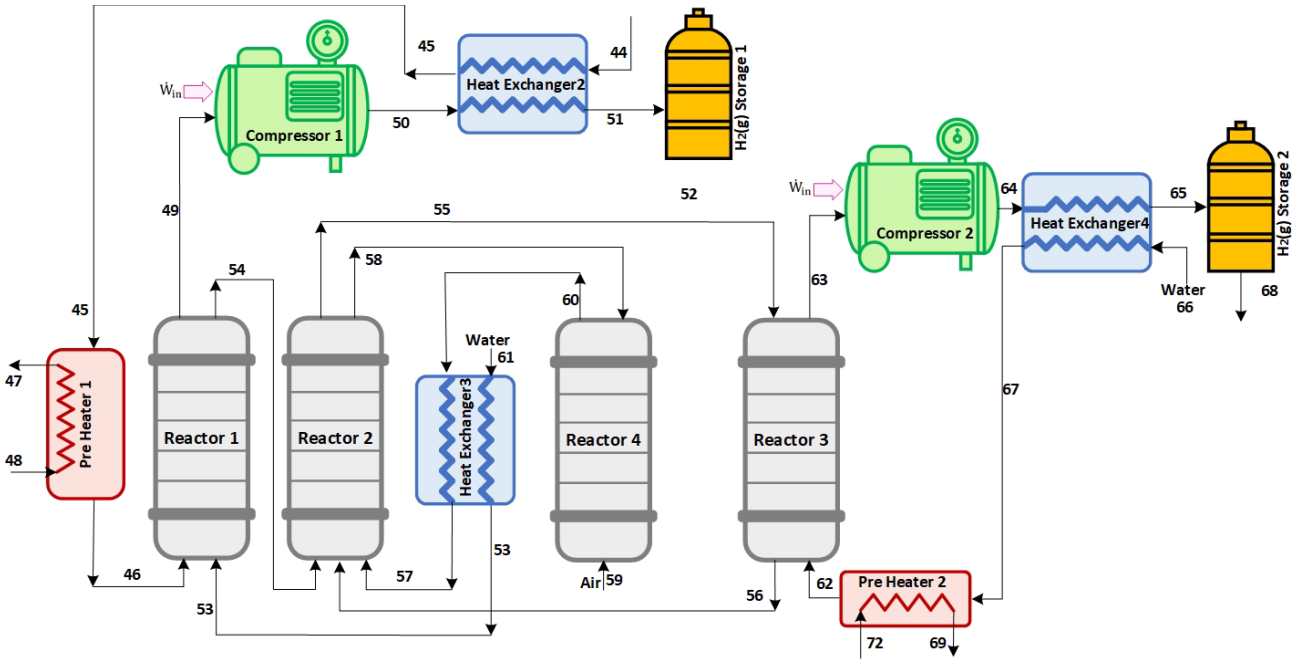

Figure 4.8 Schematic of hydrogen production of system 2

The following equations represent the balance of mass, energy, entropy, and exergy for all components related to the subsystem of system 2.

For compressor 1:

$$\dot{m}_{49} = \dot{m}_{50} \tag{4.187}$$

$$\dot{m}_{49}h_{49} + \dot{W}_{in} = \dot{m}_{50}h_{50} \tag{4.188}$$

$$\dot{S}_{gen} + \dot{m}_{49}s_{49} = \dot{m}_{50}s_{50} \tag{4.189}$$

$$\dot{m}_{49}ex_{49} + \dot{W}_{in} = \dot{E}x_{d} + \dot{m}_{50}ex_{50} \tag{4.190}$$

For compressor 2:

$$\dot{m}_{63} = \dot{m}_{64} \tag{4.191}$$

$$\dot{W}_{in} + \dot{m}_{63}h_{63} = \dot{m}_{64}h_{64} \tag{4.192}$$

$$\dot{S}_{gen} + \dot{m}_{63}s_{63} = \dot{m}_{64}s_{64} \tag{4.193}$$

$$\dot{W}_{in} + \dot{m}_{63}ex_{63} = \dot{E}x_{d} + \dot{m}_{64}ex_{64} \tag{4.194}$$

For heat exchanger 2:

$$\dot{m}_{44} + \dot{m}_{50} = \dot{m}_{51} + \dot{m}_{45} \tag{4.195}$$

$$\dot{m}_{44}h_{44} + \dot{m}_{50}h_{50} = \dot{m}_{51}h_{51} + \dot{m}_{45}h_{45} \tag{4.196}$$

$$\dot{S}_{gen} + \dot{m}_{44}s_{44} + \dot{m}_{50}s_{50} = \dot{m}_{51}s_{51} + \dot{m}_{45}s_{45} \tag{4.197}$$

$$\dot{m}_{44}ex_{44} + \dot{m}_{50}ex_{50} = \dot{m}_{51}ex_{51} + \dot{m}_{45}ex_{45} + \dot{E}x_{d} \tag{4.198}$$

For heat exchanger 3:

$$\dot{m}_{60} + \dot{m}_{61} = \dot{m}_{53} + \dot{m}_{57} \tag{4.199}$$

$$\dot{m}_{60}h_{60} + \dot{m}_{61}h_{61} = \dot{m}_{53}h_{53} + \dot{m}_{57}h_{57} \tag{4.200}$$

$$\dot{S}_{gen} + \dot{m}_{60}s_{60} + \dot{m}_{61}s_{61} = \dot{m}_{53}s_{53} + \dot{m}_{57}s_{57} \tag{4.201}$$

$$\dot{m}_{60}ex_{60} + \dot{m}_{61}ex_{61} = \dot{m}_{53}ex_{53} + \dot{m}_{57}ex_{57} + \dot{E}x_{d} \tag{4.202}$$

For heat exchanger 4:

$$\dot{m}_{64} + \dot{m}_{66} = \dot{m}_{65} + \dot{m}_{67} \tag{4.203}$$

$$\dot{m}_{64}h_{64} + \dot{m}_{66}h_{66} = \dot{m}_{65}h_{65} + \dot{m}_{67}h_{67} \tag{4.204}$$

$$\dot{S}_{gen} + \dot{m}_{64}s_{64} + \dot{m}_{66}s_{66} = \dot{m}_{65}s_{65} + \dot{m}_{67}s_{67} \tag{4.205}$$

$$\dot{m}_{64}ex_{64} + \dot{m}_{66}ex_{66} = \dot{m}_{65}ex_{65} + \dot{m}_{67}ex_{67} + \dot{E}x_{d} \tag{4.206}$$

For preheater 1:

$$\dot{m}_{45} + \dot{m}_{48} = \dot{m}_{46} + \dot{m}_{47} \tag{4.207}$$

$$\dot{m}_{45}h_{45} + \dot{m}_{48}h_{48} = \dot{m}_{46}h_{46} + \dot{m}_{47}h_{47} \tag{4.208}$$

$$\dot{S}_{gen} + \dot{m}_{45}s_{45} + \dot{m}_{48}s_{48} = \dot{m}_{46}s_{46} + \dot{m}_{47}s_{47} \tag{4.209}$$

$$\dot{m}_{45}ex_{45} + \dot{m}_{48}ex_{48} = \dot{m}_{46}ex_{46} + \dot{m}_{47}ex_{47} + \dot{E}x_{d} \tag{4.210}$$

For preheater 2:

$$\dot{m}_{67} + \dot{m}_{72} = \dot{m}_{69} + \dot{m}_{62} \tag{4.211}$$

$$\dot{m}_{67}h_{67} + \dot{m}_{72}h_{72} = \dot{m}_{69}h_{69} + \dot{m}_{62}h_{62} \quad (4.212)$$

$$\dot{S}_{gen} + \dot{m}_{67}s_{67} + \dot{m}_{72}s_{72} = \dot{m}_{69}s_{69} + \dot{m}_{62}s_{62} \quad (4.213)$$

$$\dot{m}_{67}ex_{67} + \dot{m}_{72}ex_{72} = \dot{m}_{69}ex_{69} + \dot{m}_{62}ex_{62} + \dot{E}x_d \quad (4.214)$$

For reactor 1, the physical balance equations are as follows:

$$\dot{m}_{53} + \dot{m}_{46} = \dot{m}_{54} + \dot{m}_{49} \quad (4.215)$$

$$\dot{m}_{46}h_{46} + \dot{m}_{53}h_{53} + \dot{Q}_{in} = \dot{m}_{54}h_{54} + \dot{m}_{49}h_{49} \quad (4.216)$$

$$\dot{S}_{gen} + \dot{m}_{46}s_{46} + \dot{m}_{53}s_{53} + \frac{\dot{Q}_{in}}{T_s} = \dot{m}_{54}s_{54} + \dot{m}_{49}s_{49} \quad (4.217)$$

$$\dot{m}_{46}ex_{46} + \dot{m}_{53}ex_{53} + \dot{Q}_{in}(1 - \frac{T_0}{T_s}) = \dot{m}_{54}ex_{54} + \dot{m}_{49}ex_{49} + \dot{E}x_d \quad (4.218)$$

For reactor 2, the physical balance equations are as follows:

$$\dot{m}_{54} + \dot{m}_{56} + \dot{m}_{57} = \dot{m}_{55} + \dot{m}_{58} + \dot{m}_{75} \quad (4.219)$$

$$\dot{m}_{54}h_{54} + \dot{m}_{56}h_{56} + \dot{m}_{57}h_{57} + \dot{Q}_{in} = \dot{m}_{55}h_{55} + \dot{m}_{58}h_{58} + \dot{m}_{75}h_{75} \quad (4.220)$$

$$\dot{S}_{gen} + \dot{m}_{54}s_{54} + \dot{m}_{56}s_{56} + \dot{m}_{57}s_{57} + \frac{\dot{Q}_{in}}{T_s} = \dot{m}_{55}s_{55} + \dot{m}_{58}s_{58} + \dot{m}_{75}s_{75} \quad (4.221)$$

$$\dot{m}_{54}ex_{54} + \dot{m}_{56}ex_{56} + \dot{m}_{57}ex_{57} + \dot{Q}_{in}(1 - \frac{T_0}{T_s}) = \dot{m}_{55}ex_{55} + \dot{m}_{58}ex_{58} + \dot{m}_{75}ex_{75} + \dot{E}x_d \quad (4.222)$$

For reactor 3, the physical balance equations are as follows:

$$\dot{m}_{62} + \dot{m}_{55} = \dot{m}_{63} + \dot{m}_{56} \quad (4.223)$$

$$\dot{m}_{62}h_{62} + \dot{m}_{55}h_{55} = \dot{m}_{63}h_{63} + \dot{m}_{56}h_{56} + \dot{Q}_{out} \quad (4.224)$$

$$\dot{S}_{gen} + \dot{m}_{62}s_{62} + \dot{m}_{55}s_{55} = \dot{m}_{63}s_{63} + \dot{m}_{56}s_{56} + \frac{\dot{Q}_{out}}{T_b} \quad (4.225)$$

$$\dot{m}_{62}ex_{62} + \dot{m}_{55}ex_{55} = \dot{m}_{63}ex_{63} + \dot{m}_{56}ex_{56} + \dot{Q}_{out}(1 - \frac{T_0}{T_s}) + \dot{E}x_d \quad (4.226)$$

For reactor 4, the physical balance equations are as follows:

$$\dot{m}_{58} + \dot{m}_{59} = \dot{m}_{60} \tag{4.227}$$

$$\dot{Q}_{in} + \dot{m}_{58}h_{58} + \dot{m}_{59}h_{59} = \dot{m}_{60}h_{60} \tag{4.228}$$

$$\dot{S}_{gen} + \dot{m}_{58}s_{58} + \dot{m}_{59}s_{59} + \frac{\dot{Q}_{in}}{T_s} = \dot{m}_{60}s_{60} \tag{4.229}$$

$$\dot{m}_{58}ex_{58} + \dot{m}_{59}ex_{59} + \dot{Q}_{in}(1 - \frac{T_0}{T_s}) = \dot{m}_{60}ex_{60} + \dot{E}x_d \tag{4.230}$$

4.2.4 Carbon Capturing Subsystem

As described earlier in the system description, carbon dioxide is captured using an absorber and stripper system based on an amine solution from the flue gas of a coal-fired power plant. Two heat exchangers have also been integrated to balance the heat transfer between the system components. After the carbon dioxide has been captured, the mixture of gas and water is passed through condenser 1 to separate the CO_2, and then it is compressed and stored in a CO_2 storage tank. Figure 4.9 depicts this unit in depth so that each component may be viewed separately.

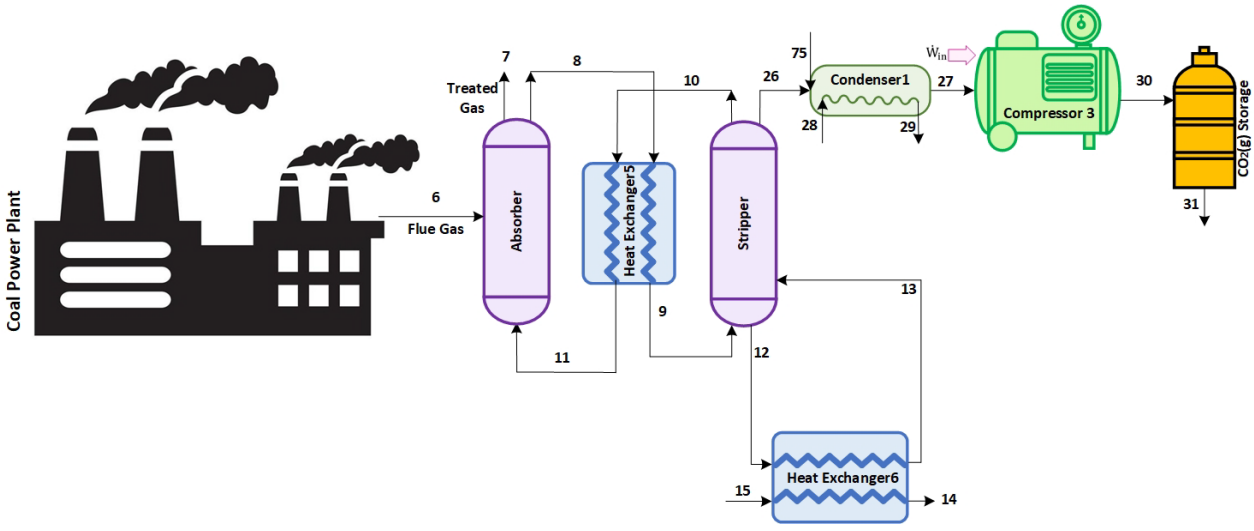

Figure 4.9 Schematic of carbon capturing from coal power plant of system 2

As with previous sections, determining the thermodynamic balance equations is essential. Consequently, the mass, energy, enthalpy, and exergy balance equations of the carbon capturing subsystem of system 2 have been determined and are displayed as follows:

For stripper:

$$\dot{m}_9 + \dot{m}_{13} = \dot{m}_{10} + \dot{m}_{12} + \dot{m}_{26} \tag{4.231}$$

$$\dot{Q}_{in} + \dot{m}_9 h_9 + \dot{m}_{13} h_{13} = \dot{m}_{10} h_{10} + \dot{m}_{12} h_{12} + \dot{m}_{26} h_{26} \tag{4.232}$$

$$\dot{S}_{gen} + \frac{\dot{Q}_{in}}{T_s} + \dot{m}_9 s + \dot{m}_{13} s_{13} = \dot{m}_{10} h_{10} + \dot{m}_{12} s_{12} + \dot{m}_{26} s_{26} \tag{4.233}$$

$$\dot{Q}_{in}\left(1 - \frac{T_0}{T_s}\right) + \dot{m}_9 ex_9 + \dot{m}_{13} ex_{13} = \dot{m}_{10} ex_{10} + \dot{m}_{12} ex_{12} + \dot{m}_{26} ex_{26} + \dot{E}x_d \tag{4.234}$$

For absorber:

$$\dot{m}_{11} + \dot{m}_6 = \dot{m}_8 + \dot{m}_7 \tag{4.235}$$

$$\dot{m}_{11} h_{11} + \dot{m}_6 h_6 = \dot{m}_8 h_8 + \dot{m}_7 h_7 + \dot{Q}_{out} \tag{4.236}$$

$$\dot{m}_{11} s_{11} + \dot{m}_6 s_6 = \dot{m}_8 s_8 + \dot{m}_7 s_7 + \frac{\dot{Q}_{out}}{T_b} \tag{4.237}$$

$$\dot{m}_{11} ex_{11} + \dot{m}_6 ex_6 = \dot{m}_8 ex_8 + \dot{m}_7 ex_7 + \dot{Q}_{out}(1 - \frac{T_0}{T_b}) + \dot{E}x_d \tag{4.238}$$

For compressor 3:

$$\dot{m}_{27} = \dot{m}_{30} \tag{4.239}$$

$$\dot{W}_{in} + \dot{m}_{27} h_{27} = \dot{m}_{30} h_{30} \tag{4.240}$$

$$\dot{S}_{gen} + \dot{m}_{27} s_{27} = \dot{m}_{30} s_{30} \tag{4.241}$$

$$\dot{W}_{in} + \dot{m}_{27} ex_{27} = \dot{E}x_d + \dot{m}_{30} ex_{30} \tag{4.242}$$

For heat exchanger 5:

$$\dot{m}_8 + \dot{m}_{10} = \dot{m}_{11} + \dot{m}_9 \tag{4.243}$$

$$\dot{m}_8 h_8 + \dot{m}_{10} h_{10} = \dot{m}_{11} h_{11} + \dot{m}_9 h_9 \tag{4.244}$$

$$\dot{S}_{gen} + \dot{m}_8 s_8 + \dot{m}_{10} s_{10} = \dot{m}_{11} s_{11} + \dot{m}_9 s_9 \tag{4.245}$$

$$\dot{m}_8 ex_8 + \dot{m}_{10} ex_{10} = \dot{m}_{11} ex_{11} + \dot{m}_9 ex_9 + \dot{E}x_d \tag{4.246}$$

For heat exchanger 6:

$$\dot{m}_{12} + \dot{m}_{15} = \dot{m}_{13} + \dot{m}_{14} \tag{4.247}$$

$$\dot{m}_{12}h_{12} + \dot{m}_{15}h_{15} = \dot{m}_{13}h_{13} + \dot{m}_{14}h_{14} \tag{4.248}$$

$$\dot{S}_{gen} + \dot{m}_{12}s_{12} + \dot{m}_{15}s_{15} = \dot{m}_{13}s_{13} + \dot{m}_{14}s_{14} \tag{4.249}$$

$$\dot{m}_{12}ex_{12} + \dot{m}_{15}ex_{15} = \dot{m}_{13}ex_{13} + \dot{m}_{14}ex_{14} + \dot{E}x_d \tag{4.250}$$

For condenser 1:

$$\dot{m}_{26} + \dot{m}_{28} = \dot{m}_{27} + \dot{m}_{29} \tag{4.251}$$

$$\dot{m}_{26}h_{26} + \dot{m}_{28}h_{28} = \dot{m}_{27}h_{27} + \dot{m}_{29}h_{29} + \dot{Q}_{out} \tag{4.252}$$

$$\dot{m}_{26}s_{26} + \dot{m}_{28}s_{28} = \dot{m}_{27}s_{27} + \dot{m}_{29}s_{29} + \frac{\dot{Q}_{out}}{T_b} \tag{4.253}$$

$$\dot{m}_{26}ex_{26} + \dot{m}_{28}ex_{28} = \dot{m}_{27}ex_{27} + \dot{m}_{29}ex_{29} + \dot{Q}_{out}(1 - \frac{T_0}{T_b}) + \dot{E}x_d \tag{4.254}$$

4.2.5 Methane Production Subsystem

In this subsystem, as shown in Figure 4.10, methane production occurs in Reactor 5, where hydrogen and carbon dioxide are converted into methane via the Sabatier reaction. Within this catalytic reaction, hydrogen and carbon dioxide are combined under meticulously regulated conditions, leading to the formation of methane and water.

Prior to this reaction, the gases are mixed and preheated, necessitating the presence of a gas mixer, preheater, and Heat Exchanger 8 positioned before Reactor 5 to ready the gases for the forthcoming reaction.

This approach not only enables carbon dioxide sequestration but also provides a sustainable means to produce methane, an essential energy vector. Following the reaction, the resultant products are processed through Condenser 3 and a separator to isolate methane from other byproducts, after which the methane is stored for subsequent utilization.

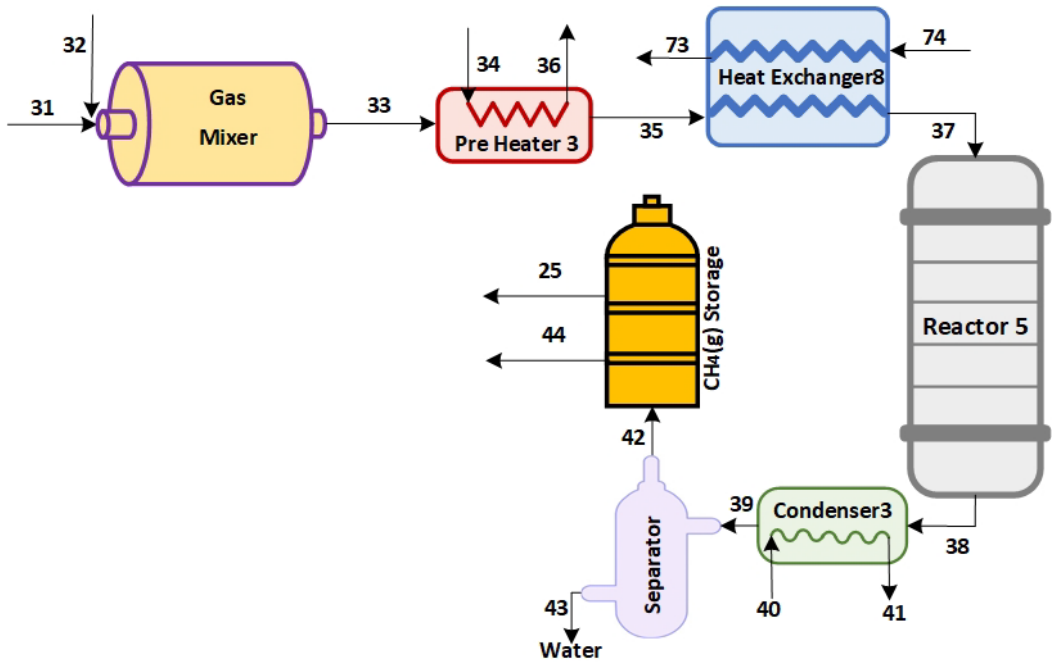

Figure 4.10 Schematic of methane production subsystem of system 2

Similar to earlier sections, establishing the thermodynamic balance equations remains crucial. As a result, the mass, energy, enthalpy, and exergy balance equations for the methane production in system 2 have been ascertained and presented below:

For gas mixer:

$$\dot{m}_{31} + \dot{m}_{32} = \dot{m}_{33} \tag{4.255}$$

$$\dot{m}_{31}h_{31} + \dot{m}_{32}h_{32} = \dot{m}_{33}h_{33} \tag{4.256}$$

$$\dot{S}_{gen} + \dot{m}_{31}s_{31} + \dot{m}_{32}s_{32} = \dot{m}_{33}s_{33} \tag{4.257}$$

$$\dot{m}_{31}ex_{31} + \dot{m}_{32}ex_{32} = \dot{m}_{33}ex_{33} + \dot{E}x_{d} \tag{4.258}$$

For preheater 3:

$$\dot{m}_{33} + \dot{m}_{34} = \dot{m}_{35} + \dot{m}_{36} \tag{4.259}$$

$$\dot{m}_{33}h_{33} + \dot{m}_{34}h_{34} = \dot{m}_{35}h_{35} + \dot{m}_{36}h_{36} \tag{4.260}$$

$$\dot{S}_{gen} + \dot{m}_{33}s_{33} + \dot{m}_{34}s_{34} = \dot{m}_{35}s_{35} + \dot{m}_{36}s_{36} \tag{4.261}$$

$$\dot{m}_{33}ex_{33} + \dot{m}_{34}ex_{34} = \dot{m}_{35}ex_{35} + \dot{m}_{36}ex_{36} + \dot{E}x_{d} \tag{4.262}$$

For heat exchanger 8:

$$\dot{m}_{35} + \dot{m}_{74} = \dot{m}_{37} + \dot{m}_{73} \tag{4.263}$$

$$\dot{m}_{35}h_{35} + \dot{m}_{74}h_{74} = \dot{m}_{37}h_{37} + \dot{m}_{73}h_{73} \tag{4.264}$$

$$\dot{S}_{gen} + \dot{m}_{35}s_{35} + \dot{m}_{74}s_{74} = \dot{m}_{37}s_{37} + \dot{m}_{73}s_{73} \tag{4.265}$$

$$\dot{m}_{35}ex_{35} + \dot{m}_{74}ex_{74} = \dot{m}_{37}ex_{37} + \dot{m}_{73}ex_{73} + \dot{E}x_d \tag{4.266}$$

The physical balance equations for reactor 5 are as follows:

$$\dot{m}_{37} = \dot{m}_{38} \tag{4.267}$$

$$\dot{m}_{37}h_{37} = \dot{m}_{38}h_{38} + \dot{Q}_{out} \tag{4.268}$$

$$\dot{S}_{gen} + \dot{m}_{37}s_{37} = \dot{m}_{38}s_{38} + \frac{\dot{Q}_{out}}{T_b} \tag{4.269}$$

$$\dot{m}_{37}ex_{37} = \dot{m}_{38}ex_{38} + \dot{Q}_{out}(1 - \frac{T_0}{T_s}) + \dot{E}x_d \tag{4.270}$$

The chemical balance equations for reactor 5 are as follows:

$$\dot{n}_{H2} + \dot{n}_{CO2} = \dot{n}_{CH4} + \dot{n}_{H2O} \tag{4.271}$$

$$\dot{n}_{H2}(\overline{h_f^0} + \bar{h} - \overline{h^0} - P\bar{v})_{H2} + \dot{n}_{CO2}(\overline{h_f^0} + \bar{h} - \overline{h^0} - P\bar{v})_{CO2} = \dot{n}_{H2O}(\overline{h_f^0} + \bar{h} - \overline{h^0} - P\bar{v})_{H2O} + \dot{n}_{CH4}(\overline{h_f^0} + \bar{h} - \overline{h^0} - P\bar{v})_{CH4} + \dot{Q}_{out} \tag{4.272}$$

$$\dot{S}_{gen} + \dot{n}_{CO2}(\overline{s_f^0} + \bar{s} - \overline{s^0})_{CO2} + \dot{n}_{H2}(\overline{s_f^0} + \bar{s} - \overline{s^0})_{H2} = \dot{n}_{CH4}(\overline{s_f^0} + \bar{s} - \overline{s^0})_{CH4} + \dot{n}_{H2O}(\overline{s_f^0} + \bar{s} - \overline{s^0})_{H2O} + \frac{\dot{Q}_{out}}{T_b} \tag{4.273}$$

$$\dot{n}_{H2}(\overline{ex_f^0} + \overline{ex} - \overline{ex^0} - P\bar{v})_{H2} + \dot{n}_{CO2}(\overline{ex_f^0} + \overline{ex} - \overline{ex^0} - P\bar{v})_{CO2} = \dot{n}_{CH4}(\overline{ex_f^0} + \overline{ex} - \overline{ex^0} - P\bar{v})_{CH4} + \dot{n}_{H2O}(\overline{ex_f^0} + \overline{ex} - \overline{ex^0} - P\bar{v})_{H2O} + \dot{E}x_d + \dot{Q}_{out}(1 - \frac{T_0}{T_b}) \tag{4.274}$$

For condenser 3:

$$\dot{m}_{38} + \dot{m}_{40} = \dot{m}_{39} + \dot{m}_{41} \tag{4.275}$$

$$\dot{m}_{38}h_{38} + \dot{m}_{40}h_{40} = \dot{m}_{39}h_{39} + \dot{m}_{41}h_{41} + \dot{Q}_{out} \quad (4.276)$$

$$\dot{m}_{38}s_{38} + \dot{m}_{40}s_{40} = \dot{m}_{39}s_{39} + \dot{m}_{41}s_{41} + \frac{\dot{Q}_{out}}{T_b} \quad (4.277)$$

$$\dot{m}_{38}ex_{38} + \dot{m}_{40}ex_{40} = \dot{m}_{39}ex_{39} + \dot{m}_{41}ex_{41} + \dot{Q}_{out}(1 - \frac{T_0}{T_b}) + \dot{E}x_d \quad (4.278)$$

For separator:

$$\dot{m}_{39} = \dot{m}_{42} + \dot{m}_{43} \quad (4.279)$$

$$\dot{m}_{39}h_{39} = \dot{m}_{42}h_{42} + \dot{m}_{43}h_{43} \quad (4.280)$$

$$\dot{m}_{39}s_{39} + \dot{S}_{gen} = \dot{m}_{42}s_{42} + \dot{m}_{43}s_{43} \quad (4.281)$$

$$\dot{m}_{39}ex_{39} = \dot{m}_{42}ex_{42} + \dot{m}_{43}ex_{43} + \dot{E}x_d \quad (4.282)$$

4.2.6 Modelling and Analysis

In alignment with the system 2 design, it was subjected to an in-depth assessment encompassing thermodynamic analysis and energy and exergy efficiency measurement. After establishing the balance equations for every system segment, this framework simulated the system using EES and Aspen Plus tools.

All subsystems of system 2, except the solar thermal energy unit, are simulated in Aspen Plus and demonstrated in Figure 4.11.

This simulation process encompassed the examination of efficiency, exergy destruction, and other thermodynamic attributes pertinent to each discrete element and the collective system. Calculations were performed and subsequently analyzed comparatively.

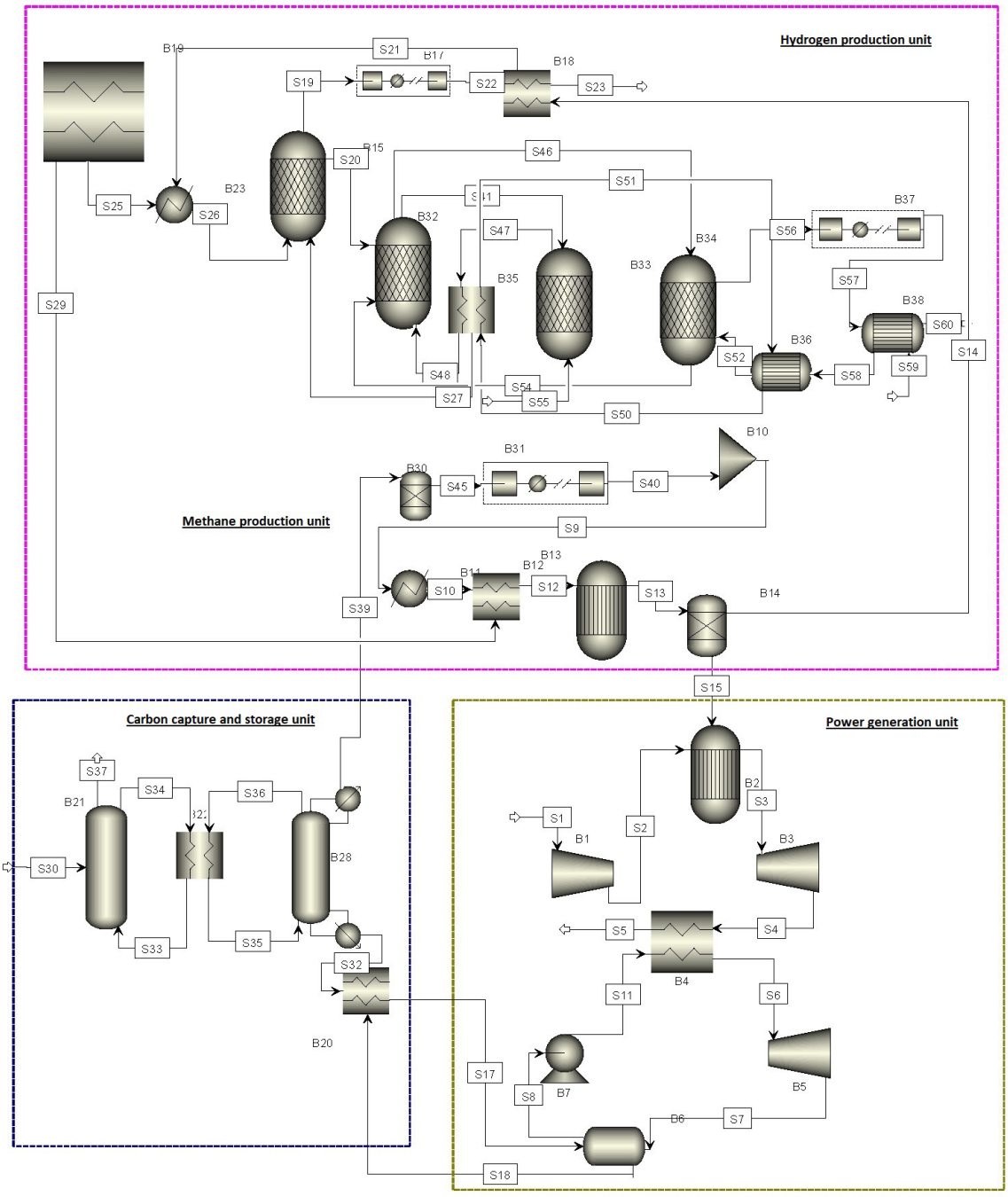

Figure 4.11 Aspen Plus simulation for multiple subsystems of system 2

Based on the balance equations, component interactions, assumptions, and simulations of the initial system's elements using Aspen Plus, thermodynamic parameters, including mass flow rate, pressure, temperature, specific enthalpy, specific entropy, and specific exergy of all state points within system 1 were determined via EES software and presented in Table 4.2.

Table 4.2 Thermodynamic properties of all state points of system 2

State Point	Working Fluid	Mass flow Rate (kg/s)	Pressure (kPa)	Temperature (℃)	Specific Enthalpy (kJ/kg)	Specific Entropy (kJ/kg.K)	Specific exergy (kJ/kg)
1	Molten salt	0.6	101	650	5213	15.371	3854
2	Molten salt	0.6	101	632	5189	14.724	3778
3	Molten salt	0.6	112	601	4813	11.976	2857
4	Molten salt	0.6	106	334	2511	6.895	1511
5	Molten salt	0.6	101	330	2172	4.782	1186
6	Flue Gas	50	101	250	103.5	7.343	454.6
7	Treated Gas	104.5	150	43.5	314.4	35.17	102.6
8	CO_2+MEA+H_2O	138.6	101	100	206.3	5.721	92.3
9	CO_2+MEA+H_2O	138.6	101	25	106.5	1.552	0
10	MEA+H_2O	121.2	101	25	87.3	1.164	0
11	MEA+H_2O	121.2	101	100	325.1	4.342	65.8
12	H_2O	1	101	50	114.8	0.542	56.4
13	H_2O	1	101	150	883.6	5.69	258.7
14	H_2O	1	101	50	114.8	0.542	56.4
15	H_2O	1	101	150	883.6	5.69	258.7
16	H_2O	3	150	20	236.4	0.422	44.9
17	Saturated water (l)	3	10	20	171.8	0.649	23.5
18	H_2O	3	5500	50	201.9	0.956	211.2
19	H_2O	3	5500	500	3400	6.55	1400
20	Air	10	101	25	298.6	5.697	0
21	Air	10	880	500	1125	5.285	211.8
22	Air	10	890	958	2457	6.596	851.9
23	Air	10	101	525	930.5	7.696	289.1
24	Exhaust gases	10	101	177	452.3	7.113	182.3
25	CH_4	0.001	430	85	266.7	2.138	227.4
26	CO_2	37.87	101	340	4117	2.955	207.2
27	CO_2	40	101	80	3414	1.153	133.3
28	H_2O	1	101	25	105.5	0.367	0
29	H_2O	1	101	110	562.1	3.37	183.1
30	CO_2	40	500	90	4520	2.637	216.5
31	CO_2	0.006	430	85	4298	2.165	120.3
32	H_2	0.001	430	85	4835	55.14	613.8
33	CO_2+H_2	0.007	430	85	1184	6.261	NA
34	H_2O	1	101	200	927.2	6.133	382
35	CO_2+H_2	0.007	430	267	1215	9.436	NA
36	H_2O	1	101	45	109.2	0.452	27.8
37	CO_2+H_2	0.007	430	400	1206	8.453	NA
38	CH_4+H_2O	0.007	430	270	2317	5.431	1094
39	CH_4+H_2O	0.007	430	145	1891	4.679	975.7

40	H_2O	1	101	25	105	0.367	0
41	H_2O	1	101	110	562.1	3.37	183.1
42	CH_4	0.0048	430	85	266.7	2.138	227.4
43	H_2O	0.005	430	85	231.5	1.366	163
44	CH_4	0.001	430	85	83.35	1.069	113.7
45	CH_4	0.001	430	256	369.8	3.745	327.4
46	CH_4	0.001	430	443	734.4	5.371	810.6
47	H_2O	1	101	110	562.1	3.37	183.1
48	H_2O	1	101	324	1218	7.754	522.1
49	H_2	0.0008	101	110	4886	60.423	697.3
50	H_2	0.0008	630	223	8517	44.438	2547
51	H_2	0.0008	630	85	8410	41.612	2503
52	H_2	0.0004	430	85	4835	55.14	613.8
53	H_2O	1	101	450	2082	8.64	809.4
54	CO	2.13	900	50	421.7	7.474	561.4
55	Fe	1.652	101	500	5597	3.346	3539
56	Fe_3O_4	2.289	101	498	2691	3.928	2588
57	Fe_3O_4	2.289	630	298	2934	3.114	2802
58	Fe	1.652	101	500	5597	3.346	3539
59	Air	2	101	25	298.6	5.697	256.8
60	Fe_3O_4	2.315	630	912	3894	7.484	2842
61	H_2O	1	101	25	105	0.367	0
62	H_2O	1	101	550	2557	8.926	1142
63	H_2	0.0032	101	110	4914	67.214	1043
64	H_2	0.0032	630	223	8546	51.237	2569
65	H_2	0.0032	630	85	8438	48.412	2514
66	H_2O	1	101	25	105	0.367	0
67	H_2O	1	101	110	862	3.37	183.1
68	H_2	0.0006	430	85	4835	55.14	613.8
69	H_2O	1	101	45	109.2	0.452	27.8
70	H_2O	2	101	45	218.4	0.904	55.6
71	H_2O	2	101	200	1854.4	1.808	764
72	H_2O	1	101	200	927.2	6.133	382
73	H_2O	1	101	25	105	0.367	0
74	H_2O	1	101	440	1987	8.054	788
75	CO_2	2.13	101	500	4325	3.15	246.1

The total exergy destruction rate includes the exergy rate of the total heating rate and the subtraction of exergy balance equations of two different relevant components. The following equations describe the calculation of the exergy destruction rate, specific exergy, and the exergy rate of the total solar heating rate, respectively.

$$\dot{E}x_d = \sum \dot{E}x_{\dot{Q}_{total}} + \sum \dot{W}_{total} + \sum \dot{m}_i ex_i - \sum \dot{m}_j ex_j \quad (4.283)$$

$$ex_i = ex_{phys,i} + ex_{chem,i} = \sum_i [(h_i - h_o) - (s_i - s_o)] + \sum_i (\mu_i^* - \mu_{i,o}) \quad (4.284)$$

$$\dot{E}x_{\dot{Q}_{total}} = \dot{Q}_{total}\left(1 - \frac{T_0}{T_{s,i}}\right) \quad (4.285)$$

The energy and exergy efficiencies of the hydrogen production subsystem can be calculated by using the following equations:

$$\eta_{H_2} = \frac{\dot{n}_{H_2} \times M_{H_2}}{\dot{Q}_{in}} \quad (4.286)$$

$$\psi_{H_2} = \frac{\dot{n}_{H_2} \times \dot{E}x_{H_2}}{\dot{Q}_{in}} \quad (4.287)$$

The energy and exergy efficiencies of the hydrogen production subsystem can be calculated by using the following equations:

$$\eta_{CH_4} = \frac{\dot{n}_{CH_4} \times M_{CH_4}}{\dot{Q}_{in}} \quad (4.288)$$

$$\psi_{CH_4} = \frac{\dot{n}_{CH_4} \times \dot{E}x_{CH_4}}{\dot{Q}_{in}} \quad (4.289)$$

The overall system efficiencies for energy and exergy are calculated as shown:

$$\eta_{Overall} = \frac{(\dot{W}_{total}) + (\dot{m}_{51} \times LHV_{H_2}) + (\dot{m}_{65} \times LHV_{H_2}) + ((\dot{m}_{25} \times LHV_{CH_4})}{\dot{Q}_{in,total}} \quad (4.290)$$

$$\psi_{Overall} = \frac{(\dot{W}_{net}) + \dot{E}x_{H_2,total} + \dot{E}x_{CH_4,total}}{\dot{E}x_{\dot{Q}_{in,total}}} \quad (4.291)$$

4.3 System 3

This part focuses on the investigation and modelling of system 3. A thorough exposition is presented regarding the thermodynamic assessment of every component within the system, along with the relevant simulation parameters. This study investigates the thermodynamic equilibrium equations for all constituents inside the system using Aspen Plus simulation and EES software. Furthermore, this study examines the characteristics of individual state

points and assesses the system's overall performance, considering its interconnected subsystems.

4.3.1 Carbon Capturing Subsystem

Since steel manufacturing is a substantial source of carbon dioxide emissions, it is essential to comprehend and enhance these systems by using comprehensive modelling and analyzing techniques. The analysis not only offers a valuable understanding of the underlying thermodynamic interactions but also allows for the optimization of process parameters to improve the overall efficiency and sustainability of the system. Figure 4.12 shows a part-by-part view of this unit so that this part can be examined in detail.

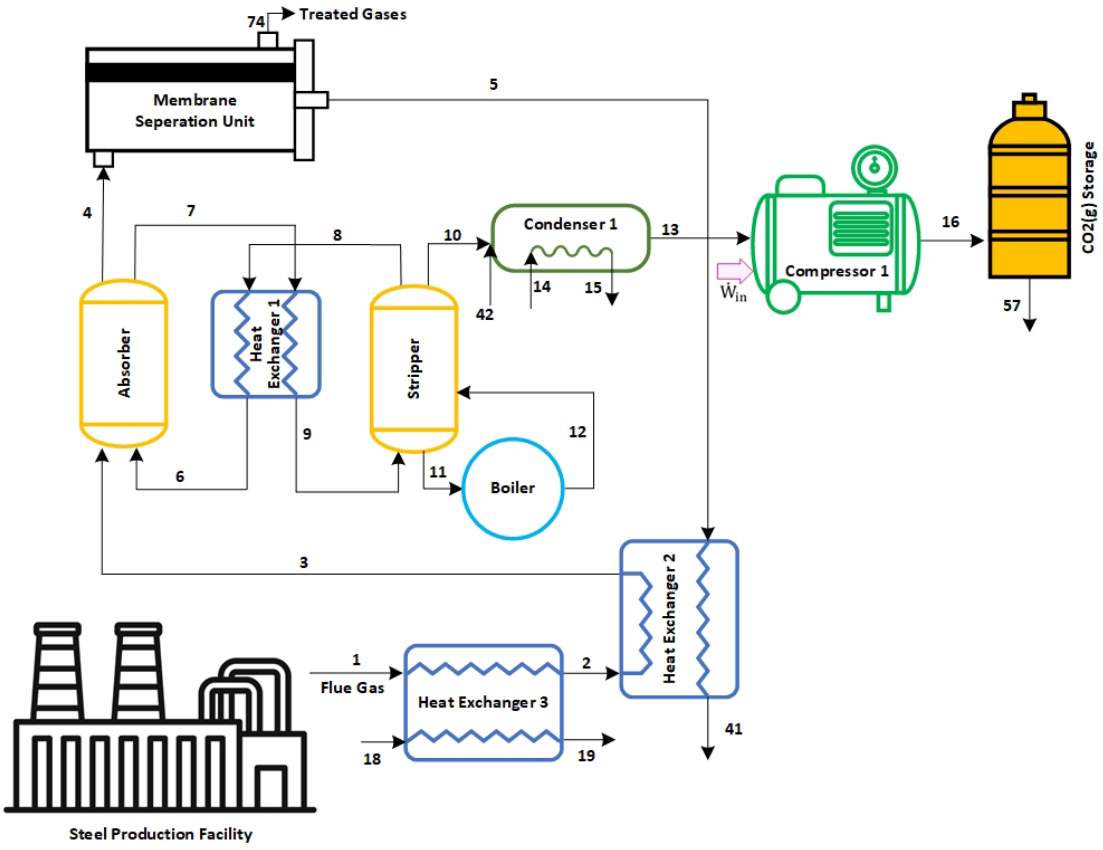

Figure 4.12 Schematic of carbon capturing from steel production facility of system 3

As with previous sections, determining the thermodynamic balance equations is essential. Consequently, the mass, energy, enthalpy, and exergy balance equations of the carbon capturing subsystem of system 3 have been determined and are displayed as follows: For stripper:

$$\dot{m}_9 + \dot{m}_{12} = \dot{m}_{10} + \dot{m}_{11} + \dot{m}_8 \tag{4.292}$$

$$\dot{Q}_{in} + \dot{m}_9 h_9 + \dot{m}_{12} h_{12} = \dot{m}_{10} h_{10} + \dot{m}_{11} h_{11} + \dot{m}_8 h_8 \tag{4.293}$$

$$\dot{S}_{gen} + \frac{\dot{Q}_{in}}{T_s} + \dot{m}_9 s + \dot{m}_{12} s_{12} = \dot{m}_{10} h_{10} + \dot{m}_{11} s_{11} + \dot{m}_8 s_8 \tag{4.294}$$

$$\dot{Q}_{in}\left(1 - \frac{T_0}{T_s}\right) + \dot{m}_9 ex_9 + \dot{m}_{12} ex_{12} = \dot{m}_{10} ex_{10} + \dot{m}_{11} ex_{11} + \dot{m}_8 ex_8 + \dot{E}x_d \tag{4.295}$$

For absorber:

$$\dot{m}_3 + \dot{m}_6 = \dot{m}_4 + \dot{m}_7 \tag{4.296}$$

$$\dot{m}_3 h_3 + \dot{m}_6 h_6 = \dot{m}_4 h_4 + \dot{m}_7 h_7 + \dot{Q}_{out} \tag{4.297}$$

$$\dot{m}_3 s_3 + \dot{m}_6 s_6 = \dot{m}_4 s_4 + \dot{m}_7 s_7 + \frac{\dot{Q}_{out}}{T_b} \tag{4.298}$$

$$\dot{m}_3 ex_3 + \dot{m}_6 ex_6 = \dot{m}_4 ex_4 + \dot{m}_7 ex_7 + \dot{Q}_{out}(1 - \frac{T_0}{T_b}) + \dot{E}x_d \tag{4.299}$$

For heat exchanger 1:

$$\dot{m}_7 + \dot{m}_8 = \dot{m}_6 + \dot{m}_9 \tag{4.300}$$

$$\dot{m}_7 h_7 + \dot{m}_8 h_8 = \dot{m}_6 h_6 + \dot{m}_9 h_9 \tag{4.301}$$

$$\dot{m}_7 s_7 + \dot{m}_8 s_8 = \dot{m}_6 s_6 + \dot{m}_9 s_9 \tag{4.302}$$

$$\dot{m}_7 ex_7 + \dot{m}_8 ex_8 = \dot{m}_6 ex_6 + \dot{m}_9 ex_9 + \dot{E}x_d \tag{4.303}$$

For boiler:

$$\dot{m}_{11} = \dot{m}_{12} \tag{4.304}$$

$$\dot{m}_{11} h_{11} + \dot{Q}_{in} = \dot{m}_{12} h_{12} \tag{4.305}$$

$$\dot{m}_{11} s_{11} + \frac{\dot{Q}_{in}}{T_s} = \dot{m}_{12} s_{12} \tag{4.306}$$

$$\dot{m}_{11} ex_{11} + \dot{Q}_{in}(1 - \frac{T_0}{T_s}) = \dot{m}_{12} ex_{12} + \dot{E}x_d \tag{4.307}$$

For condenser 1:

$$\dot{m}_{10} + \dot{m}_{14} = \dot{m}_{13} + \dot{m}_{15} \tag{4.308}$$

$$\dot{m}_{10}h_{10} + \dot{m}_{14}h_{14} = \dot{m}_{13}h_{13} + \dot{m}_{15}h_{15} + \dot{Q}_{out} \tag{4.309}$$

$$\dot{m}_{10}s_{10} + \dot{m}_{14}s_{14} = \dot{m}_{13}s_{13} + \dot{m}_{15}s_{15} + \frac{\dot{Q}_{out}}{T_b} \tag{4.310}$$

$$\dot{m}_{10}ex_{10} + \dot{m}_{14}ex_{14} = \dot{m}_{13}ex_{13} + \dot{m}_{15}ex_{15} + \dot{Q}_{out}(1 - \frac{T_0}{T_b}) + \dot{E}x_d \tag{4.311}$$

For compressor 1:

$$\dot{m}_{13} = \dot{m}_{16} \tag{4.312}$$

$$\dot{W}_{in} + \dot{m}_{13}h_{13} = \dot{m}_{16}h_{16} \tag{4.313}$$

$$\dot{S}_{gen} + \dot{m}_{13}s_{13} = \dot{m}_{16}s_{16} \tag{4.314}$$

$$\dot{W}_{in} + \dot{m}_{13}ex_{13} = \dot{E}x_d + \dot{m}_{16}ex_{16} \tag{4.315}$$

For heat exchanger 2:

$$\dot{m}_2 + \dot{m}_5 = \dot{m}_3 + \dot{m}_{41} \tag{4.316}$$

$$\dot{m}_2h_2 + \dot{m}_5h_5 = \dot{m}_3h_3 + \dot{m}_{41}h_{41} \tag{4.317}$$

$$\dot{S}_{gen} + \dot{m}_2s_2 + \dot{m}_5s_5 = \dot{m}_3s_3 + \dot{m}_{41}s_{41} \tag{4.318}$$

$$\dot{m}_2ex_2 + \dot{m}_5ex_5 = \dot{m}_3ex_3 + \dot{m}_{41}ex_{41} + \dot{E}x_d \tag{4.319}$$

For heat exchanger 3:

$$\dot{m}_1 + \dot{m}_{18} = \dot{m}_2 + \dot{m}_{19} \tag{4.320}$$

$$\dot{m}_1h_1 + \dot{m}_{18}h_{18} = \dot{m}_2h_2 + \dot{m}_{19}h_{19} \tag{4.321}$$

$$\dot{S}_{gen} + \dot{m}_1s_1 + \dot{m}_{18}s_{18} = \dot{m}_2s_2 + \dot{m}_{19}s_{19} \tag{4.322}$$

$$\dot{m}_1ex_1 + \dot{m}_{18}ex_{18} = \dot{m}_2ex_2 + \dot{m}_{19}ex_{19} + \dot{E}x_d \tag{4.323}$$

For membrane separation unit:

$$\dot{m}_4 = \dot{m}_5 + \dot{m}_{74} \tag{4.324}$$

$$\dot{m}_4 h_4 + \dot{Q}_{in} = \dot{m}_5 h_5 + \dot{m}_{74} h_{74} \tag{4.325}$$

$$\dot{m}_4 s_4 + \frac{\dot{Q}_{in}}{T_s} = \dot{m}_5 s_5 + \dot{m}_{74} s_{74} \tag{4.326}$$

$$\dot{m}_4 ex_4 + \dot{Q}_{in}\left(1 - \frac{T_0}{T_s}\right) = \dot{m}_5 ex_5 + \dot{m}_{74} ex_{74} + \dot{E}x_d \tag{4.327}$$

4.3.2 Power Generation Subsystem

Figure 4.13 offers a visual depiction that demonstrates the operational dynamics of the power generation mechanism in system 3, which is achieved by integrating three distinct cycles.

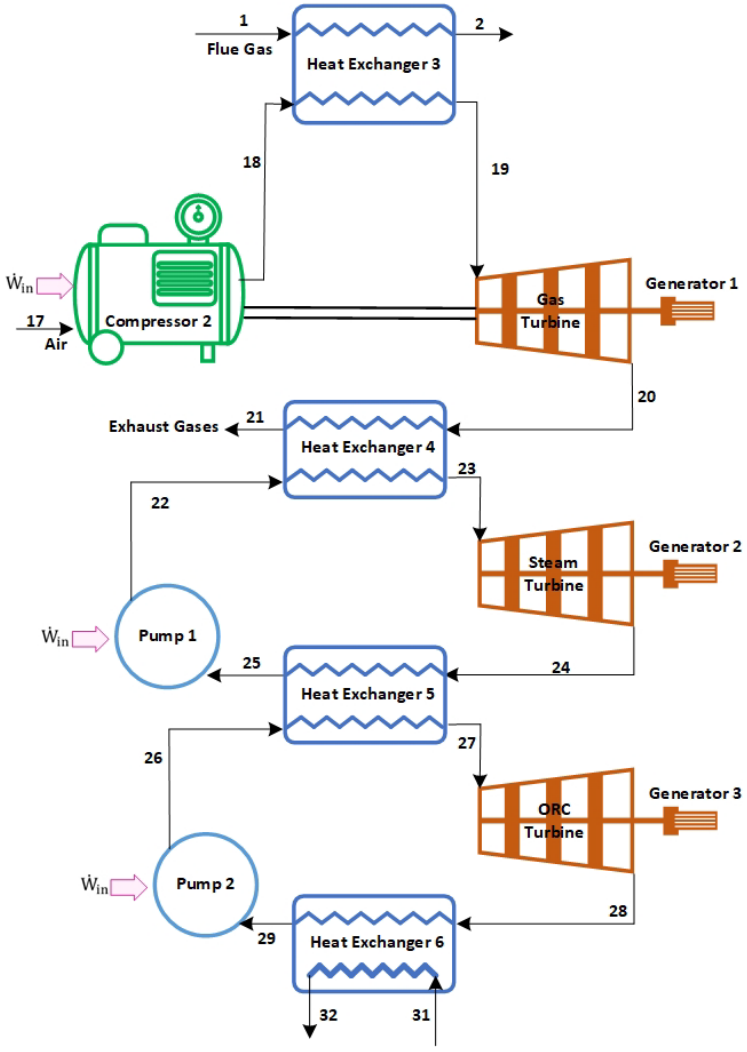

Figure 4.13 Schematic of power generation subsystem of system 3

The subsequent analysis elucidates the rationale behind transitioning from previous power generation systems to this new version, incorporating the Organic Rankine Cycle and seawater desalination to produce fresh water. As with previous sections, the following mass, energy, enthalpy, and exergy balance equations of the power generation subsystem of system 3 are determined to analyze the subsystem thermodynamically.

For pump 1:

$$\dot{m}_{25} = \dot{m}_{22} \tag{4.328}$$

$$\dot{m}_{25}h_{25} + \dot{W}_{in} = \dot{m}_{22}h_{22} \tag{4.329}$$

$$\dot{S}_{gen} + \dot{m}_{25}s_{25} = \dot{m}_{22}s_{22} \tag{4.330}$$

$$\dot{m}_{25}ex_{25} + \dot{W}_{in} = \dot{E}x_{d} + \dot{m}_{22}ex_{22} \tag{4.331}$$

For pump 2:

$$\dot{m}_{29} = \dot{m}_{26} \tag{4.332}$$

$$\dot{m}_{29}h_{29} + \dot{W}_{in} = \dot{m}_{26}h_{26} \tag{4.333}$$

$$\dot{S}_{gen} + \dot{m}_{29}s_{29} = \dot{m}_{26}s_{26} \tag{4.334}$$

$$\dot{m}_{29}ex_{29} + \dot{W}_{in} = \dot{E}x_{d} + \dot{m}_{26}ex_{26} \tag{4.335}$$

For heat exchanger 3:

$$\dot{m}_{1} + \dot{m}_{18} = \dot{m}_{2} + \dot{m}_{19} \tag{4.336}$$

$$\dot{m}_{1}h_{1} + \dot{m}_{18}h_{18} = \dot{m}_{2}h_{2} + \dot{m}_{19}h_{19} \tag{4.337}$$

$$\dot{S}_{gen} + \dot{m}_{1}s_{1} + \dot{m}_{18}s_{18} = \dot{m}_{2}s_{2} + \dot{m}_{19}s_{19} \tag{4.338}$$

$$\dot{m}_{1}ex_{1} + \dot{m}_{18}ex_{18} = \dot{m}_{2}ex_{2} + \dot{m}_{19}ex_{19} + \dot{E}x_{d} \tag{4.339}$$

For heat exchanger 4:

$$\dot{m}_{20} + \dot{m}_{22} = \dot{m}_{21} + \dot{m}_{23} \tag{4.340}$$

$$\dot{m}_{20}h_{20} + \dot{m}_{22}h_{22} = \dot{m}_{21}h_{21} + \dot{m}_{23}h_{23} \tag{4.341}$$

$$\dot{S}_{gen} + \dot{m}_{20}s_{20} + \dot{m}_{22}s_{22} = \dot{m}_{21}s_{21} + \dot{m}_{23}s_{23} \quad (4.342)$$

$$\dot{m}_{20}ex_{20} + \dot{m}_{22}ex_{22} = \dot{m}_{21}ex_{21} + \dot{m}_{23}ex_{23} + \dot{E}x_d \quad (4.343)$$

For heat exchanger 5:

$$\dot{m}_{24} + \dot{m}_{26} = \dot{m}_{25} + \dot{m}_{27} \quad (4.344)$$

$$\dot{m}_{24}h_{24} + \dot{m}_{26}h_{26} = \dot{m}_{25}h_{25} + \dot{m}_{27}h_{27} \quad (4.345)$$

$$\dot{S}_{gen} + \dot{m}_{24}s_{24} + \dot{m}_{26}s_{26} = \dot{m}_{25}s_{25} + \dot{m}_{27}s_{27} \quad (4.346)$$

$$\dot{m}_{24}ex_{24} + \dot{m}_{26}ex_{26} = \dot{m}_{25}ex_{25} + \dot{m}_{27}ex_{27} + \dot{E}x_d \quad (4.347)$$

For heat exchanger 6:

$$\dot{m}_{28} + \dot{m}_{31} = \dot{m}_{29} + \dot{m}_{32} \quad (4.348)$$

$$\dot{m}_{28}h_{28} + \dot{m}_{31}h_{31} = \dot{m}_{29}h_{29} + \dot{m}_{32}h_{32} \quad (4.349)$$

$$\dot{S}_{gen} + \dot{m}_{28}s_{28} + \dot{m}_{31}s_{31} = \dot{m}_{29}s_{29} + \dot{m}_{32}s_{32} \quad (4.350)$$

$$\dot{m}_{28}ex_{28} + \dot{m}_{31}ex_{31} = \dot{m}_{29}ex_{29} + \dot{m}_{32}ex_{32} + \dot{E}x_d \quad (4.351)$$

For steam turbine:

$$\dot{m}_{23} = \dot{m}_{24} \quad (4.352)$$

$$\dot{m}_{23}h_{23} = \dot{m}_{24}h_{24} + \dot{W}_{out} \quad (4.353)$$

$$\dot{S}_{gen} + \dot{m}_{23}s_{23} = \dot{m}_{24}s_{24} \quad (4.354)$$

$$\dot{m}_{23}ex_{23} = \dot{E}x_d + \dot{m}_{24}ex_{24} + \dot{W}_{out} \quad (4.355)$$

For gas turbine:

$$\dot{m}_{19} = \dot{m}_{20} \quad (4.356)$$

$$\dot{m}_{19}h_{19} = \dot{m}_{20}h_{20} + \dot{W}_{out} \quad (4.357)$$

$$\dot{S}_{gen} + \dot{m}_{19}s_{19} = \dot{m}_{20}s_{20} \quad (4.358)$$

$$\dot{m}_{19}ex_{19} = \dot{E}x_d + \dot{m}_{20}ex_{20} + \dot{W}_{out} \quad (4.359)$$

For Organic Rankine cycle turbine:

$$\dot{m}_{27} = \dot{m}_{28} \quad (4.360)$$

$$\dot{m}_{27}h_{27} = \dot{m}_{28}h_{28} + \dot{W}_{out} \quad (4.361)$$

$$\dot{S}_{gen} + \dot{m}_{27}s_{27} = \dot{m}_{28}s_{28} \quad (4.362)$$

$$\dot{m}_{27}ex_{27} = \dot{E}x_d + \dot{m}_{28}ex_{28} + \dot{W}_{out} \quad (4.363)$$

For compressor 2:

$$\dot{m}_{17} = \dot{m}_{18} \quad (4.364)$$

$$\dot{W}_{in} + \dot{m}_{17}h_{17} = \dot{m}_{18}h_{18} \quad (4.365)$$

$$\dot{S}_{gen} + \dot{m}_{17}s_{17} = \dot{m}_{18}s_{18} \quad (4.366)$$

$$\dot{W}_{in} + \dot{m}_{17}ex_{17} = \dot{E}x_d + \dot{m}_{18}ex_{18} \quad (4.367)$$

4.3.3 Hydrogen Production Subsystem

This system incorporates a distinct approach to hydrogen production. It encompasses two hydrogen-generating methods: one through a three-stage iron-based chemical looping system and the other via an electrolyzer. These two sections operate independently, and the hydrogen produced from both is compressed and stored in a tank for subsequent use.

Figure 4.14 illustrates the detailed interrelation of the components. In order to perform a detailed analysis of the system, the thermodynamic balance equations for each component must be established. The chemical balance equations for reactors 2, 3, and 4 are already represented in (4.73), (4.81), and (4.89), respectively.

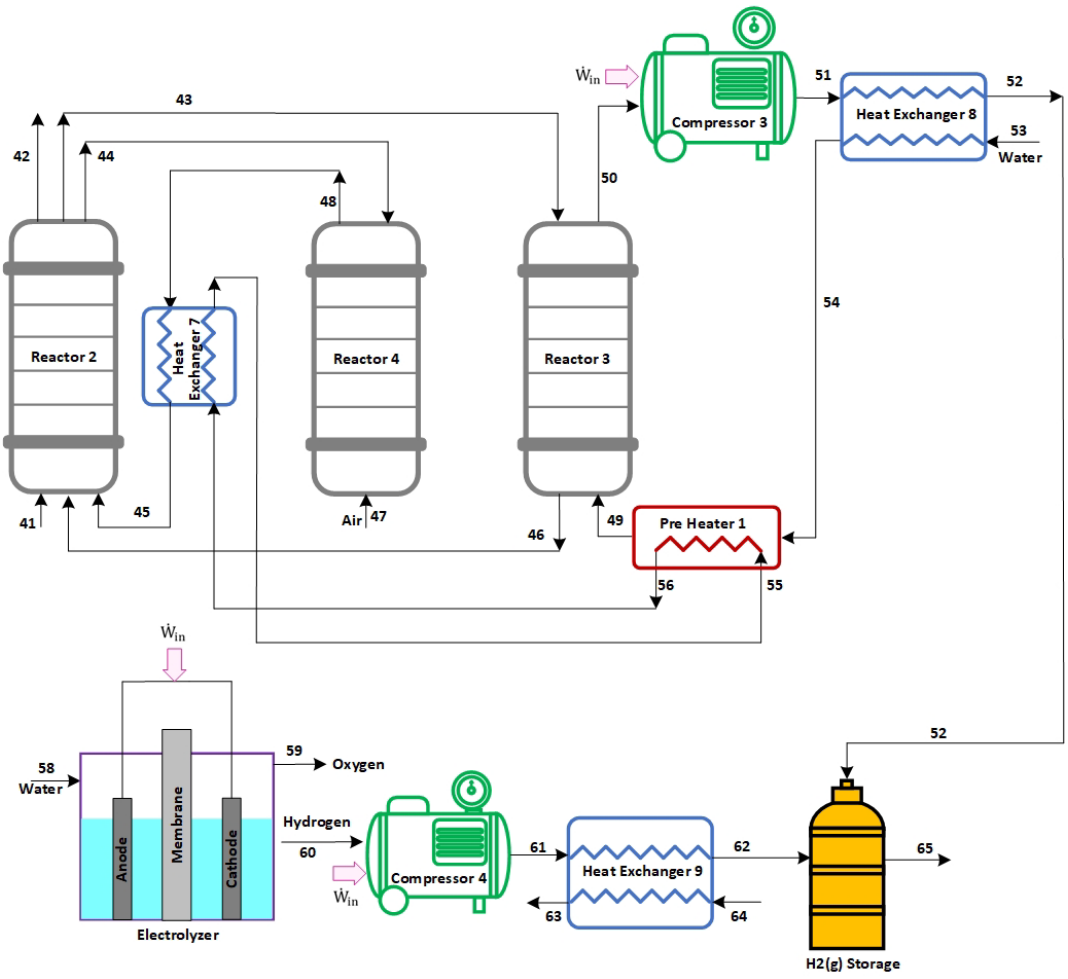

Figure 4.14 Schematic of hydrogen production of system 3

The following equations reflect the mass, energy, entropy, and exergy balances for all components connected to system 3's hydrogen-generating subsystems.

For compressor 3:

$$\dot{m}_{50} = \dot{m}_{51} \tag{4.368}$$

$$\dot{m}_{50}h_{50} + \dot{W}_{in} = \dot{m}_{51}h_{51} \tag{4.369}$$

$$\dot{S}_{gen} + \dot{m}_{50}s_{50} = \dot{m}_{51}s_{51} \tag{4.370}$$

$$\dot{m}_{50}ex_{50} + \dot{W}_{in} = \dot{E}x_{d} + \dot{m}_{51}ex_{51} \tag{4.371}$$

For compressor 4:

$$\dot{m}_{60} = \dot{m}_{61} \tag{4.372}$$

$$\dot{W}_{in} + \dot{m}_{60} h_{60} = \dot{m}_{61} h_{61} \tag{4.373}$$

$$\dot{S}_{gen} + \dot{m}_{60} s_{60} = \dot{m}_{61} s_{61} \tag{4.374}$$

$$\dot{W}_{in} + \dot{m}_{60} ex_{60} = \dot{E}x_{d} + \dot{m}_{61} ex_{61} \tag{4.375}$$

For heat exchanger 7:

$$\dot{m}_{48} + \dot{m}_{56} = \dot{m}_{55} + \dot{m}_{45} \tag{4.376}$$

$$\dot{m}_{48} h_{48} + \dot{m}_{56} h_{56} = \dot{m}_{55} h_{55} + \dot{m}_{45} h_{45} \tag{4.377}$$

$$\dot{S}_{gen} + \dot{m}_{48} s_{48} + \dot{m}_{56} s_{56} = \dot{m}_{55} s_{55} + \dot{m}_{45} s_{45} \tag{4.378}$$

$$\dot{m}_{48} ex_{48} + \dot{m}_{56} ex_{56} = \dot{m}_{55} ex_{55} + \dot{m}_{45} ex_{45} + \dot{E}x_{d} \tag{4.379}$$

For heat exchanger 8:

$$\dot{m}_{51} + \dot{m}_{53} = \dot{m}_{52} + \dot{m}_{54} \tag{4.380}$$

$$\dot{m}_{51} h_{51} + \dot{m}_{53} h_{53} = \dot{m}_{52} h_{52} + \dot{m}_{54} h_{54} \tag{4.381}$$

$$\dot{S}_{gen} + \dot{m}_{51} s_{51} + \dot{m}_{53} s_{53} = \dot{m}_{52} s_{52} + \dot{m}_{54} s_{54} \tag{4.382}$$

$$\dot{m}_{51} ex_{51} + \dot{m}_{53} ex_{53} = \dot{m}_{52} ex_{52} + \dot{m}_{54} ex_{54} + \dot{E}x_{d} \tag{4.383}$$

For heat exchanger 9:

$$\dot{m}_{64} + \dot{m}_{61} = \dot{m}_{62} + \dot{m}_{63} \tag{4.384}$$

$$\dot{m}_{64} h_{64} + \dot{m}_{61} h_{61} = \dot{m}_{62} h_{62} + \dot{m}_{63} h_{63} \tag{4.385}$$

$$\dot{S}_{gen} + \dot{m}_{64} s_{64} + \dot{m}_{61} s_{61} = \dot{m}_{62} s_{62} + \dot{m}_{63} s_{63} \tag{4.386}$$

$$\dot{m}_{64} ex_{64} + \dot{m}_{61} ex_{61} = \dot{m}_{62} ex_{62} + \dot{m}_{63} ex_{63} + \dot{E}x_{d} \tag{4.387}$$

For preheater 1:

$$\dot{m}_{54} + \dot{m}_{55} = \dot{m}_{49} + \dot{m}_{56} \tag{4.388}$$

$$\dot{m}_{54}h_{54} + \dot{m}_{55}h_{55} = \dot{m}_{49}h_{49} + \dot{m}_{56}h_{56} \quad (4.389)$$

$$\dot{S}_{gen} + \dot{m}_{54}s_{54} + \dot{m}_{55}s_{55} = \dot{m}_{49}s_{49} + \dot{m}_{56}s_{56} \quad (4.390)$$

$$\dot{m}_{54}ex_{54} + \dot{m}_{55}ex_{55} = \dot{m}_{49}ex_{49} + \dot{m}_{56}ex_{56} + \dot{E}x_d \quad (4.391)$$

For electrolyzer:

$$\dot{m}_{58} = \dot{m}_{59} + \dot{m}_{60} \quad (4.392)$$

$$\dot{m}_{58}h_{58} + \dot{W}_{in} = \dot{m}_{59}h_{59} + \dot{m}_{60}h_{60} \quad (4.393)$$

$$\dot{S}_{gen} + \dot{m}_{58}s_{58} = \dot{m}_{59}s_{59} + \dot{m}_{60}s_{60} \quad (4.394)$$

$$\dot{m}_{58}ex_{58} + \dot{W}_{in} = \dot{E}x_d + \dot{m}_{59}ex_{59} + \dot{m}_{60}ex_{60} \quad (4.395)$$

For reactor 2, the physical balance equations are as follows:

$$\dot{m}_{41} + \dot{m}_{45} + \dot{m}_{46} = \dot{m}_{42} + \dot{m}_{43} + \dot{m}_{44} \quad (4.396)$$

$$\dot{m}_{41}h_{41} + \dot{m}_{45}h_{45} + \dot{m}_{46}h_{46} + \dot{Q}_{in} = \dot{m}_{42}h_{42} + \dot{m}_{43}h_{43} + \dot{m}_{44}h_{44} \quad (4.397)$$

$$\dot{S}_{gen} + \dot{m}_{41}s_{41} + \dot{m}_{45}s_{45} + \dot{m}_{46}s_{46} + \frac{\dot{Q}_{in}}{T_s} = \dot{m}_{42}s_{42} + \dot{m}_{43}s_{43} + \dot{m}_{44}s_{44} \quad (4.398)$$

$$\dot{m}_{41}ex_{41} + \dot{m}_{45}ex_{45} + \dot{m}_{46}ex_{46} + \dot{Q}_{in}(1 - \frac{T_0}{T_s}) = \dot{m}_{42}ex_{42} + \dot{m}_{43}ex_{43} + \dot{m}_{44}ex_{44} + \dot{E}x_d \quad (4.399)$$

For reactor 3, the physical balance equations are as follows:

$$\dot{m}_{43} + \dot{m}_{49} = \dot{m}_{50} + \dot{m}_{46} \quad (4.400)$$

$$\dot{m}_{43}h_{43} + \dot{m}_{49}h_{49} = \dot{m}_{50}h_{50} + \dot{m}_{46}h_{46} + \dot{Q}_{out} \quad (4.401)$$

$$\dot{S}_{gen} + \dot{m}_{43}s_{43} + \dot{m}_{49}s_{49} = \dot{m}_{50}s_{50} + \dot{m}_{46}s_{46} + \frac{\dot{Q}_{out}}{T_b} \quad (4.402)$$

$$\dot{m}_{43}ex_{43} + \dot{m}_{49}ex_{49} = \dot{m}_{50}ex_{50} + \dot{m}_{46}ex_{46} + \dot{Q}_{out}(1 - \frac{T_0}{T_s}) + \dot{E}x_d \quad (4.403)$$

For reactor 4, the physical balance equations are as follows:

$$\dot{m}_{47} + \dot{m}_{44} = \dot{m}_{48} \quad (4.404)$$

$$\dot{Q}_{in} + \dot{m}_{47}h_{47} + \dot{m}_{44}h_{44} = \dot{m}_{48}h_{48} \tag{4.405}$$

$$\dot{S}_{gen} + \dot{m}_{47}s_{47} + \dot{m}_{44}s_{44} + \frac{\dot{Q}_{in}}{T_s} = \dot{m}_{48}s_{48} \tag{4.406}$$

$$\dot{m}_{47}ex_{47} + \dot{m}_{44}ex_{44} + \dot{Q}_{in}(1 - \frac{T_0}{T_s}) = \dot{m}_{48}ex_{48} + \dot{E}x_d \tag{4.407}$$

4.3.4 Methanol Production Subsystem

As shown in Figure 4.15, methanol is produced in this system in Reactor 1 by converting hydrogen and carbon dioxide into methanol. Before this reaction, the gases have to be mixed and heated up, which necessitates the existence of a gas mixer, preheater 2, and Heat Exchanger 10 located before Reactor 1.

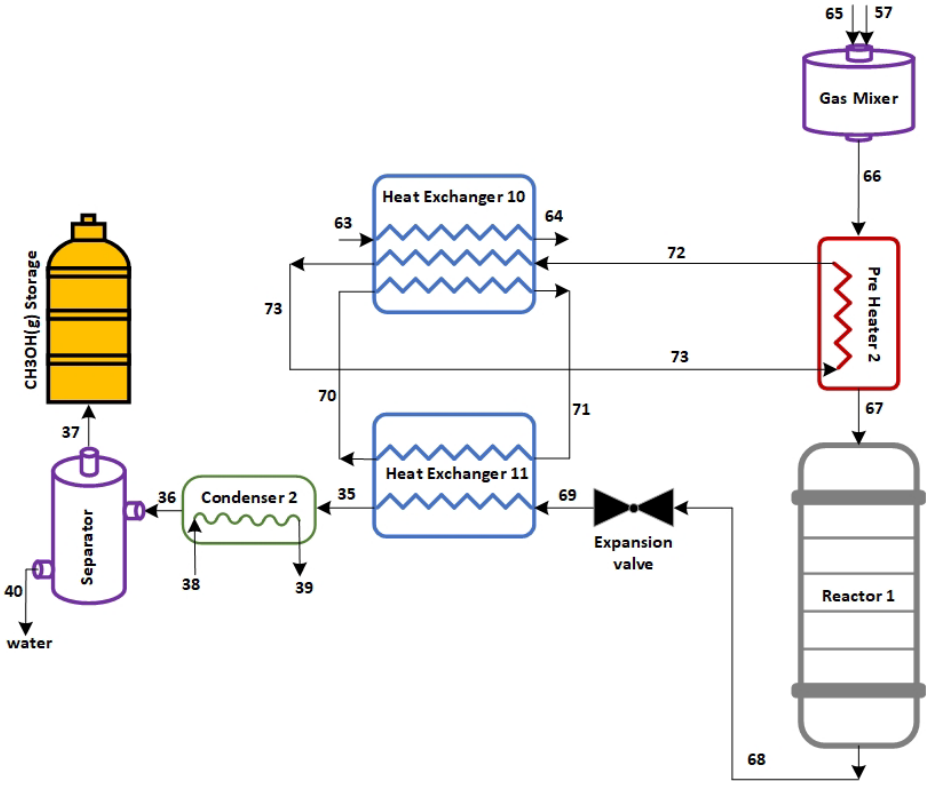

Figure 4.15 Schematic of methanol production subsystem of system 3

The resultant mixture then reacts under precise circumstances, producing methanol and water. Following the reaction, the products head out through an expansion valve and heat exchanger 11 to decrease the heat and pressure. The methanol was then separated from the water using Condenser 2 and a separator before being stored for future use. For analyzing

the system thermodynamically, the mass, energy, enthalpy, and exergy balance equations for the methanol production subsystem have been determined and written as follows:

For gas mixer:

$$\dot{m}_{65} + \dot{m}_{57} = \dot{m}_{66} \tag{4.408}$$

$$\dot{m}_{65}h_{65} + \dot{m}_{57}h_{57} = \dot{m}_{66}h_{66} \tag{4.409}$$

$$\dot{S}_{gen} + \dot{m}_{65}s_{65} + \dot{m}_{57}s_{57} = \dot{m}_{66}s_{66} \tag{4.410}$$

$$\dot{m}_{65}ex_{65} + \dot{m}_{57}ex_{57} = \dot{m}_{66}ex_{66} + \dot{E}x_{d} \tag{4.411}$$

For preheater 2:

$$\dot{m}_{73} + \dot{m}_{66} = \dot{m}_{67} + \dot{m}_{72} \tag{4.412}$$

$$\dot{m}_{73}h_{73} + \dot{m}_{66}h_{66} = \dot{m}_{67}h_{67} + \dot{m}_{72}h_{72} \tag{4.413}$$

$$\dot{S}_{gen} + \dot{m}_{73}s_{73} + \dot{m}_{66}s_{66} = \dot{m}_{67}s_{67} + \dot{m}_{72}s_{72} \tag{4.414}$$

$$\dot{m}_{73}ex_{73} + \dot{m}_{66}ex_{66} = \dot{m}_{67}ex_{67} + \dot{m}_{72}ex_{72} + \dot{E}x_{d} \tag{4.415}$$

For heat exchanger 10:

$$\dot{m}_{63} + \dot{m}_{70} + \dot{m}_{72} = \dot{m}_{71} + \dot{m}_{73} + \dot{m}_{64} \tag{4.416}$$

$$\dot{m}_{63}h_{63} + \dot{m}_{70}h_{70} + \dot{m}_{72}h_{72} = \dot{m}_{71}h_{71} + \dot{m}_{73}h_{73} + \dot{m}_{64}h_{64} \tag{4.417}$$

$$\dot{S}_{gen} + \dot{m}_{63}s_{63} + \dot{m}_{70}s_{70} + \dot{m}_{72}s_{72} = \dot{m}_{71}s_{71} + \dot{m}_{73}s_{73} + \dot{m}_{64}s_{64} \tag{4.418}$$

$$\dot{m}_{63}ex_{63} + \dot{m}_{70}ex_{70} + \dot{m}_{72}ex_{72} = \dot{m}_{71}ex_{71} + \dot{m}_{73}ex_{73} + \dot{m}_{64}ex_{64} + \dot{E}x_{d} \tag{4.419}$$

For heat exchanger 11:

$$\dot{m}_{69} + \dot{m}_{71} = \dot{m}_{35} + \dot{m}_{70} \tag{4.420}$$

$$\dot{m}_{69}h_{69} + \dot{m}_{71}h_{71} = \dot{m}_{35}h_{35} + \dot{m}_{70}h_{70} \tag{4.421}$$

$$\dot{S}_{gen} + \dot{m}_{69}s_{69} + \dot{m}_{71}s_{71} = \dot{m}_{35}s_{35} + \dot{m}_{70}s_{70} \tag{4.422}$$

$$\dot{m}_{69}ex_{69} + \dot{m}_{71}ex_{71} = \dot{m}_{35}ex_{35} + \dot{m}_{70}ex_{70} + \dot{E}x_{d} \tag{4.423}$$

The physical balance equations for reactor 1 are as follows:

$$\dot{m}_{67} = \dot{m}_{68} \tag{4.424}$$

$$\dot{m}_{67}h_{67} = \dot{m}_{68}h_{68} + \dot{Q}_{out} \tag{4.425}$$

$$\dot{S}_{gen} + \dot{m}_{67}s_{67} = \dot{m}_{68}s_{68} + \frac{\dot{Q}_{out}}{T_b} \tag{4.426}$$

$$\dot{m}_{67}ex_{67} = \dot{m}_{68}ex_{68} + \dot{Q}_{out}(1 - \frac{T_0}{T_s}) + \dot{E}x_d \tag{4.427}$$

The chemical balance equations for reactor 1 are as follows:

$$\dot{n}_{H2} + \dot{n}_{CO2} = \dot{n}_{CH3OH} + \dot{n}_{H2O} \tag{4.428}$$

$$\dot{n}_{H2}(\overline{h_f^0} + \bar{h} - \overline{h^0} - P\bar{v})_{H2} + \dot{n}_{CO2}(\overline{h_f^0} + \bar{h} - \overline{h^0} - P\bar{v})_{CO2} = \dot{n}_{H2O}(\overline{h_f^0} + \bar{h} - \overline{h^0} - P\bar{v})_{H2O} + \dot{n}_{CH3OH}(\overline{h_f^0} + \bar{h} - \overline{h^0} - P\bar{v})_{CH3OH} + \dot{Q}_{out} \tag{4.429}$$

$$\dot{S}_{gen} + \dot{n}_{CO2}(\overline{s_f^0} + \bar{s} - \overline{s^0})_{CO2} + \dot{n}_{H2}(\overline{s_f^0} + \bar{s} - \overline{s^0})_{H2} = \dot{n}_{CH3OH}(\overline{s_f^0} + \bar{s} - \overline{s^0})_{CH3OH} + \dot{n}_{H2O}(\overline{s_f^0} + \bar{s} - \overline{s^0})_{H2O} + \frac{\dot{Q}_{out}}{T_b} \tag{4.430}$$

$$\dot{n}_{H2}(\overline{ex_f^0} + \overline{ex} - \overline{ex^0} - P\bar{v})_{H2} + \dot{n}_{CO2}(\overline{ex_f^0} + \overline{ex} - \overline{ex^0} - P\bar{v})_{CO2} = \dot{n}_{CH3OH}(\overline{ex_f^0} + \overline{ex} - \overline{ex^0} - P\bar{v})_{CH3OH} + \dot{n}_{H2O}(\overline{ex_f^0} + \overline{ex} - \overline{ex^0} - P\bar{v})_{H2O} + \dot{E}x_d + \dot{Q}_{out}(1 - \frac{T_0}{T_b}) \tag{4.431}$$

For condenser 2:

$$\dot{m}_{38} + \dot{m}_{35} = \dot{m}_{39} + \dot{m}_{36} \tag{4.432}$$

$$\dot{m}_{38}h_{38} + \dot{m}_{35}h_{35} = \dot{m}_{39}h_{39} + \dot{m}_{36}h_{36} + \dot{Q}_{out} \tag{4.433}$$

$$\dot{m}_{38}s_{38} + \dot{m}_{35}s_{35} = \dot{m}_{39}s_{39} + \dot{m}_{36}s_{36} + \frac{\dot{Q}_{out}}{T_b} \tag{4.434}$$

$$\dot{m}_{38}ex_{38} + \dot{m}_{35}ex_{35} = \dot{m}_{39}ex_{39} + \dot{m}_{36}ex_{36} + \dot{Q}_{out}(1 - \frac{T_0}{T_b}) + \dot{E}x_d \tag{4.435}$$

For separator:

$$\dot{m}_{36} = \dot{m}_{40} + \dot{m}_{37} \tag{4.436}$$

$$\dot{m}_{36}h_{36} = \dot{m}_{40}h_{40} + \dot{m}_{37}h_{37} \tag{4.437}$$

$$\dot{m}_{36}s_{36} + \dot{S}_{gen} = \dot{m}_{40}s_{40} + \dot{m}_{37}s_{37} \quad (4.438)$$

$$\dot{m}_{36}ex_{36} = \dot{m}_{40}ex_{40} + \dot{m}_{37}ex_{37} + \dot{E}x_{d} \quad (4.439)$$

For expansion valve:

$$\dot{m}_{68} = \dot{m}_{69} \quad (4.440)$$

$$\dot{m}_{68}h_{68} = \dot{m}_{69}h_{69} \quad (4.441)$$

$$\dot{S}_{gen} + \dot{m}_{68}s_{68} = \dot{m}_{69}s_{69} \quad (4.442)$$

$$\dot{m}_{68}ex_{68} = \dot{m}_{69}ex_{69} + \dot{E}x_{d} \quad (4.443)$$

4.3.5 Freshwater Production Subsystem

This additional desalination process for freshwater production is integrated into system 3 to develop sustainability and use the existing heat of the ORG in a suitable manner. Figure 4.16 displays a better understanding of the multiple-stage desalination system to obtain a better subsystem output.

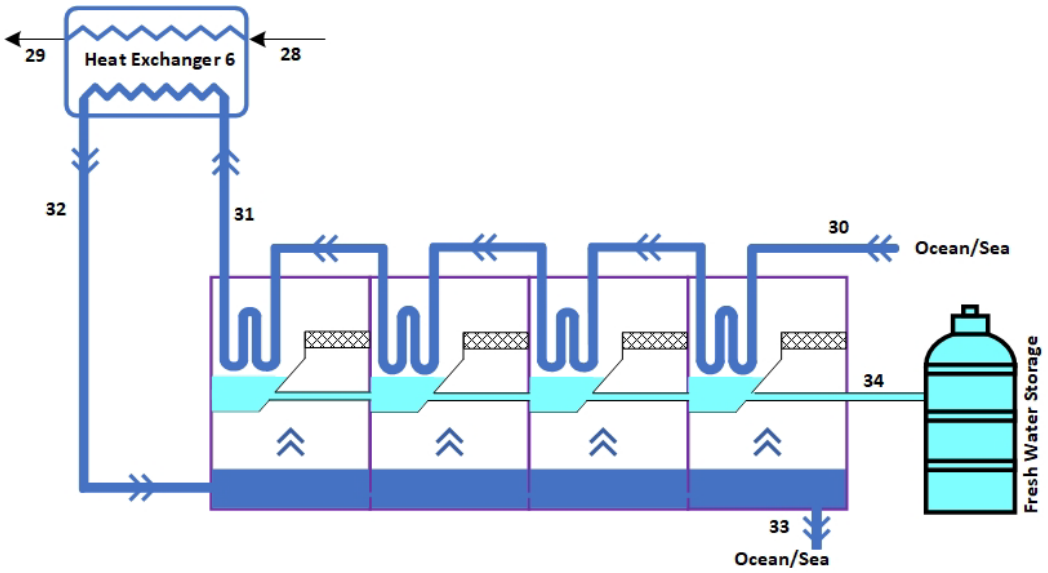

Figure 4.16 Schematic of ocean water desalination to produce freshwater of system 3

The primary technique used for desalinating seawater in this system is the distillation method, which entails the evaporation of saltwater followed by condensing the resulting vapour into freshwater, separating the salts and contaminants. In this approach, the

saltwater is subjected to heat exchanger 6 for heating until it attains its boiling point and starts the process of evaporation.

The water vapour, devoid of salts and contaminants, ascends and is then guided by cooling mechanisms or condensation chambers. During the cooling process, the gaseous state of water undergoes condensation, resulting in the formation of droplets that constitute freshwater.

The collection of freshwater occurs inside a distinct chamber or vessel. Filters may be included at different phases of this process, including pre-heating filtration to eliminate more significant contaminants and post-condensation filtration to guarantee the attainment of required purity levels in the resultant freshwater; therefore, it successfully separates freshwater from the dissolved salts and other contaminants found in sea or ocean water. The desalination unit to produce freshwater is divided into the multiple-stage distillation section and heat exchanger 6. Previously, the mass, energy, entropy, and exergy balance equations of heat exchanger 6 are presented in (4.348), (4.349), (4.350) and (4.351) equations.

4.3.6 Modelling and Analysis

In accordance with the system 3 design, it was put through a thorough evaluation that included thermodynamic analysis, energy and exergy efficiency measurement, and other factors.

Within this theoretical framework, after the balance equations were derived for each system component, the entire setup underwent simulation using the EES and Aspen Plus software tools.

All subsystems of system 3, except for the freshwater production unit, have been simulated using Aspen Plus software and are shown in Figure 4.17. The simulation procedure included the analysis of efficiency, exergy destruction, and other thermodynamic characteristics relevant to each individual component and the overall system.

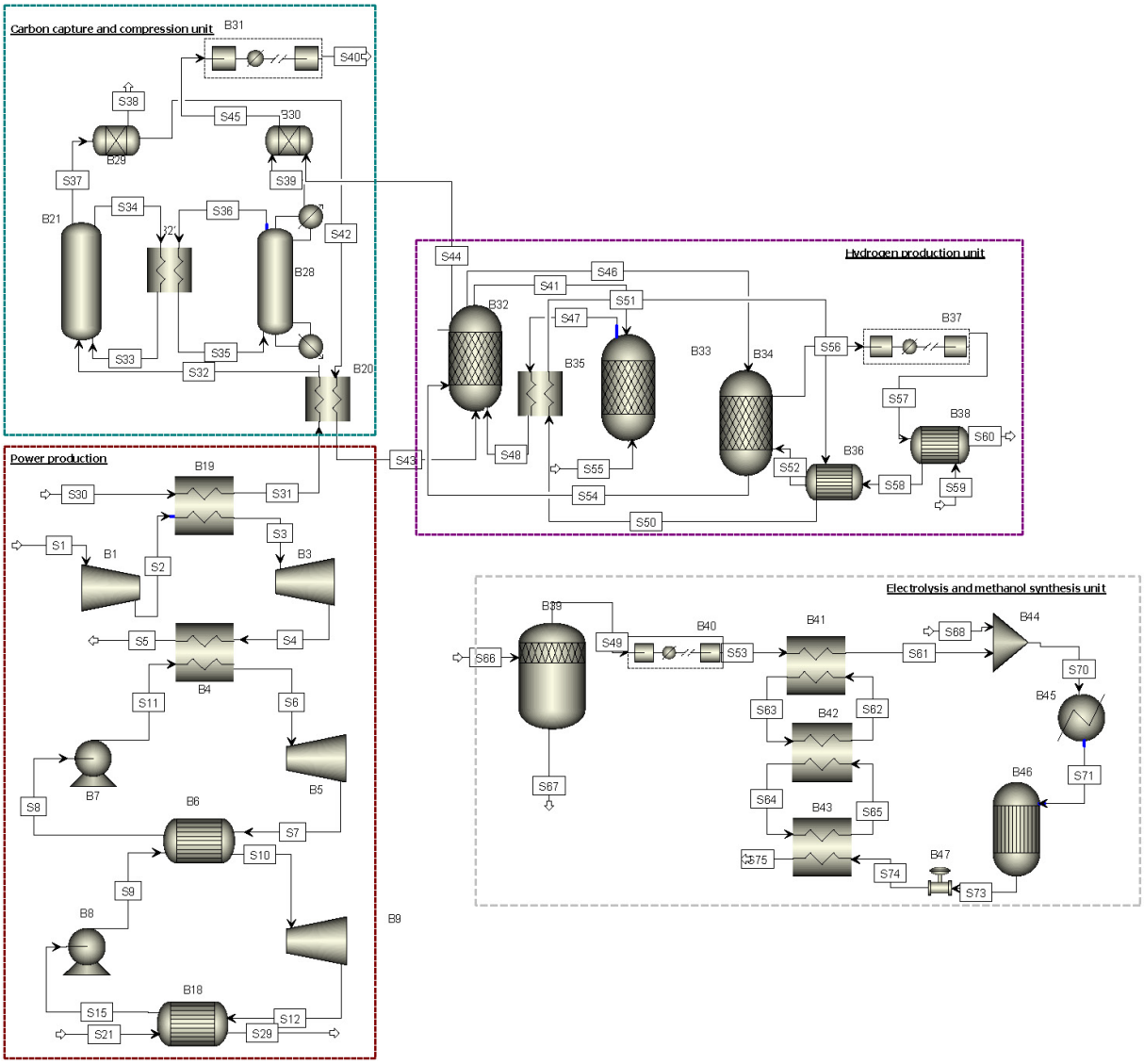

Figure 4.17 Aspen Plus simulation for multiple subsystems of system 3

The calculations were conducted and later examined using an analytical method. The mass flow rate, pressure, temperature, specific enthalpy, specific entropy, and specific exergy of all state points in system 3 were determined by applying physical and chemical balance equations, interactions, Aspen Plus simulation, and calculations and assumptions of system 3 components. These values were obtained using EES software and are presented in Table 4.3.

Table 4.3 Thermodynamic properties of all state points of system 3

State Point	Working Fluid	Mass flow Rate (kg/s)	Pressure (kPa)	Temperature (℃)	Specific Enthalpy (kJ/kg)	Specific Entropy (kJ/kg.K)	Specific exergy (kJ/kg)
1	Flue Gas	150	101	1000	2237	28.679	852.4
2	Flue Gas	150	101	450	1738	15.932	630.1
3	Flue Gas	150	101	150	726.2	6.42	264
4	Treated Gas + CO	30	101	95	314.4	35.17	102.6
5	CO	2.87	101	113	325.1	6.43	61.1
6	MEA+H_2O	18.6	101	100	325.1	4.342	65.8
7	CO_2+MEA+H_2O	138.6	101	100	206.3	5.721	92.3
8	MEA+H_2O	18.6	101	25	87.3	1.164	0
9	CO_2+MEA+H_2O	138.6	101	25	106.5	1.552	0
10	CO_2	117.13	101	340	4117	2.955	207.2
11	H_2O	1	101	50	114.8	0.542	56.4
12	H_2O	1	101	150	883.6	5.69	258.7
13	CO_2	120	101	80	3414	1.153	133.3
14	H_2O	1	101	25	105.5	0.367	0
15	H_2O	1	101	110	562.1	3.37	183.1
16	CO_2	120	500	90	4520	2.637	216.5
17	Air	10	101	25	298.6	5.697	0
18	Air	10	909	500	1125	5.285	211.8
19	Superheated air	10	909	978	2457	6.689	862.4
20	Air	10	101	525	930.5	7.696	289.1
21	Exhaust gases	10	101	177	452.3	7.113	182.3
22	H_2O	3	5500	50	201.9	0.956	211.2
23	Superheated vapour water	3	5500	500	3400	6.55	1400
24	H_2O	3	150	20	236.4	0.422	44.9
25	Saturated liquid water	3	10	20	171.8	0.649	23.5
26	H_2O	3	5500	35	201.9	0.956	211.2
27	Superheated vapour water	3	5500	130	3400	6.55	1400
28	H_2O	3	150	58	236.4	0.422	44.9
29	Saturated water (l)	3	10	35	171.8	0.649	23.5
30	seawater	500	101	25	105.5	0.367	0
31	seawater	500	101	55	428.1	1.62	53.9
32	seawater	500	101	85	531.2	1.647	138.8
33	seawater	400	101	45	351.1	1.18	47.1
34	freshwater	100	101	45	165.5	0.77	10.2
35	CH_3OH+ H_2O	0.007	430	145	1891	4.79	975.7

36	$CH_3OH + H_2O$	0.007	430	145	1891	4.79	975.7
37	CH_3OH	0.0048	430	85	266.7	2.38	227.4
38	H_2O	1	101	25	105	0.37	0
39	H_2O	1	101	110	562.1	3.37	183.1
40	H_2O	0.0023	101	55	231.5	1.36	163
41	CO	2.87	180	350	422.1	19.43	207.8
42	CO_2	2.87	101	500	4325	3.15	246.1
43	Fe	1.652	101	500	5597	3.36	3539
44	Fe	1.652	101	500	5597	3.36	3539
45	Fe_3O_4	2.289	630	298	2934	3.14	2802
46	Fe_3O_4	2.289	101	498	2691	3.28	2588
47	Air	2	101	25	298.6	5.67	256.8
48	Fe_3O_4	2.315	630	912	3894	7.4	2842
49	H_2O	1	101	550	2557	8.6	1142
50	H2	0.0032	101	110	4914	67.14	1043
51	H2	0.0032	630	223	8546	51.27	2569
52	H2	0.0032	630	85	8438	48.12	2514
53	H_2O	1	101	25	105	0.367	0
54	H_2O	1	101	110	862	3.7	183.1
55	H_2O	1	101	200	927.2	6.33	382
56	H_2O	1	101	45	109.2	0.52	27.8
57	CO_2	0.006	430	85	4298	2.16	120.3
58	H_2O	0.018	101	25	105	0.37	0
59	O_2	0.032	101	95	563	38.7	148
60	H_2	0.002	101	95	1886	60.43	697.3
61	H_2	0.002	630	181	8517	44.38	2547
62	H_2	0.002	630	85	8410	41.62	2503
63	H_2O	2	101	200	1854.4	1.808	764
64	H_2O	2	101	45	218.4	0.904	55.6
65	H_2	0.001	430	85	4835	55.14	613.8
66	CO_2+ H_2	0.007	430	85	1184	6.261	NA
67	CO_2+ H_2	0.007	430	400	1206	8.5	NA
68	$CH_3OH + H_2O$	0.007	430	270	2317	55.41	1094
69	$CH_3OH + H_2O$	0.007	101	270	2317	32.11	472
70	H_2O	1	101	440	1987	8.05	788
71	H_2O	1	101	25	105	0.36	0
72	H_2O	1	101	110	562.1	3.3	183.1
73	H_2O	1	101	324	1218	7.74	522.1
74	Treated Gas	82.5	101	95	314.4	35.7	102.6

Chapter 5. Results and Discussion

This section comprehensively presents outcomes from the intricate modelling and simulation experiments. Each meticulously developed system and its respective subsystems have been thoroughly assessed. Additionally, a rigorous comparative analysis to discern these systems' relative performance and characteristics is provided. In evaluating each system, the EES and Aspen Plus software were deployed to compute parameters such as energy and energy efficiencies, exergy destruction rate, hydrogen production and carbon capturing mass flow rates, and heat and work rates. Finally, the effect of specific parameters, such as ambient temperature, on these parameters has been reviewed and presented.

5.1 System 1 Results

Figure 5.1 displays the heating rate for each system component. It has been established that the thermal energy generated by solar power derived from the condenser and reactor 3 provides heat for further reactors, the combustion chamber, and the pyrolizer.

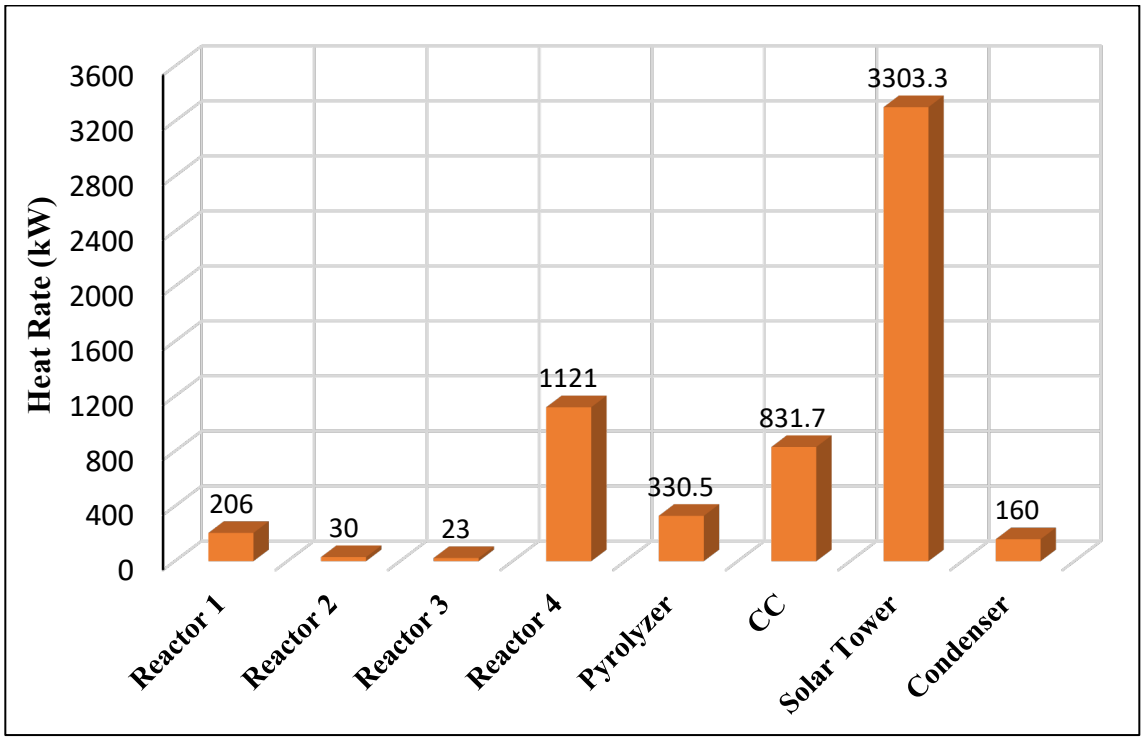

Figure 5.1 Heating rate analysis of components of system 1

Based on the findings presented in Figure 5.1, it has been shown that the primary heat source for the system is derived from the solar system, having a heating rate of 3303.3 kW. Among all the components, the Fe-based CLHP reactor 4, with a heating rate of 1121 kW and the combustion chamber, with an 831.7 kW heating rate, demonstrates a higher use of this heat compared to any other component within the system.

Figure 5.2 represents the working rate for each component of the system. It has been previously described that in this system, the power is generated by the gas turbine and the steam turbine, and then these generated powers are used in several components of the system. Therefore, the collective contribution of both the gas and steam turbines is instrumental in augmenting the system's overall output.

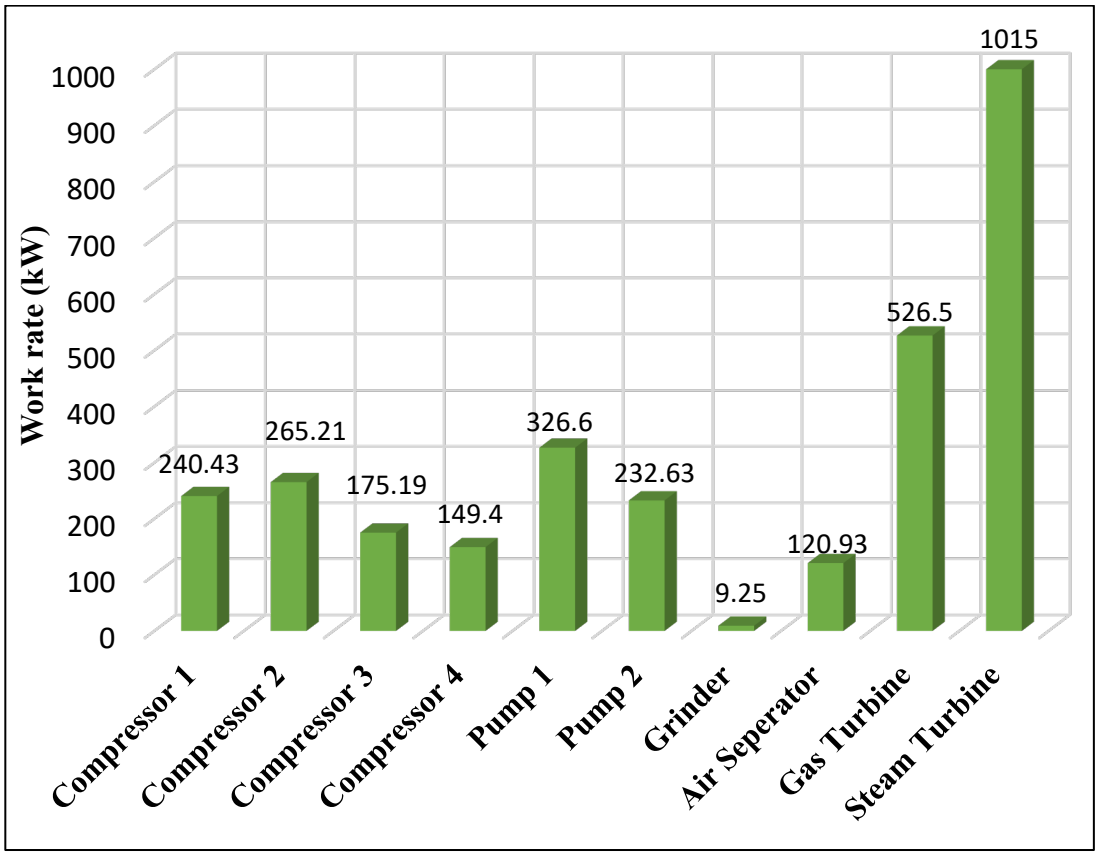

Figure 5.2 Working rate analysis of components of system 1

The steam turbine generates 1015 kW of power, almost two times more than the gas turbine power generation, which is 526.5 kW. Notably, the primary consumption of this generated power is by pumps and compressors, which have the crucial task of elevating the pressure of fluids like hydrogen and carbon dioxide, facilitating their storage, or their desired

destination post-pressurization component. It is also worth noting that the energy produced by gas and steam turbines is efficient, and output is allocated across the system, powering components such as a grinder, air separator, four distinct compressors, and a pair of pumps. Figure 5.3 illustrates the energy and exergy efficiencies within the power generating system, solar system, and iron-based chemical looping.

The power-generating subsystem decreases energy efficiency by 3.3% compared to the exergy efficiency, which is measured at 68.9%. In contrast, it may be shown that energy efficiency surpasses exergy efficiency inside the solar system. The energy and exergy efficiency of the solar heating system are reported as 73.22% and 69.4%, respectively. In addition, it is worth noting that the Fe-based CLHP subsystem exhibits energy and exergy efficiencies of 56.38% and 52.62%, respectively.

The solar heating system exhibits the following demonstration of maximum energy efficiency, with a recorded value of 73.22%. Similarly, the power-generating subsystem also showcases a notable level of energy efficiency, with a recorded value of 65.6%. In contrast, the power generating cycle and solar system exhibit the greatest levels of exergy, with percentages of 69.4% and 68.9%, respectively. The hydrogen generation subsystem has the lowest energy and exergy efficiencies.

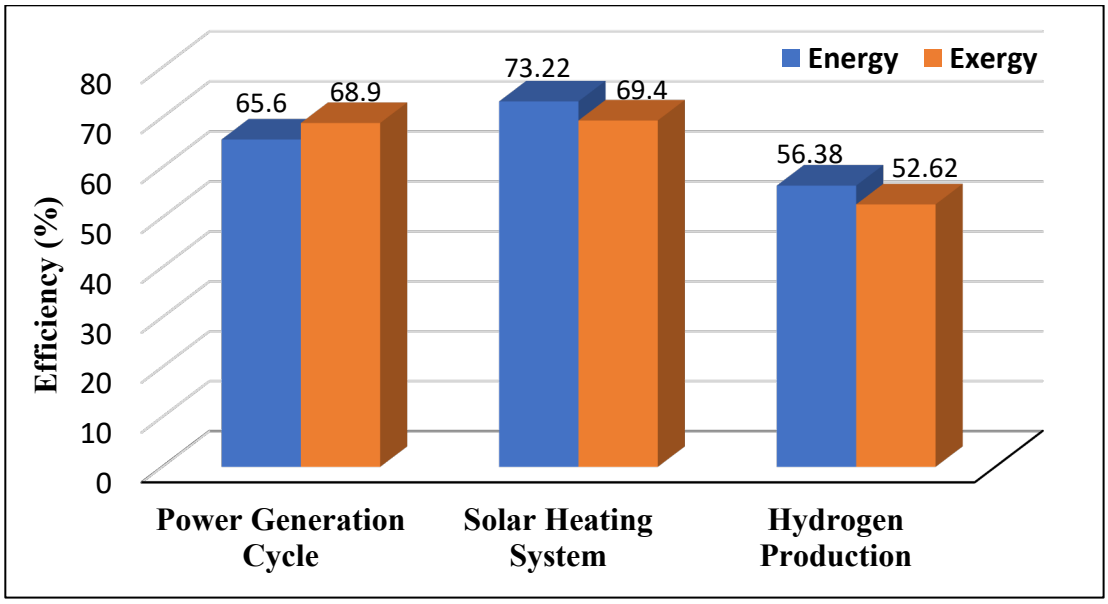

Figure 5.3 Energy and exergy efficiencies of subsystems of system 1

Figure 5.4 illustrates the exergy destruction rates associated with each component within each subsystem of System 1. At a temperature of 25℃, the exergy destruction rates for iron-based chemical looping, the combined Brayton-Rankine cycle, and the solar heating system have been determined to be 425.34 MW, 305.415 MW, and 369.4 MW, respectively.

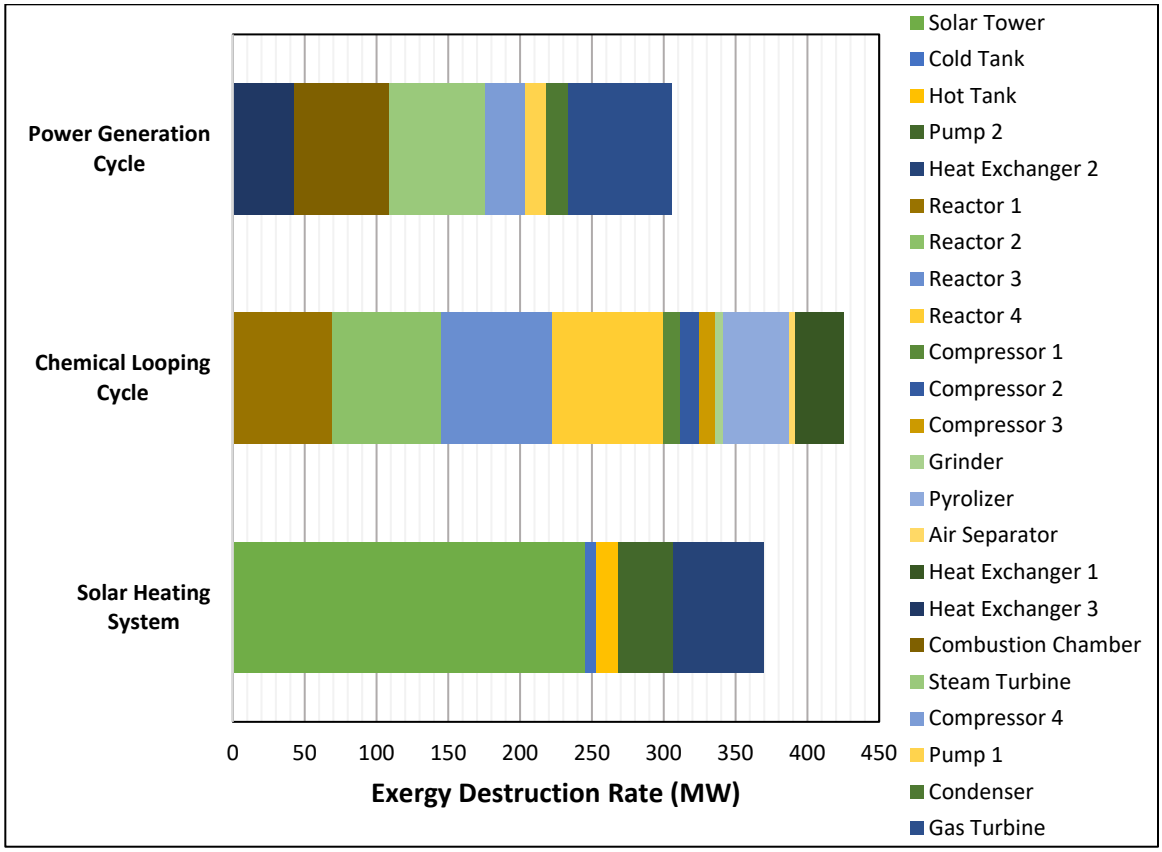

Figure 5.4 Exergy destruction rate of all the components of each subsystem of system 1

According to Figure 5.5, the exergy destruction rate will be elevated with the rise in ambient temperature. The exergy destruction rate of the Fe-based CLHP is found to be the greatest. On the other hand, it can be seen that the power-generating cycle exhibits the lowest rate of exergy destruction.

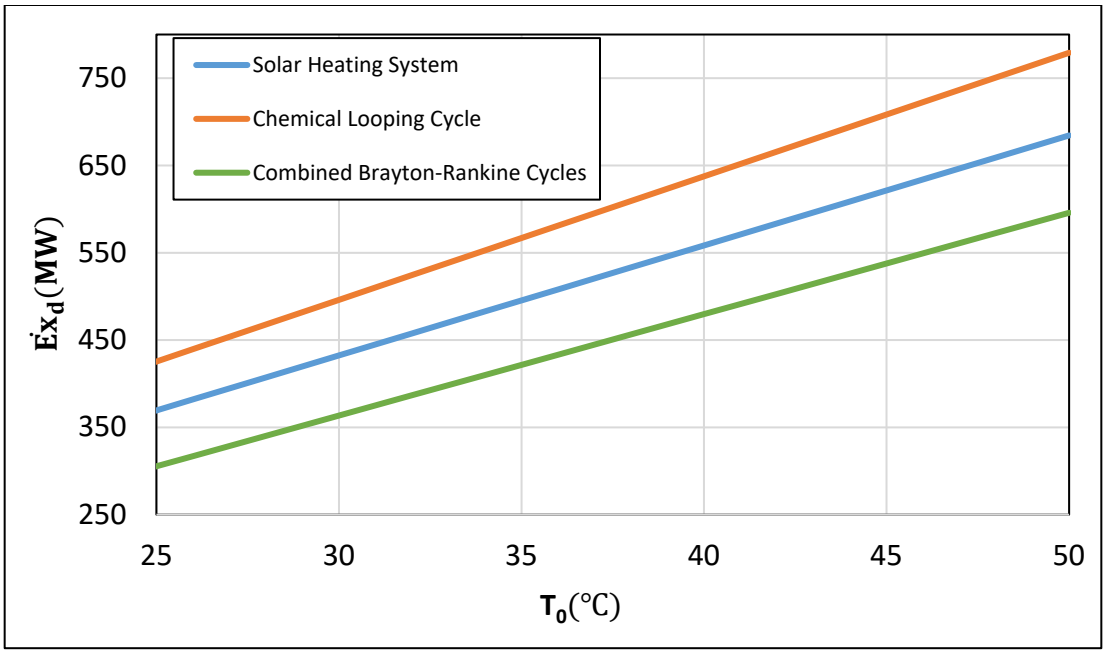

Figure 5.5 Effect of ambient temperature on exergy destruction rate of subsystems of system 1

Figure 5.6 shows that by increasing the direct normal irradiance of the solar system, the rate of hydrogen production and carbon capturing within the system increases. This happens due to increasing the heating rate input to the system by increasing the irradiance.

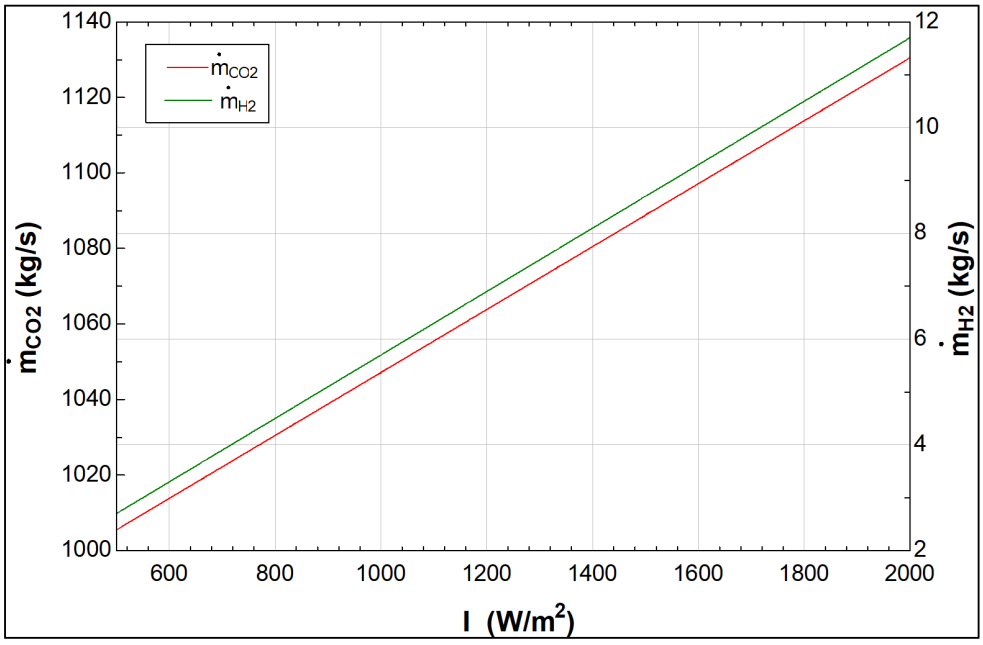

Figure 5.6 Effect of direct normal irradiance on the hydrogen production and carbon capturing flow rate in system 1

Therefore, as the heat input rate of the hydrogen production reactors goes up, the rate of the produced hydrogen increases. Since the carbon is captured directly from reactor 2, the captured carbon also increases.

On the other hand, as shown in Figure 5.7, it is observed that increasing the solar system's heating rate increases the system's overall energy and exergy efficiencies. Therefore, if it goes higher than an optimum point, the rate of hydrogen production and the system's efficiency increases due to the increase in heat loss and excess exergy destruction throughout the system.

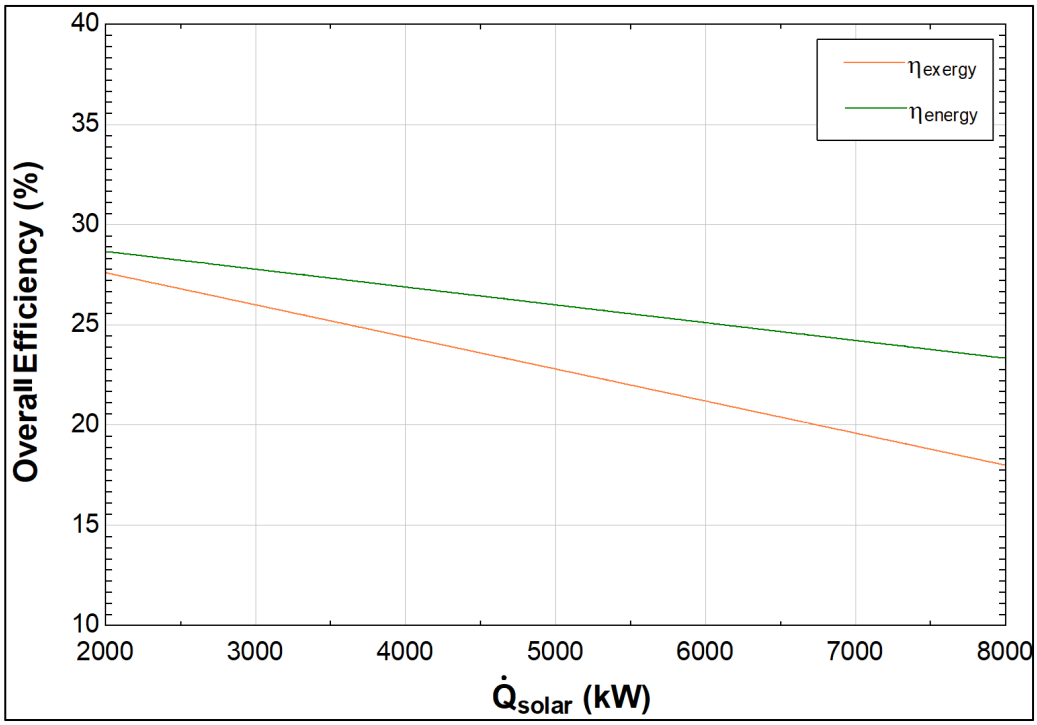

Figure 5.7 Effect of solar heating rate on the overall energy and exergy efficiencies in system 1

After evaluating the exergy destruction rate of the components, efficiencies, and the effect of the solar heating system, the change in the amount of iron oxide and the polypropylene input rate on hydrogen production and carbon capture are investigated.

Figure 5.8 illustrates the effect of the iron oxide input rate on the chemical looping hydrogen production rate. It has been proved that increasing the mass flow rate of iron oxide enhances the hydrogen and carbon produced within the chemical looping. However, the rate of increase gets lower at the higher mass flow rates of iron oxide. During the

chemical reaction of the hydrogen production in reactor 2, iron oxide reacts with the carbon monoxide to produce carbon monoxide and iron to proceed to other reactors for CLHP. The amount of iron oxide that reacts with carbon monoxide is limited; therefore, after some point, the hydrogen production rate increases and carbon capturing decreases.

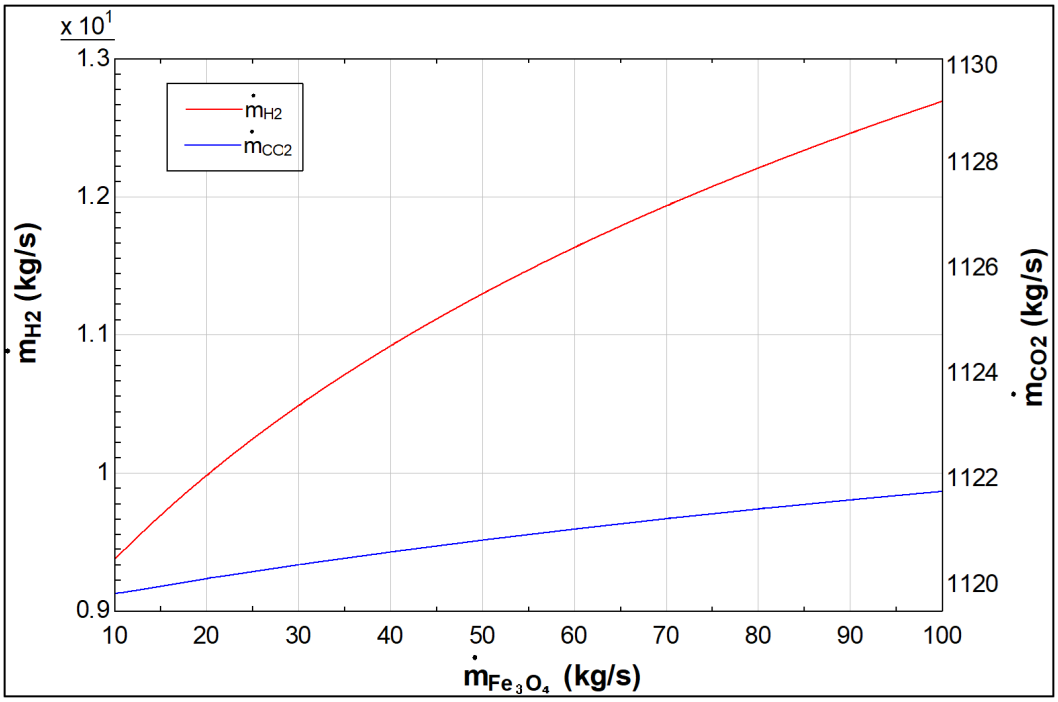

Figure 5.8 Effect of Fe_3O_4 mass flow rate on hydrogen production rate and carbon dioxide capturing rate of system 1

In the detailed analysis presented in Figure 5.9, it becomes evident that the increase in the mass flow rate of the inlet polypropylene results in a significant surge in both hydrogen production and carbon capturing capabilities. When the system intake is at a measured 11.5 kg/s of polypropylene, the output yields a substantial 10.5 kg/s of H_2 and an impressive capture rate of 1120 kg/s for CO_2. Referring to equation (4.126), it's evident that a rise in ambient temperature correlates with an increase in exergy destruction. Furthermore, within this intricately designed system, which comprises three subsystems operating under distinct thermal conditions, each characterized by its own set of heat losses, irreversibilities, and specific heat transfer limitations between the components, it has been empirically verified that elevating the ambient temperature for such a configuration led to an apparent reduction in both energy and exergy efficiencies.

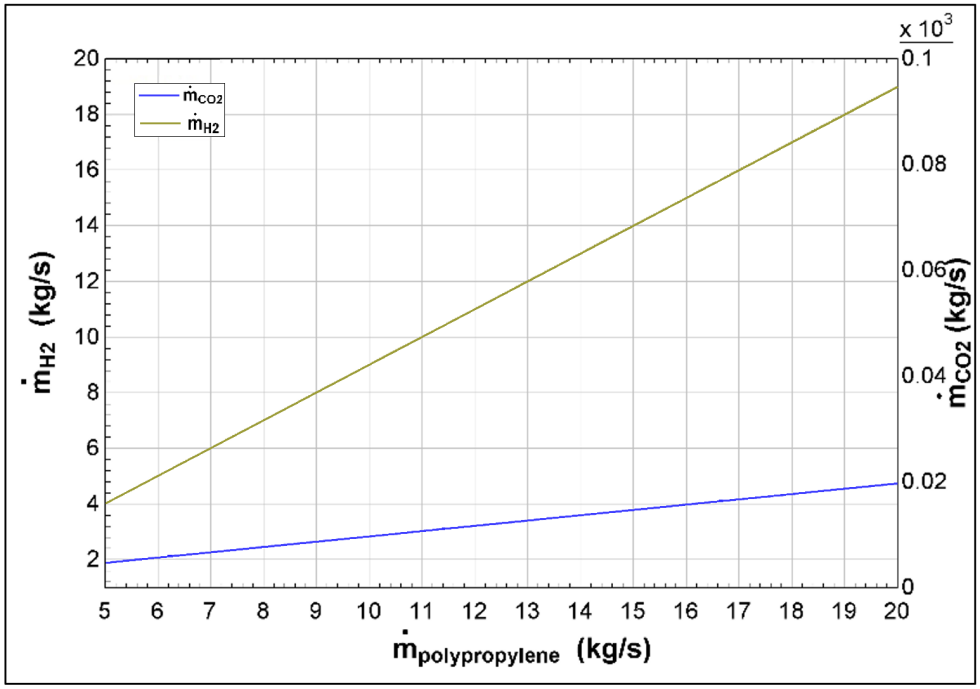

Figure 5.9 Effect of polypropylene mass flow rate on hydrogen production rate and carbon dioxide capturing rate of system 1

The effect of changing the ambient temperature on the work rate of the gas turbine and steam turbine is shown in Figure 5.10, which helps to analyze the power generation system.

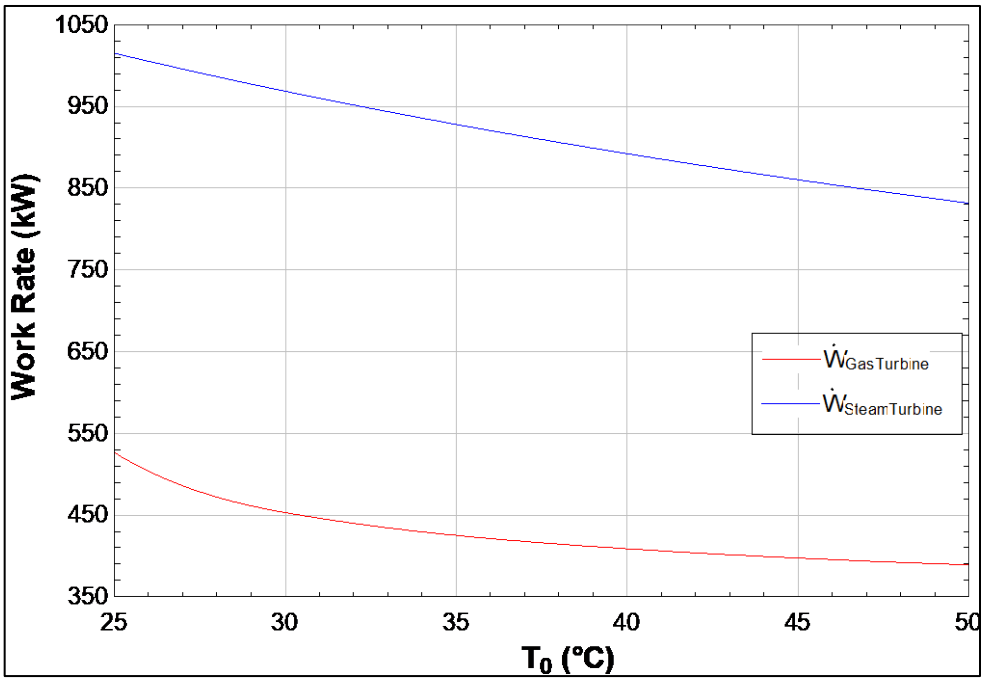

Figure 5.10 Effect of ambient temperature on work rate of different cycles of system 1

Figure 5.11 presents a comprehensive analysis of the energy and exergy efficiencies in relation to varying ambient temperatures. As illustrated, by enhancing the ambient temperature, the work output rate of both turbines decreases as their efficiency lowers due to working in higher ambient temperatures. Also, it might be because of the operational limitations in higher ambient temperatures and changing the properties of the fluid properties in higher temperatures.

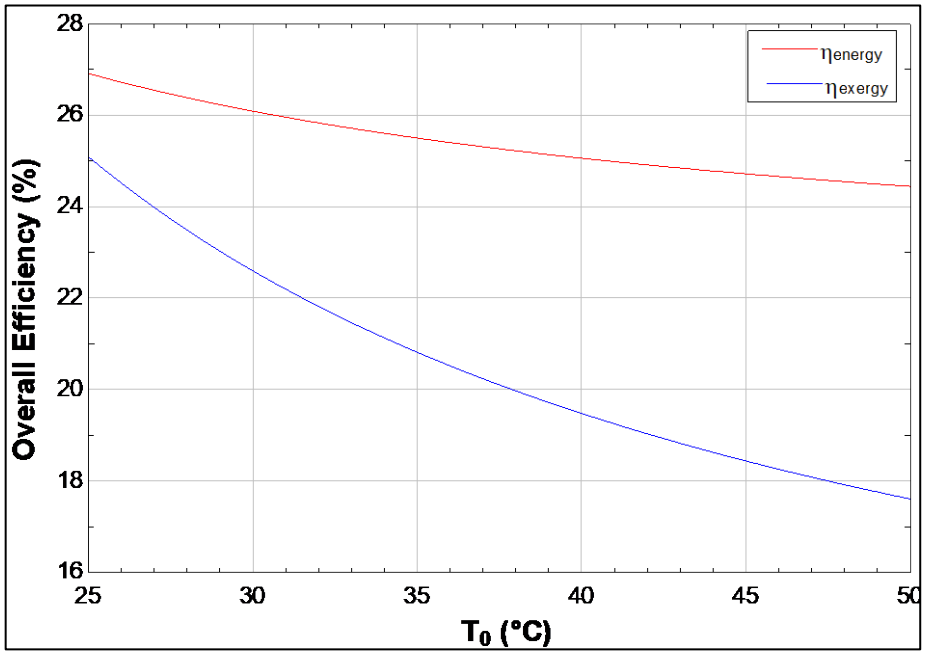

Figure 5.11 Effect of ambient temperature on overall energy and exergy efficiencies of system 1

Observed evidence suggests that an elevation in the ambient temperature inversely affects both energy and exergy efficiencies within this particular system.

5.2 System 2 Results

Figure 5.12 illustrates the exergy destruction rate for all subsystems of system 2. The data shown in this figure clearly indicates that the exergy destruction rate, represented as $\dot{E}x_d$, for the solar tower is at 97.7 MW. The specific factor is recognized as the primary cause of irreversibility throughout the overall system. Simultaneously, the power generation sector and the integrated hydrogen production system, which includes both the SMR process and the subsequent Fe-based CLHP system, exhibit significant exergy destructions, measuring 74.76 MW and 67.5 MW, respectively.

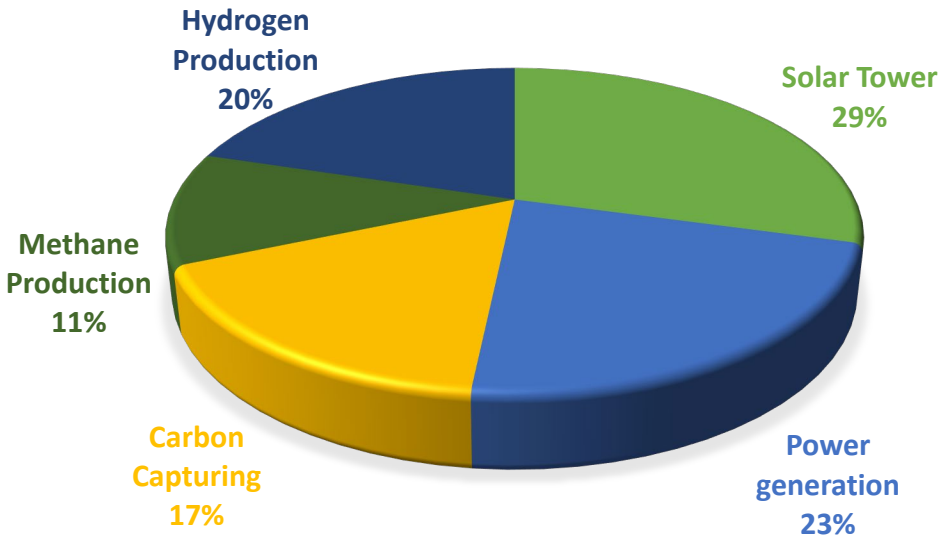

Figure 5.12 Exergy destruction rate of subsystems in system 2

Figure 5.13 displays the impact of the ambient temperature on the exergy destruction rate on the subsystems. As seen in this figure, it can be implied that the exergy destruction rate would rise by elevating the ambient temperature of all subsystems. This is attributed to the amplified disparity between the reference temperature and the ambient temperature.

By considering both figures, it can be concluded that there is a significant reduction in the efficiency of exergy usage within the system. Upon conducting a more in-depth study, it has been determined that the combustion chamber continues to be the primary factor responsible for the reported irreversibility in power generation. On the other hand, heat exchangers and preheaters, which are used to enhance heat transmission between different components, have low rates of exergy destruction. Inside the domain of carbon capture, a significant proportion of the irreversibility is ascribed to the chemical processes taken on inside the stripper.

The carbon capture subsystem has an $\dot{E}x_d$ value of 56.4 MW. In contrast, the methane production subsystem has a minimum recorded value $\dot{E}x_d$ of 37.4 MW. It is important to note that the only source of exergy destruction in this subsystem is seen in reactor 5. This may be qualified for the exothermic Sabatier reaction that is used for methane synthesis.

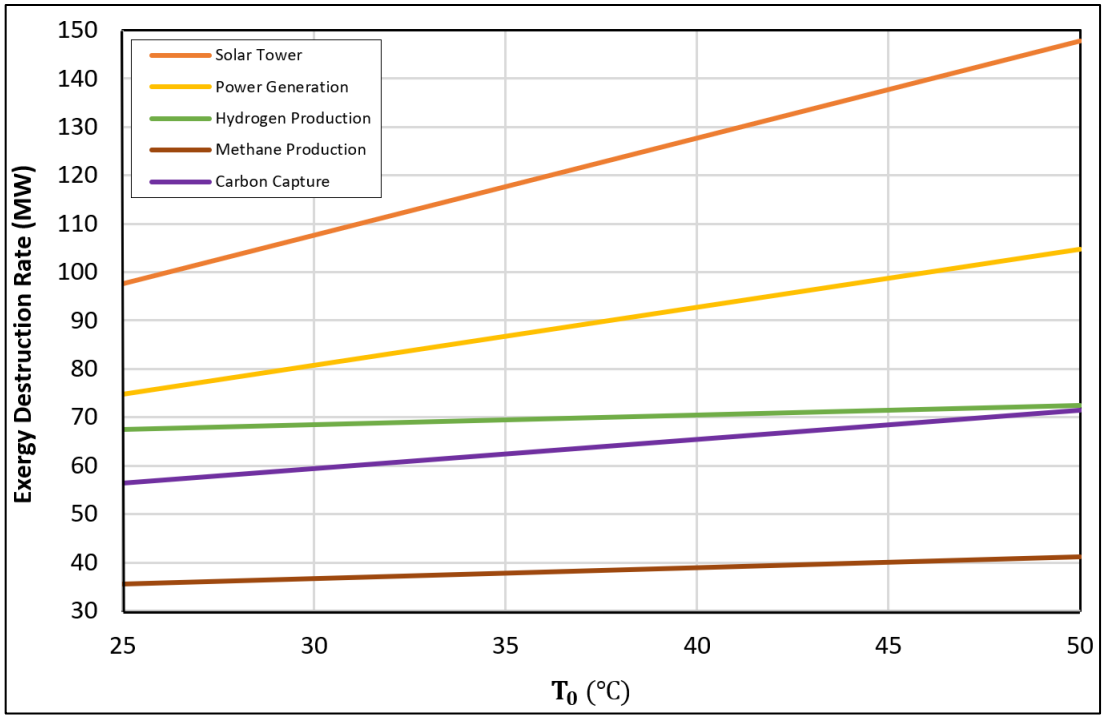

Figure 5.13 Effect of ambient temperature on exergy destruction rate of subsystems in system 2

Figure 5.14 compares the work input and output rate of all components of the system that are using or producing power within the system.

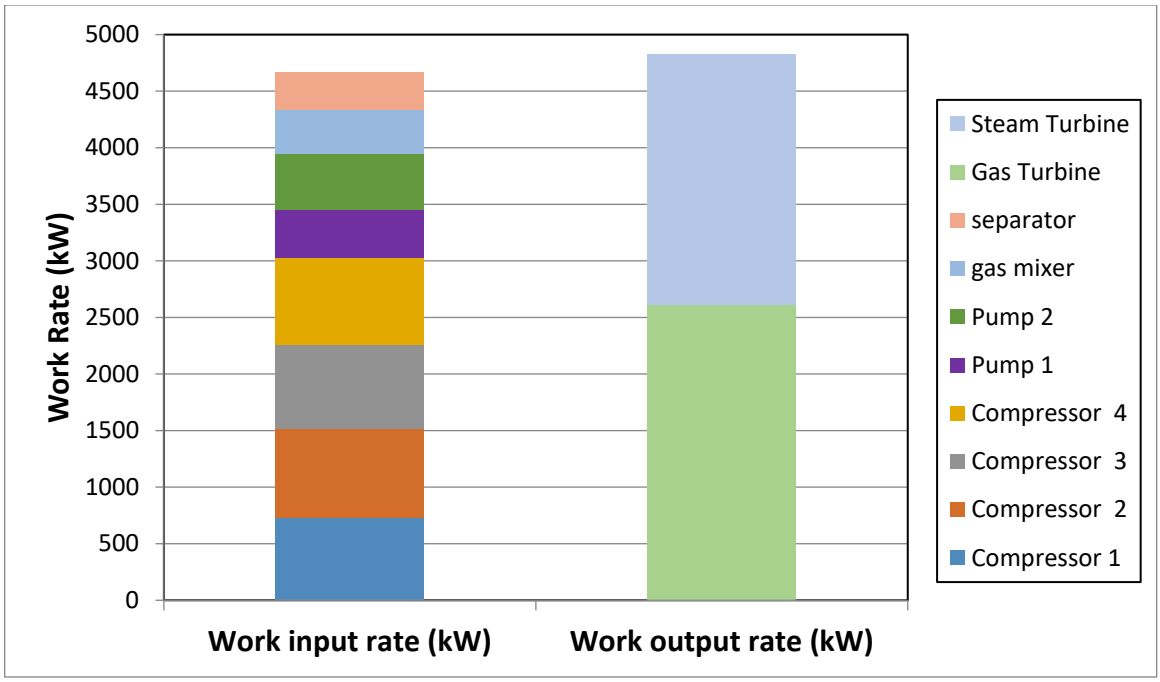

Figure 5.14 Working input and output rate analysis of components of system 2

It is shown that the amount of work produced by the combined Brayton-Rankine cycle is enough to supply the required work input for components that require work input.

Figure 5.15 shows the effect of changing ambient temperature on hydrogen and methane production rates and carbon capturing rates. It has been proved that as ambient temperature rises, the rate of methane and hydrogen production and carbon capture increase.

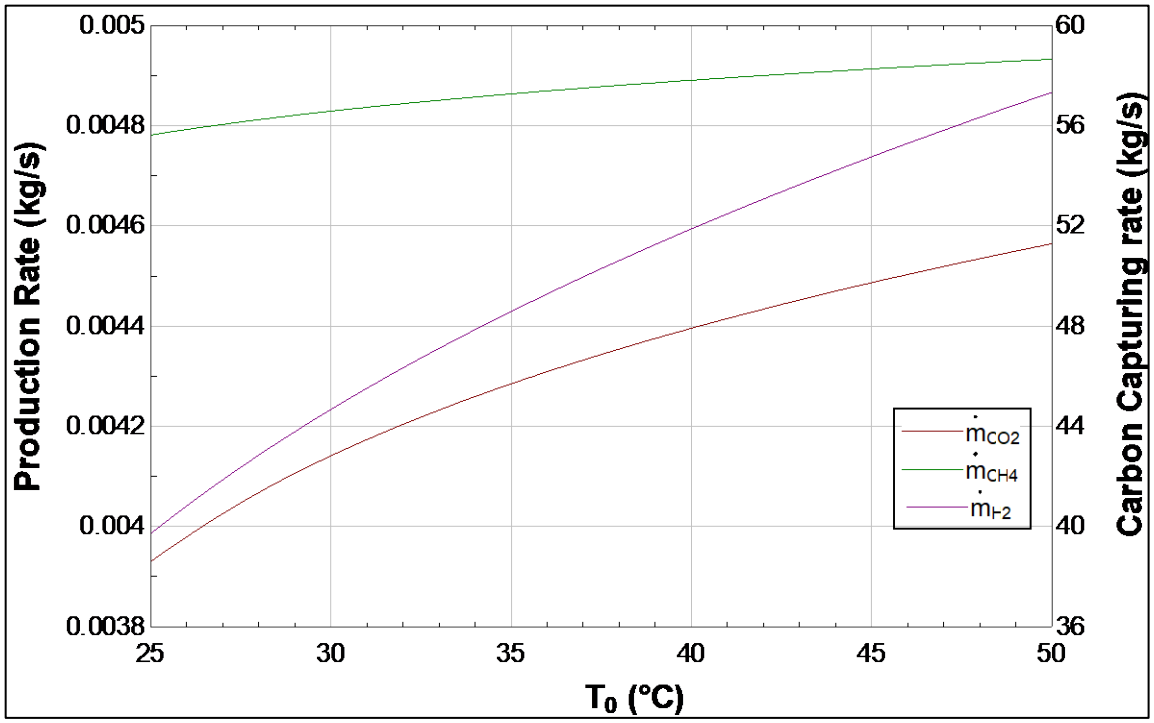

Figure 5.15 Effect of ambient temperature on hydrogen and methane production rate and carbon dioxide capturing rate of system 2

Initially, the rate might be steeper. However, as the temperature continues to increase, the system approaches operational and efficiency limits, causing the rate of production to become slower.

Figure 5.16 illustrates the amount of energy and exergy efficiencies within the power generating system, solar heating system, hydrogen production system, carbon capturing system and methane production system. It is shown that methane production has the most energy efficiency, and the solar heating system has the lowest energy and exergy efficiency in this system.

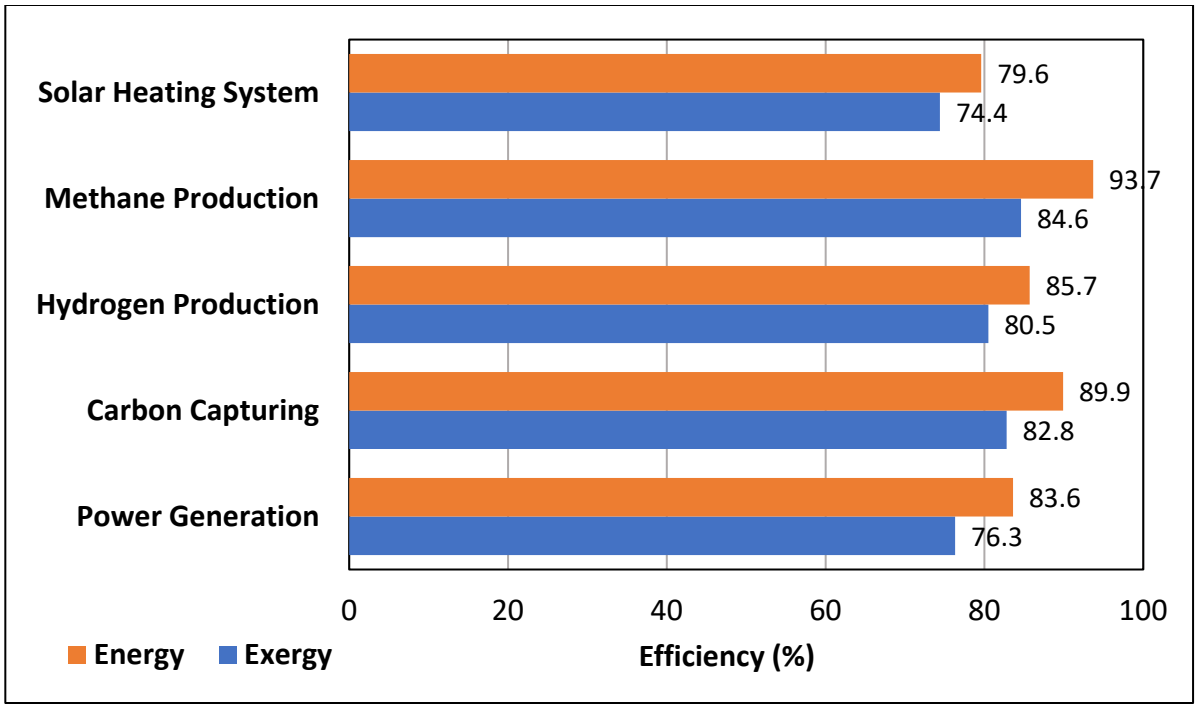

Figure 5.16 Energy and exergy efficiencies of subsystems of system 2

The graphical representation in Figure 5.17 illustrates the relationship between the solar heating rate and the system's performance. It is evident that an increase in heating rates leads to a noticeable reduction in both energy and exergy efficiencies.

This phenomenon may be attributed to the fact that higher temperatures need a greater amount of energy to be sustained, hence diminishing the overall energy efficiency of the system. Moreover, the heightened heat input induces intricate thermodynamic alterations, resulting in augmented exergy dissipation and diminished exergy efficiency, which quantifies the system's capacity to use accessible energy efficiently.

The foregoing pattern underscores the complex elements involved in the performance of our system, hence necessitating more inquiry to enhance the efficiency of sustainable energy consumption.

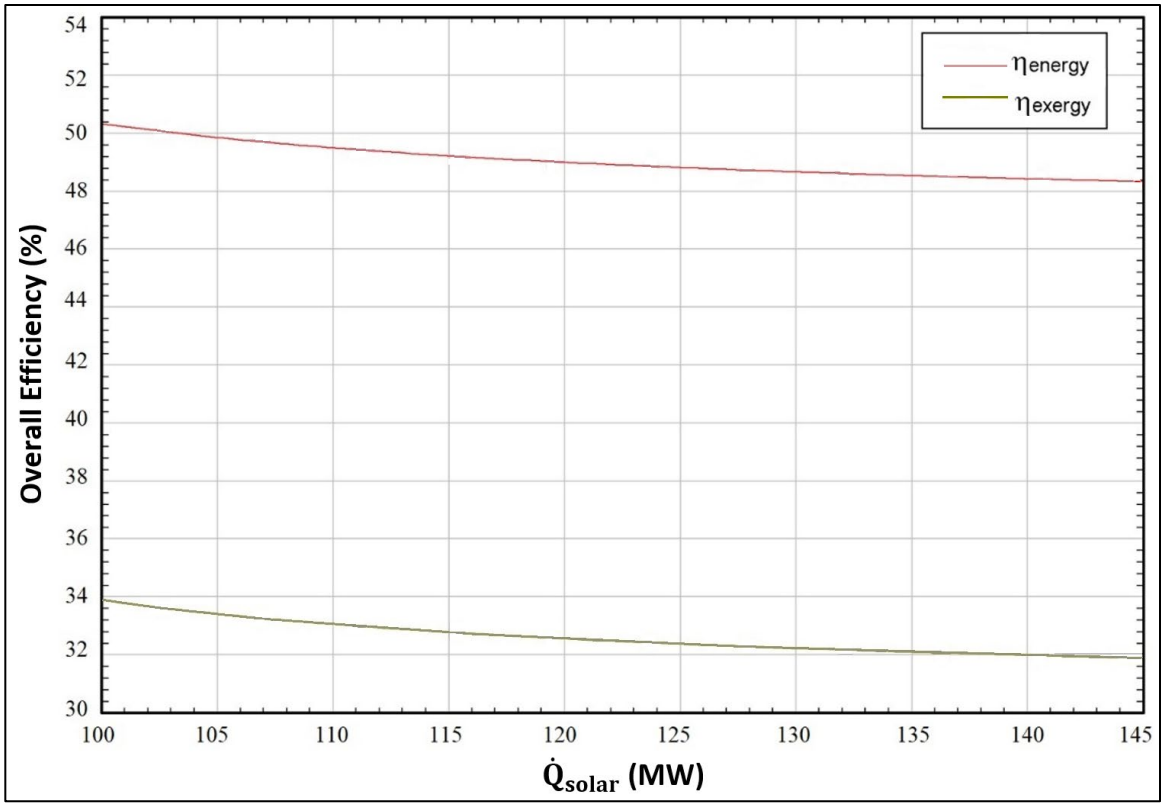

Figure 5.17 Effect of solar heating rate on the overall energy and exergy efficiencies in System 2

Figure 5.18 shows that increased irradiance increases hydrogen and methane emissions. Increases in solar radiation speed up the endothermic reactions necessary to produce hydrogen by Fe-based CLHP, the transformation of methane in steam, and the synthesis of methane via the Sabatier process.

These chemical reactions become energetically advantageous with increasing thermal energy input, resulting in increased hydrogen and methane outputs. This demonstrates how increased thermal energy has a direct impact on reaction efficiency, ultimately leading to increased hydrogen and methane outputs.

Insights about how to improve the system's long-term energy efficiency may be gleaned from the implied relationship between heat inputs and chemical activity.

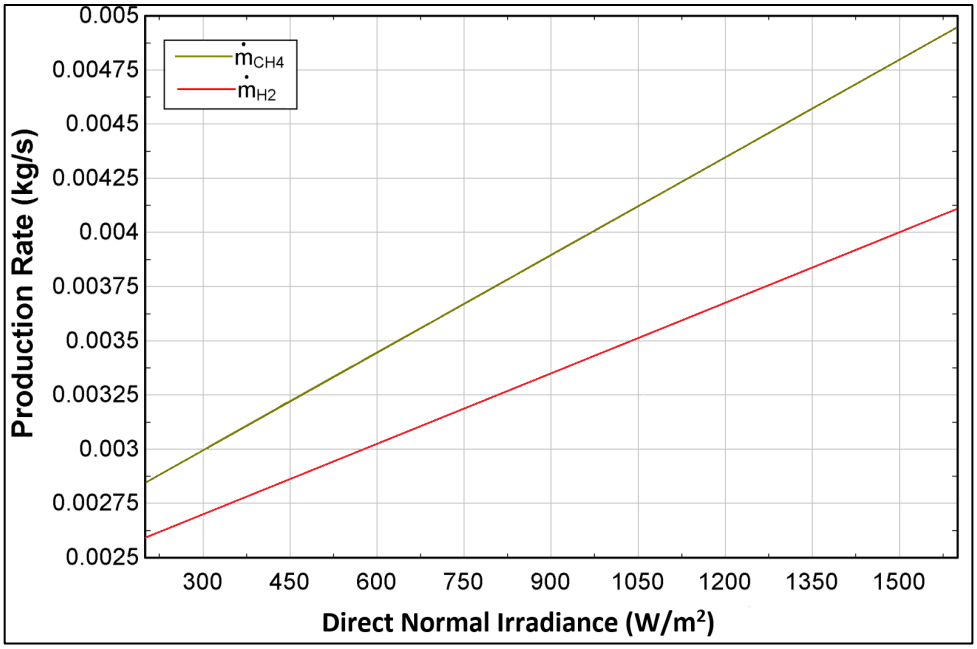

Figure 5.18 Effect of direct normal irradiance on the hydrogen and methane production in system 2

Increasing the concentration of the amine-based solution in the stripper increases carbon capture, as seen in Figure 5.19.

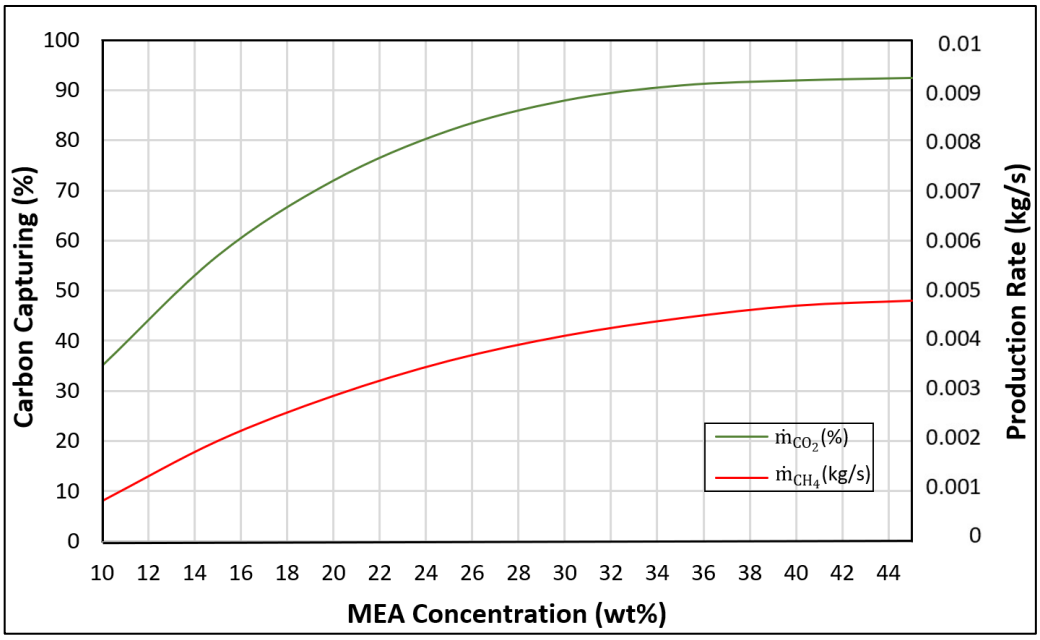

Figure 5.19 Effect of amine-based solution concentration on carbon capturing and methane production rate in system 2

The quantity of methane generated will either increase or decrease in direct proportion to the amount of CO_2. Although it has been shown that increasing concentrations of MEA reduce the rate of carbon absorption, increasing concentrations of MEA also slow down the pace at which methane is produced.

Figure 5.20 displays the effect of the iron oxide input rate in the chemical looping hydrogen production rate. It has been proved that increasing the mass flow rate of iron oxide enhances the hydrogen and carbon produced within the chemical looping. However, the rate of increase gets lower at the higher mass flow rates of iron oxide.

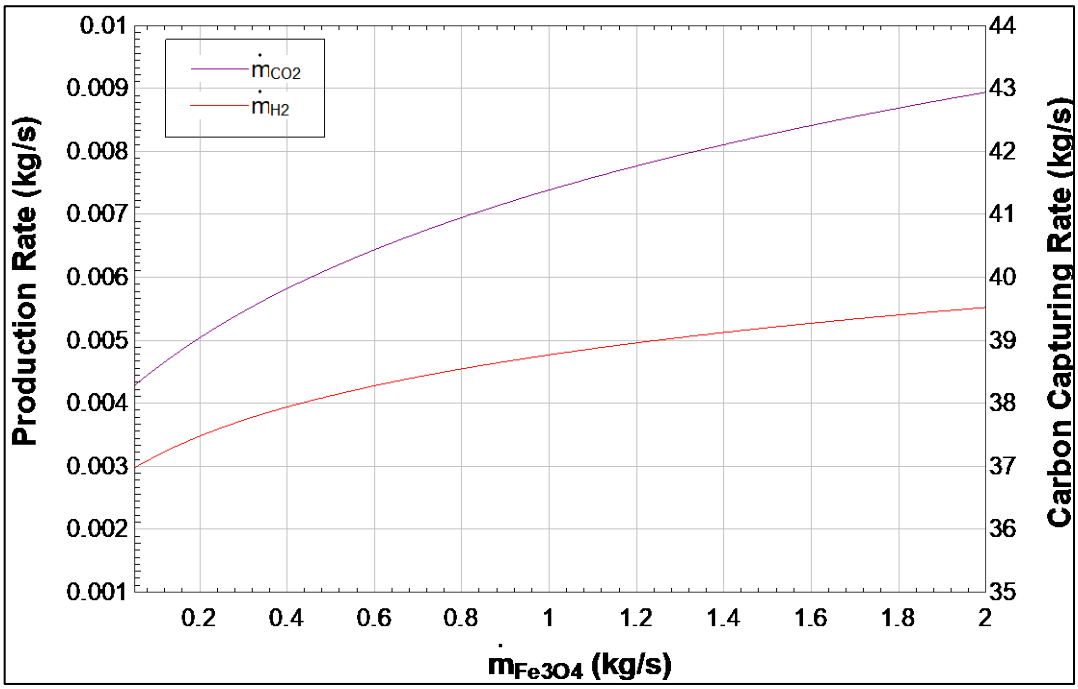

Figure 5.20 Effect of Fe_3O_4 mass flow rate on hydrogen production rate and carbon dioxide capturing rate of system 2

The effect of changing the ambient temperature on the work rate of the gas turbine and steam turbine is shown in Figure 5.21 to help analyze the power generation system. As illustrated, by enhancing the ambient temperature, the work output rate of both turbines decreases.

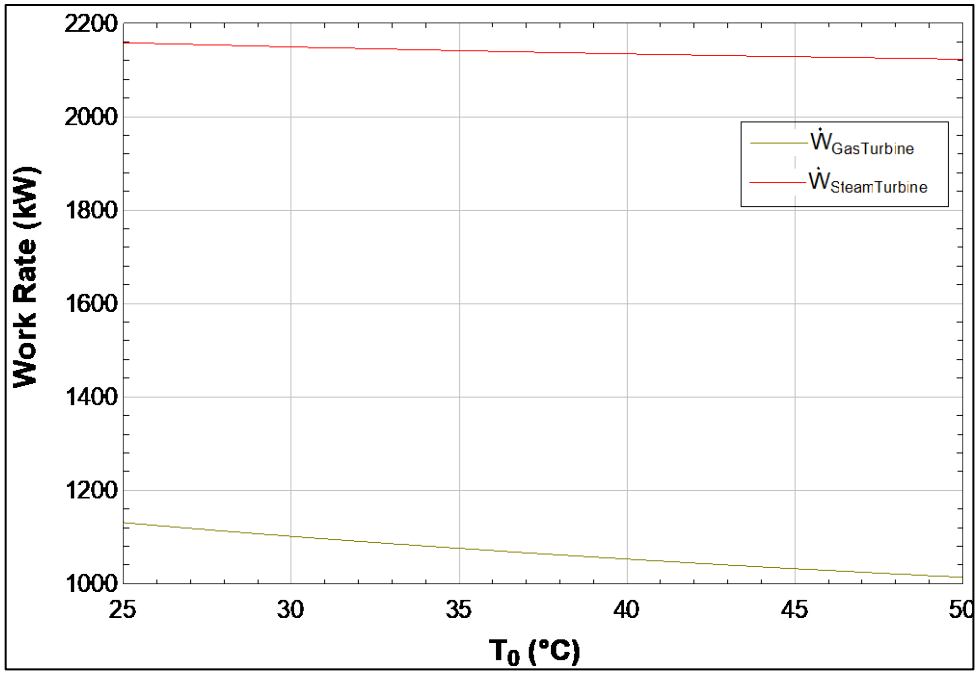

Figure 5.21 Effect of ambient temperature on work rate of different cycles of system 2

The overall energy and exergy efficiency as a function of temperature is shown in Fig. 5.22. Data has been observed to suggest that increasing the ambient temperature will decrease the system's energy and exergy efficiency. Energy efficiency, on the other hand, suffers a far more modest loss in comparison to exergy efficiency.

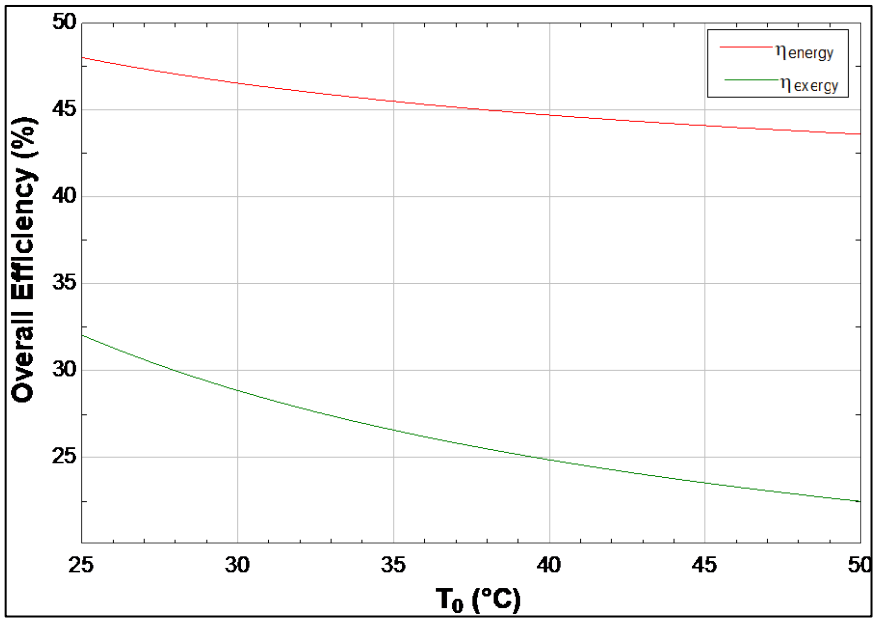

Figure 5.22 Effect of ambient temperature on the overall energy and exergy efficiencies in system 2

At 25℃, it is said that the energy efficiency is 48% and the exergy efficiency is 32%. It has been shown that an increase in temperature leads to a greater loss of exergy. In addition, five distinct subsystems characterized by distinct temperatures have been identified inside this system. There is heat loss, irreversibility, and restricted heat movement between components in each of these subsystems. It is well known that increasing the system's ambient temperature reduces its energy and exergy efficiency.

5.3 System 3 Results

As illustrated in Figure 5.23, elevating the flue gas mass flow rate within a steel production facility leads to a proportional increase in the generation of H_2 and CH_3OH. For instance, when a mere 150 kg/s of flue gas from a steel production facility is introduced into the carbon capturing subsystem, it yields 0.0052 kg/s of hydrogen and 0.0048 kg/s of methanol.

By using the amine-based carbon capturing method after receiving most of the heat of the flue gas by two heat exchangers, it is proved that 120 kg/s of carbon dioxide can be captured from 150 kg/s of flue gas and stored for further use. As shown in Figure 5.23, by increasing the mass flow rate of the flue gas, the rate of carbon capture and the amount of hydrogen and methanol produced will eventually increase.

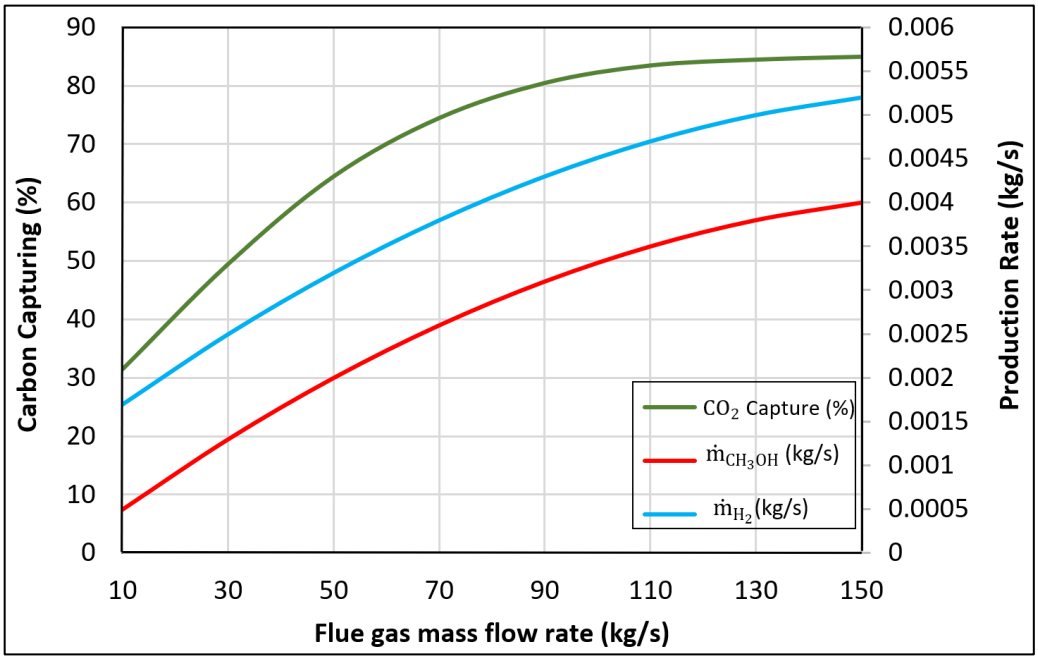

Figure 5.23 Effect of flue gas mass flow rate on carbon capture percent and hydrogen and methanol production rate

Figure 5.24 illustrates the amount of energy and exergy efficiencies within the power generating system, H_2 production system, CO_2 capturing system and CH_3OH production system. It is shown that power generation has the most energy and exergy efficiencies, and hydrogen production has the lowest energy and exergy efficiencies in this system.

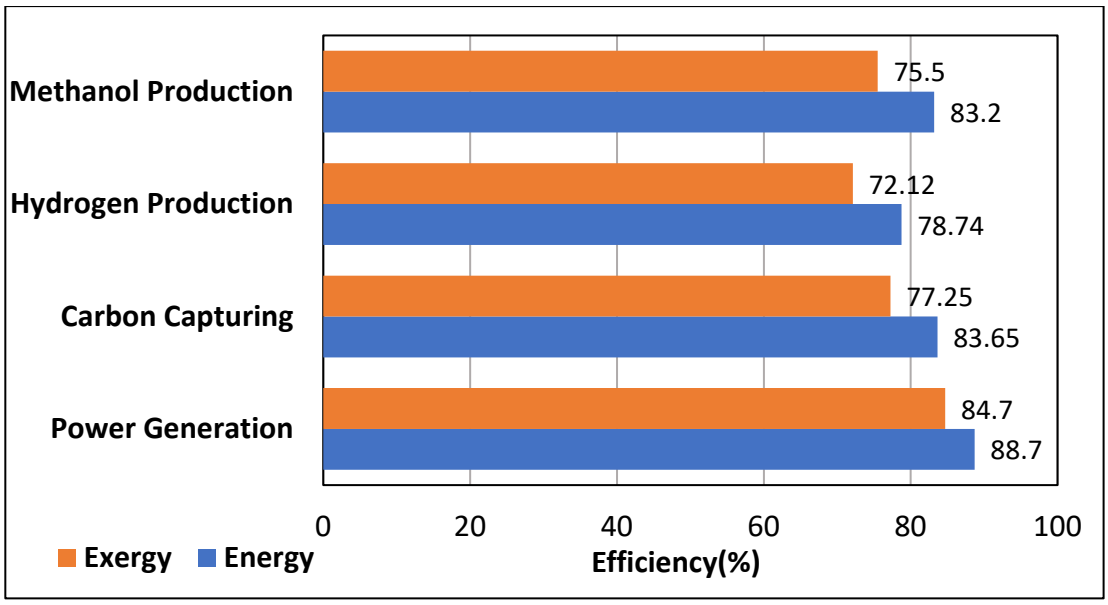

Figure 5.24 Energy and exergy efficiencies of subsystems of system 3

.

Table 5.1 showcases the results of calculations for the production of potable water, hydrogen generation, and the quantity of carbon dioxide sequestered. The calculations detailed in this study are grounded in the foundational assumptions of system 3, which encompasses the following statements:

- The steel manufacturing plant emits flue gas at a rate of 150 kg/s, which comprises both carbon dioxide and carbon monoxide.
- This flue gas has a recorded temperature of 1000 ℃ and a pressure of 101 kPa. Furthermore, the electrolyzer employed for hydrogen production operates with an efficiency of 70% and at a power of 515 kW.
- The multi-stage distillation process utilized for freshwater extraction achieves a recovery ratio of 20%, with an intake rate for saltwater set at 500 kg/s.

Table 5.1 Mass flow rate of system productions

	Mass flow rate (kg/s)
Captured carbon dioxide	120
Total generated hydrogen	0.0052
Electrolyzed hydrogen	0.002
Chemical looping hydrogen produced	0.0032
Methanol Produced	0.0048
Freshwater	100

In the subsequent illustration in Figure 5.25, a comprehensive comparison outlines the precise quantities of electrical output and input across system components. Evidently, the tertiary system encompasses a multitude of elements necessitating electrical supply. Consequently, to accommodate this demand, the power generation sub-structure of the tertiary system integrates three synergistically linked cycles. Notably, the electrical output surpasses the input requisites, providing a surplus that holds potential for subsequent utilization. As it is shown, compressors consume the most work rate, and gas turbines, which are included in the Brayton cycle, produce the most power output, which can alone provide the required work input rate for three compressors.

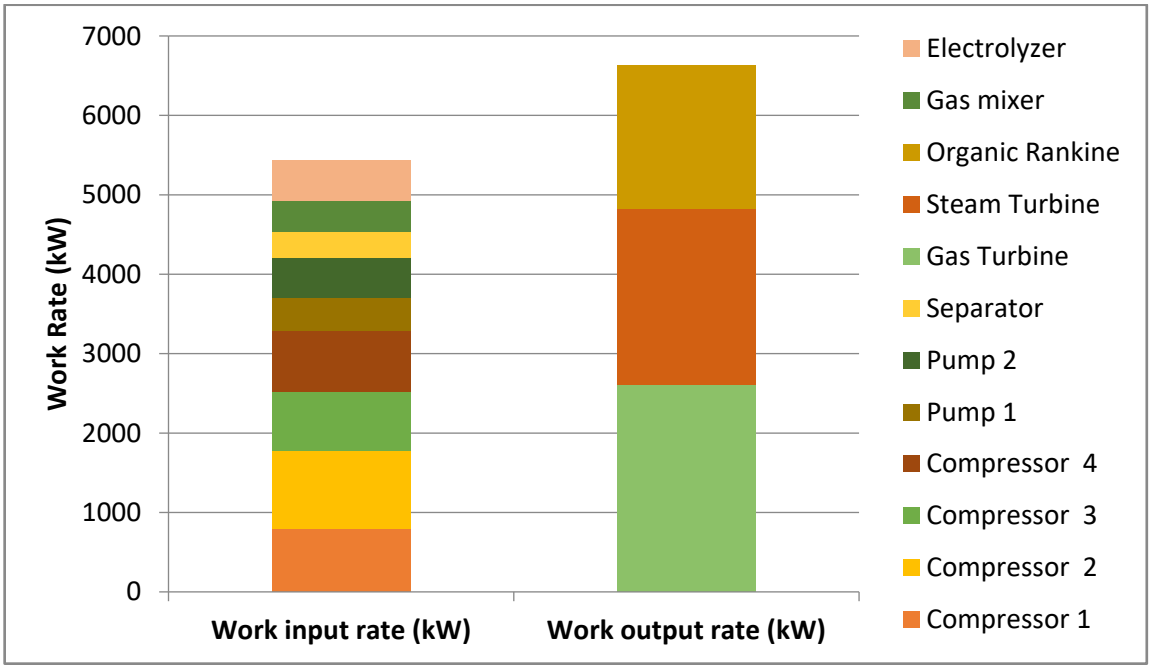

Figure 5.25 Working input and output rate analysis of components of system 3

Figure 5.26 displays the change in work rate in three power generation cycles based on ambient temperature.

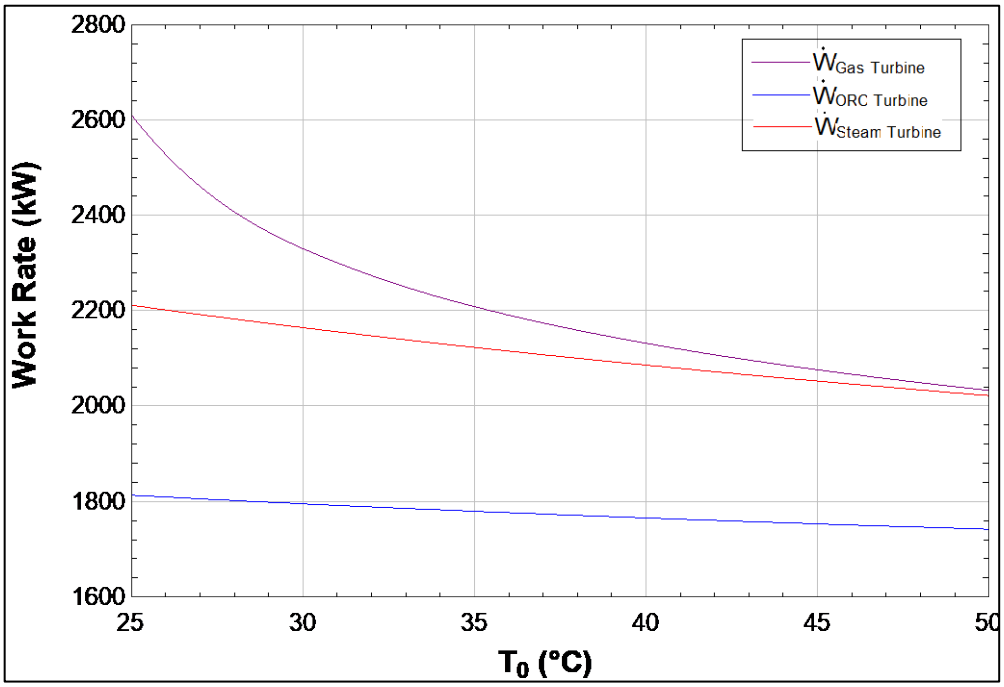

Figure 5.26 Effect of ambient temperature on work rate of different cycles of system 3

As shown in Figure 5.26, the gas turbine has the highest work rate at 25 ℃, but as the ambient temperature increases, the rate of the decrease in its work rate is higher than the other two cycles. On the other hand, the Organic Rankine cycle has the lowest work rate at 25 ℃, but its decrease rate as the ambient temperature goes up is much slower than the other two cyclesThe sustainability of system 3 is also being investigated by calculating all the components and the subsystems exergy destructions.

Figure 5.27 illustrates the percentage of each subsystem's exergy destruction rate within the system. It shows that the chemical looping system has the highest exergy destruction, which will lower its exergy efficiency, and the lowest exergy destruction is for the carbon-capturing system. For a better and deeper investigation of the issue, the range of their change with the change of ambient temperature and flue gas temperature is also determined.

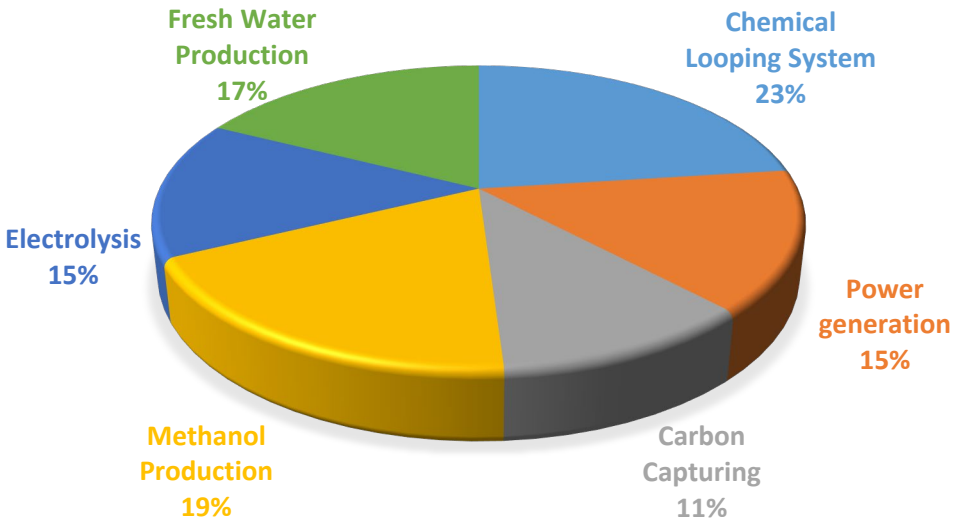

Figure 5.27 Exergy destruction rate of subsystems in system 3

Figure 5.28 illustrates the growth of the exergy destruction rate for each subsystem of system 3 by increasing the ambient temperature from 15 ℃ to 45 Celsius. It is shown that at 25 ℃, the chemical looping hydrogen production has the highest exergy destruction rate with the amount of 103.2 MW, while the carbon capturing subsystem has the lowest exergy destruction rate with the amount of 44.8 MW.

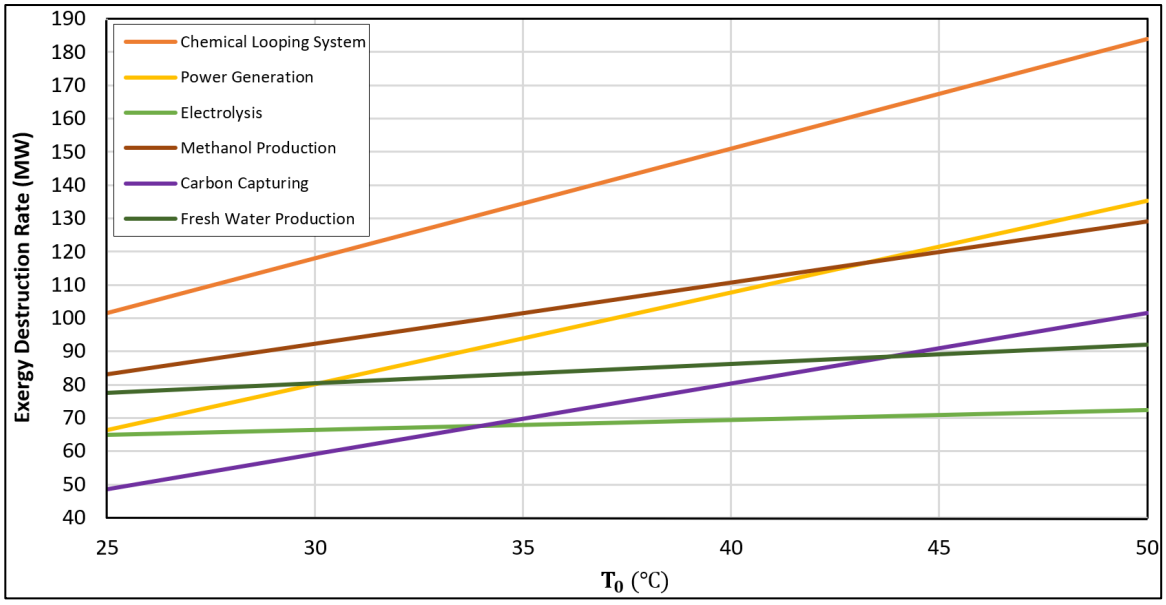

Figure 5.28 Effect of ambient temperature on exergy destruction rate of subsystems in system 3

It is shown that the sustainability of electrolysis and freshwater production is not highly affected by increasing ambient temperature. However, the exergy destructions of all subsystems are increasing as the ambient temperature keeps getting higher.

Increasing the concentration of the amine-based solution in the stripper increases carbon capture, as seen in Figure 5.29. The methanol production rate is based on both hydrogen and carbon dioxide. In this case, since the only affected material is carbon dioxide and hydrogen input, which are the same, the rate of increase in the methanol production rate is lower than the rate of increase in the carbon dioxide itself.

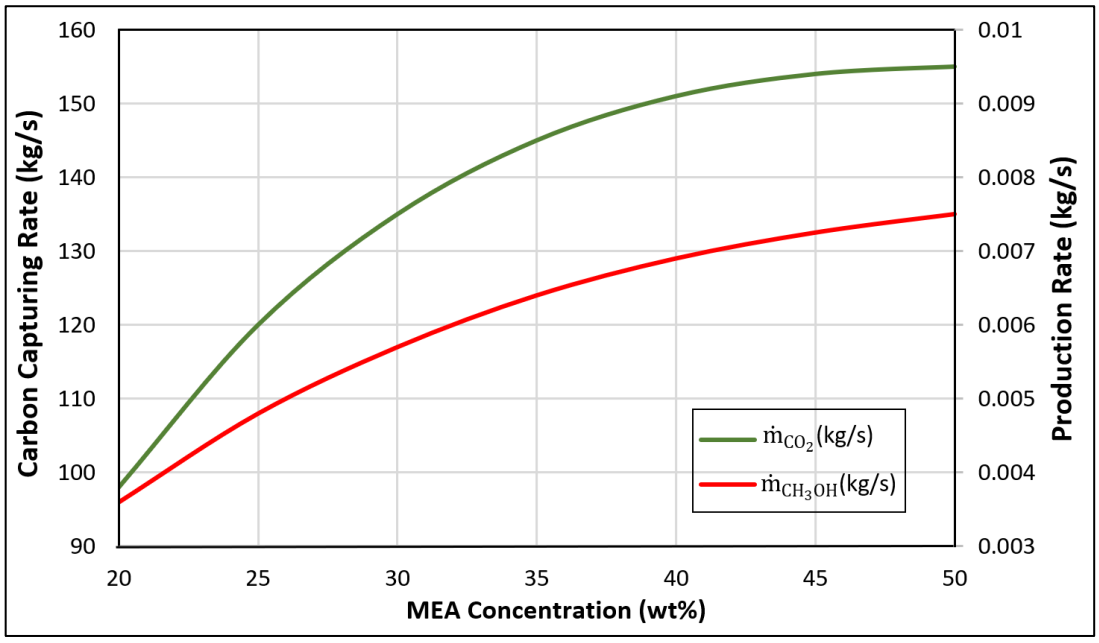

Figure 5.29 Effect of amine-based solution concentration on carbon capturing and methane production rate in system 3

Increasing the concentration of the amine-based solution in the stripper increases carbon capture, as seen in Figure 5.29. The methanol production rate is based on both hydrogen and carbon dioxide. In this case, since the only affected material is carbon dioxide and hydrogen input, which are the same, the rate of increase in the methanol production rate is lower than the rate of increase in the carbon dioxide itself.

In Figure 5.30, the change in the exergy efficiency of subsystems has been investigated by changing the temperature of the flue gas that is coming from the steel production facility. Due to having two heat exchangers before the carbon capturing process, the flue gas

temperature can directly affect the amount of heat received by the power generation cycles by increasing their temperature difference. Also, the reactors in the chemical looping H_2 production subsystem are receiving the heat from one other heat exchanger before the CCS, so by increasing this temperature, the amount of heat received by the hydrogen generation reactor will increase, too.

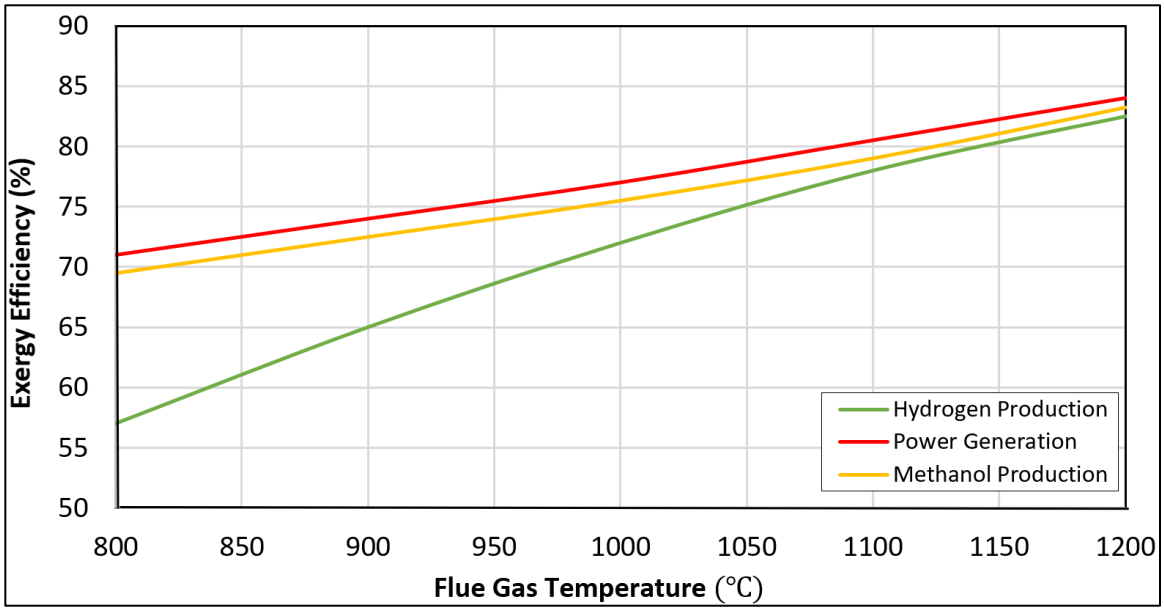

Figure 5.30 Effect of flue gas temperature on exergy efficiency of related subsystems in system 3

Therefore, as it is shown, increasing the flue gas temperature will decrease the exergy efficiency of both the power generation and the hydrogen generation subsystems. Although it is clear that as the temperature goes higher, the rate of increase in exergy efficiency of these two subsystems decreases since after the component reaches a certain optimal point, the heat losses and the material degradation will cause deficiencies, so the exergy efficiency will decrease in those subsystems in higher temperatures. The exergy efficiency of methanol production also shows an improvement but at a diminishing pace.

This outcome may be deemed plausible since methanol is produced by the reaction between hydrogen and carbon dioxide. The quantity of carbon dioxide required for this reaction is far lower than the amount generated, so the decline in exergy efficiency of the carbon capture process will not impact methanol production. Conversely, there is an observed

increase in hydrogen exergy efficiency, which subsequently impacts the exergy efficiency of the methanol-generating subsystem in a similar manner.

On the other hand, in the carbon capturing subsystem, exergy efficiency will be decreased by increasing the temperature. Elevated flue gas temperatures can potentially diminish the effectiveness of some carbon capture solvents, particularly the amine-based carbon capturing process that is used for this system.

This reduction is primarily caused by the risk of solvent degradation and the subsequent rise in energy demands for solvent regeneration. Because of this, the exergy efficiency of the carbon capture process might be reduced as a direct consequence. In system 3, the assumed temperature of flue gas is 1000 ℃. In this temperature, as is also shown in Figure 5.24, the amount of exergy efficiency for carbon capturing, power generation, methanol generation, hydrogen generation and heating system is 77.25%, 84.7%, 75.5%, 72.12 and 96.95%, respectively. Figures 5.31 and 5.32 show the change in all different subsystems based on ambient temperature. By increasing the ambient temperature, the hydrogen production rate and carbon capturing rate will increase, but at the same time, it decreases the rate of freshwater production and its efficiency.

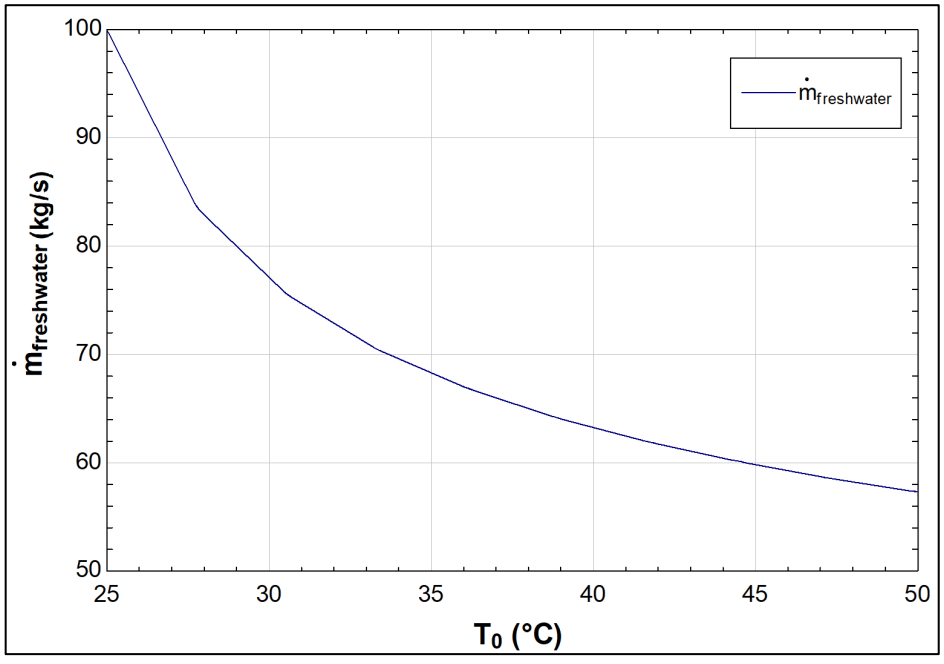

Figure 5.31 Effect of ambient temperature on the freshwater mass flow rate of system 3

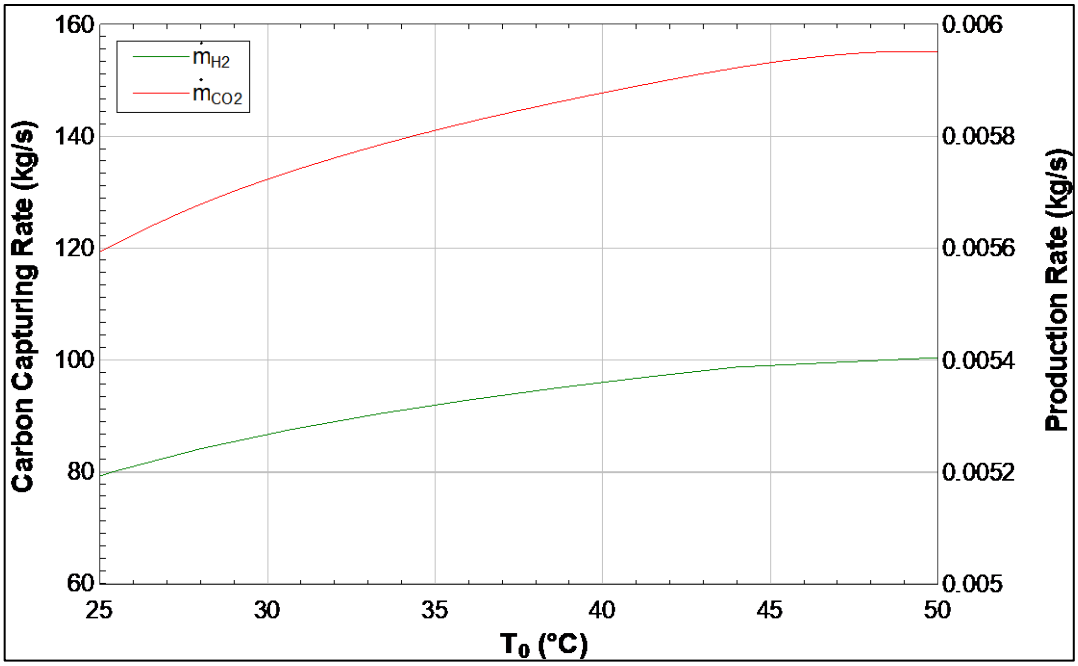

Figure 5.32 Effect of ambient temperature on hydrogen and carbon dioxide mass flow rate of system 3

Figure 5.33 proved that by increasing the mass flow rate of the iron oxide, the hydrogen production rate and carbon capturing rate will increase. However, the rate of increase gets lower at the higher mass flow rates of iron oxide.

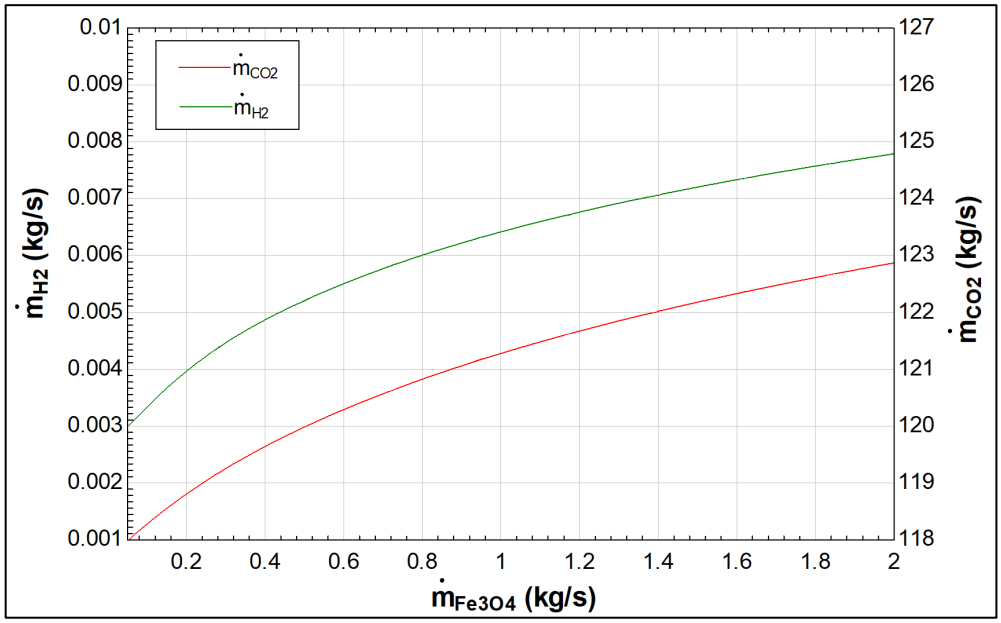

Figure 5.33 Effect of Fe_3O_4 mass flow rate on hydrogen production rate and carbon dioxide capturing rate of system 3

Figure 5.34 illustrates the relationship between temperature and the total energy and exergy efficiency. Empirical evidence indicates a negative correlation between the rise in ambient temperature and the energy and exergy efficiency of the system. In contrast, energy efficiency experiences a much greater degree of loss as compared to exergy efficiency.

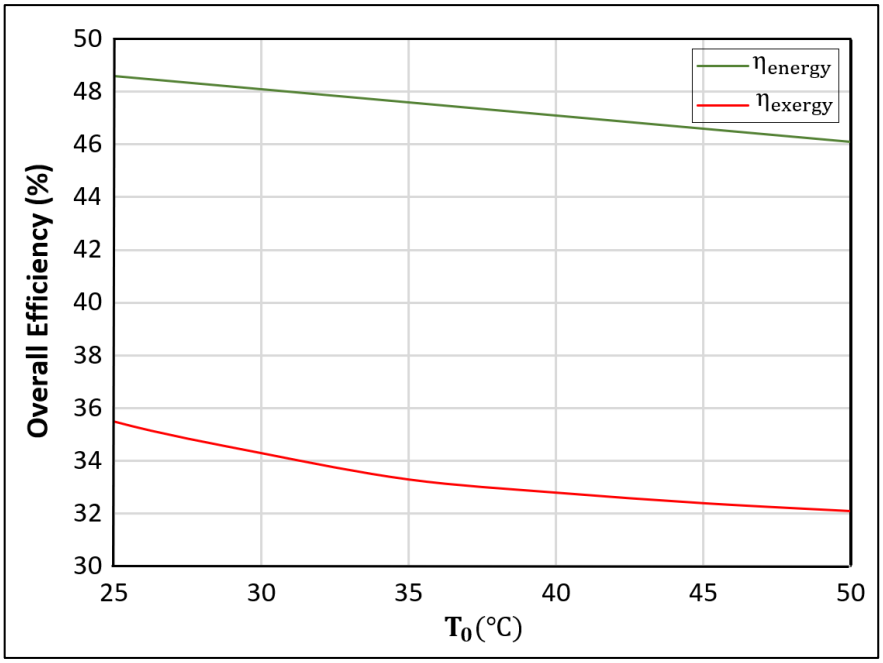

Figure 5.34 Effect of ambient temperature on energy and exergy efficiencies of system 3

According to the literature, at a temperature of 25°C, the energy efficiency is reported to be 48.6%, while the exergy efficiency is documented to be 35.6%. Research has shown that an elevation in temperature results in a heightened dissipation of exergy. Furthermore, it has been determined that there are five separate subsystems inside this system, each distinguished by its own unique temperature. Each of these subsystems experiences heat loss, irreversibility, and limited heat transfer between components. It is well recognized that increasing the ambient temperature of a system leads to a decrease in both its energy and exergy efficiency.

5.4 Systems Comparison, Assessment, and Discussion

As discussed, each system operates under unique assumptions and pathways to achieve the objectives of hydrogen production and carbon capture. In system 1, the integration of plastic waste pyrolysis, a solar heating system, and steam methane reforming defines its

approach. Similarly, system 2 incorporates processes for hydrogen production via steam methane reforming, methane production, and solar heating.

In contrast, system 3 departs from the inclusion of the solar heating system due to its high exergy destruction. Instead, it utilizes heat generated internally to fulfill the thermal requirements of its components. Furthermore, the power generation scheme evolves from the first two systems' Brayton-Rankine cycles to a trio of combined Brayton-Rankine-Organic Rankine cycles, ensuring ample power supply for all system components. Notably, system 3 yields additional products in the form of freshwater and methanol. The final outcomes, encompassing overall energy and exergy efficiencies, hydrogen production rates, and carbon capture rates, are summarized in Table 5.2.

Table 5.2 Final Comparison of 3 Systems

		System 1	System 2	System 3
Energy Efficiency (%)	**Overall**	**27**	**48**	**48.6**
	H_2 Production	56.38	85.7	78.74
	Carbon Capturing	98.8	89.9	83.65
	Power Generation	65.5	83.6	88.7
	Heating System	73.22	79.6	98.62
Exergy Efficiency (%)	**Overall**	**25**	**32.1**	**35.2**
	H_2 Production	52.62	80.5	72.12
	Carbon Capturing	98.39	82.8	77.25
	Power Generation	68.9	76.3	84.7
	Heating System	69.4	74.4	96.95
Other renewable energy utilization/productions		-plastic waste pyrolysis with 85.6% exergy efficiency -Solar tower heating system	-Methane production with 84.6% exergy efficiency -Solar tower heating system	-Methanol production with 75.5% exergy efficiency -Freshwater production

It is evident that although theoretically, system 1 achieves significantly higher rates of hydrogen and carbon dioxide production than systems 2 and 3, its energy and exergy efficiencies are lower than the other two systems. System 2 has higher H_2 production and carbon capturing efficiencies than system 3, but due to its lower heating system and power generation compared to system 3, system 2 has lower overall energy and exergy

efficiencies. Comparing these systems is challenging due to differing assumptions, components, designs, and state point parameters. Nevertheless, each system successfully attains its goal of enhancing energy and exergy efficiencies.

The study's validation was founded on the thorough application of thermodynamic principles, including mass, energy, exergy, and entropy balancing equations. These fundamental equations were rigorously included in each stage of the system design process, assuring conformance to recognized thermodynamic rules. The computational study was performed utilizing two advanced software tools, EES (Engineering Equation Solver) and Aspen Plus, which are well-known for their reliability in process simulation and optimization.

The input data and modelling technique were repeatedly verified for integrity using the rigorous error detection algorithms of these software platforms. If there were any departures from thermodynamic principles or contradictions in the data, computational errors would have occurred, which would have halted the progress of the simulations. The processes were implemented perfectly in both EES and Aspen Plus, with no errors. This was a key validation mechanism that showed the procedures used were correct and the results could be trusted, which is based on the careful application of thermodynamic rules and verified using potent simulation tools, emphasizing the study's dependability and integrity.

The primary benefit of integrating sub-systems to create a multigeneration system compared to keeping systems separated pertains to efficiencies of the multigeneration system and the individual systems. For instance, if a system is modelled to have a single output of electrical power through the implementation of a conventional Rankine cycle, a substantial amount of energy will be wasted when heat is dissipated from the condenser. However, if a Rankine system were to be integrated with another system which is capable of harnessing the heat released to produce an additional useful output, the thermal energy previously dissipated by the condenser would no longer be considered wasted. System 3 combines a Rankine cycle with a multi-effect desalination sub-system linked by a heat exchanger. The heat exchanger works simultaneously as a condenser for the Rankine cycle and as a heater for the desalination system. Furthermore, this concept of integration can be

highly beneficial from a cost standpoint. Although multigeneration systems can be considered expensive to construct, they would likely be more economical to develop than generating all sub-systems separately. For example, the total cost to purchase and operate two heat exchangers (one operating as a condenser and the other as a heating exchanger) would be more expensive than a single heat exchanger operating both simultaneously.

Upon further examination of the cost analysis, it becomes evident that the integrated multigeneration system offers substantial long-term economic benefits, specifically in terms of operational and maintenance expenditures. Unlike isolated systems, the unified approach used in multigenerational systems maximizes resource usage, resulting in lower operational costs. For example, shared infrastructure, such as a single heat exchanger serving two uses, reduces both original capital investment and maintenance expenses. This consolidation results in fewer components that require frequent repair and maybe replacement, lowering the overall maintenance expense. Furthermore, the increased energy efficiency inherent in these integrated systems results in lower fuel consumption and, as a result, lower operational costs during the system's lifetime. This efficiency advantage is particularly relevant in energy-intensive processes such as desalination, where the synergistic impact of shared heat sources may significantly reduce energy needs. While the initial investment in a multigeneration system may be costlier, the cumulative cost savings realized via enhanced efficiency and decreased operations and maintenance expenditures make it a financially feasible and sustainable solution over time. This economic practicality, along with the environmental benefits of increased efficiency, puts multigeneration systems as a superior environmental and economical alternative to traditional, separated systems.

In a comparative analysis with related works, the performance of the newly designed systems stands out, especially in the domains of hydrogen and methane generation coupled with carbon capture. This comparison delineates a noteworthy progression beyond the existing scholarly contributions in this area. The research by Ishaq and Dincer [47] delineates a scenario where hydrogen is generated through a solar heating mechanism and a combined power cycle, achieving energy and exergy efficiencies of 29.9% and 31.5%, respectively. In a similar vein, Siddiqui et al. [74] demonstrated a system harnessing solar

and geothermal energy to produce hydrogen, electricity, and cooling, resulting in energy and exergy efficiencies of 19.6% and 19.1%, respectively. Contrastingly, the innovative design of the second system under study showcases remarkable energy and exergy efficiencies of 48% and 32%, respectively. Additionally, a third system exhibits high efficiencies of 35.6% and 48.6% in energy and exergy, respectively. This system is notable for its multifaceted design encompassing five subsystems. These subsystems are adept at producing not only methane and methanol but also freshwater, alongside hydrogen production, carbon capture, and power generation. Systems 1 and 2 are further enhanced by the integration of solar tower heating, which is categorized under renewable energy sources. Notably, system 1 incorporates a plastic waste pyrolysis process for methane generation, augmenting its sustainability quotient. This substantial improvement is attributed to the strategic optimization through integration with other subsystems focused on methane production and carbon dioxide capture. These comparative insights underscore the efficiency and scalability potential of the proposed system modifications in the realm of sustainable energy production.

Chapter 6. Conclusions and Recommendations

This chapter provides a concise overview of the primary outcomes, conclusions, and findings derived from the present thesis. On the basis of these results, suggestions for further research are made.

6.1 Conclusions

In the present thesis, three unique integrated chemical looping hydrogen production and carbon capturing systems have been presented to investigate the energy aspects of using chemical looping for hydrogen production as well as carbon capturing. Each system is individually integrated with two other renewable sources to achieve the highest efficiency in the most sustainable manner.

- In System 1, the Fe-based CLHP and SMR methods are used simultaneously to produce hydrogen and capture the carbon dioxide within the system. This system uses plastic waste pyrolysis as an input to provide the methane for the CLHP subsystem. The solar heating system and Brayton-Rankine cycle are integrated into this system to supply the system with heat and electricity. The key findings from System 1 analysis are:
- The overall energy and exergy efficiencies are found to be 27% and 25%, respectively. The chemical looping subsystem has the lowest energy and exergy efficiency of 56.38% and 52.62% respectively. The power generation energy and exergy efficiencies are 65.6% and 68.9%, respectively, and the solar heating system has the highest energy and exergy efficiencies, which are 73.22% and 69.4%, respectively.
- At the ambient temperature of 25℃, for 11.5 kg/s polypropylene, 10.5 kg/s H_2will be produced, and 1120 kg/s CO_2will be captured.
- The total heat rate produced by the solar system is 3303.3 kW, which supplies all the required heat of the system.
- The gas and steam turbine from the combined Brayton-Rankine cycle supply the total network output of the system, which has work rates of 1015 kW and 526.5 kW, respectively.

In System 2, hydrogen and methane are produced along with capturing carbon from the flue gas of a coal power plant using an amine solution simultaneously. Fe-based CLHP and

SMR are used in tandem to produce hydrogen. Methane is produced from the stored hydrogen and carbon dioxide. Similar to System 1, a solar heating system and a Brayton-Rankine cycle are used to provide the heat and power of the system. The highlights of System 2 are:

- At the ambient temperature of 25℃, The system achieved overall energy and exergy efficiencies of 48% and 32%, respectively.
- The $\dot{E}x_d$ of the solar tower, the power generation and the combined hydrogen production system are 97.7 MW, 74.76 MW and 67.5 MW, resulting in a lower exergy utilization efficiency. The CCS subsystem only has the $\dot{E}x_d$ of 56.4 MW, and the least $\dot{E}x_d$of 37.4 MW belongs to methane production.
- The system is capable of generating hydrogen at a rate of 0.004 kg/s and methane at a rate of 0.0048 kg/s, considering the solar heating rate as 147 MW at 25 ℃ calculated by using irradiance as 1.5 kW/m^2 and 100 heliostats with the area as 35×35 m^2 and 80% efficiency for a solar heating subsystem.
- At irradiance of 1.5 kW/m^2, the hydrogen mass flow rate is 0.004 kg/s, where 0.0008 kg/s of hydrogen is produced by the SMR method, and 0.0032 kg/s of the rest is produced by the CLHP method.
- The produced methane mass flow rate is 0.0048 kg/s. The captured carbon dioxide by using 50 kg/s of flue gas at 250 ℃ in the amine-based process is 40 kg/s.
- In the 45% concentration of the amine-based solution, the methane flow rate is 0.0048 kg/s, and the carbon capture system has 80% carbon absorption.

System 3 uses Fe-based CLHP with electrolysis methods to produce hydrogen. Carbon is captured from the flue gas of a steel production facility, and the heat is captured from the flue gas by heat exchangers to provide the required heat for the system. Methanol and freshwater are also produced within the system, as well as electricity, by using three combined Brayton-Rankine-ORC power cycles. At the ambient temperature of 25℃, the system achieved overall energy and exergy efficiencies of 48.6% and 35.6%, respectively.

- At the temperature of 1000 ℃ of flue gas, the amount of exergy efficiency for carbon capturing, power generation, methanol generation, hydrogen generation and heating system is 77.25%, 84.7%, 75.5%, 72.12 and 96.95%, respectively.

- The Fe-based CLHP subsystem has the maximum exergy destruction rate, which is 103.2 MW, while the carbon-capturing subsystem has the lowest exergy destruction rate, which is 44.8 MW.
- Using 150 kg/s of flue gas from a steel production facility, which is introduced into the carbon capturing subsystem, produces 0.0052 kg/s of hydrogen, where 0.002 kg/s of the hydrogen is from electrolysis and 0.0032 kg/s of it from CLHP. Also, 120 kg/s of carbon dioxide is then captured from 150 kg/s from the amine-based process. After that, 0.0048 kg/s of methanol is then produced from the stored CO_2 and H_2.
- 100 kg/s of freshwater is also produced by the desalination of 500 kg/s of seawater.

6.2 Recommendations

The presented thesis provides the design of three distinct and novel multigeneration systems capable of producing numerous useful outputs while simultaneously capturing carbon dioxide. Given that the project's scope was limited to modelling the systems and conducting energy and exergy analyses, several recommendations can be made to advance these studies further. The recommendations of this thesis are presented as follows:

- Expanding the study to include exergoeconomic analysis. Conducting an exergoeconomic analysis will aid in determining the financial feasibility of the project overall. The study should consist of the financial investment of purchasing various system components and the cost to operate the components.
- The integration of a multi-objective optimization study based on the presented multigeneration systems to identify the suitable conditions to minimize the exergy destruction rates without also compromising the practicality or capabilities of the current systems.
- The investigation of using alternative carbon capture technologies and exploring the feasibility of alternative options which are not amine-based. These alternative techniques would include membrane separation and calcium or chemical looping.
- Determining the sustainability of the proposed systems through adding life-cycle analyses. The life cycle analyses could be categorized into three stages (manufacturing, end of life, and transportation). The damage to existing ecosystems

and potential health consequences for people and wildlife will also be measured by considering factors such as toxicity.

- The fabrication of an experimental prototype and setup will serve as a laboratory-scale reactor and system. The physical prototype's construction will have the potential to validate simulated results.

Bibliography

[1] B. Dutcher, M. Fan, and A. G. Russell, “Amine-based CO2 capture technology development from the beginning of 2013-A review,” ACS Appl. Mater. Interfaces, vol. 7, no. 4, pp. 2137–2148, 2015, doi: 10.1021/am507465f.

[2] J. Krane, “Climate change and fossil fuel: An examination of risks for the energy industry and producer states,” MRS Energy and Sustainability, vol. 4, no. 1. Springer Nature, Dec. 01, 2017. doi: 10.1557/mre.2017.3.

[3] Z. F. Toprak, N. Hamidi, Ş. Toprak, and Z. Şen, "Climatic identity assessment of the climate change," International Journal of Global Warming, vol. 5, no. 1, p. 30, 2013, doi: 10.1504/IJGW.2013.051480.

[4] L. Stougie and H. J. Van Der Kooi, “Exergy and sustainability,” International Journal of Exergy, vol. 11, no. 4, p. 508, 2012, doi: 10.1504/IJEX.2012.050259.

[5] https://www.iea.org/data-and-statistics/data-product/greenhouse-gas-emissions-fromenergy#documentation (Accessed October27, 2023)

[6] C. Acar and I. Dincer, "The potential role of hydrogen as a sustainable transportation fuel to combat global warming," Int J Hydrogen Energy, vol. 45, no. 5, pp. 3396–3406, Jan. 2020, doi: 10.1016/j.ijhydene.2018.10.149.

[7] A. Sayigh, “Renewable energy — the way forward,” Appl Energy, vol. 64, no. 1–4, pp. 15–30, Sep. 1999, doi: 10.1016/S0306-2619(99)00117-8.

[8] U. Hamid, A. Rauf, U. Ahmed, Md. Selim Arif Sher Shah, and N. Ahmad, “Techno-economic assessment of process integration models for boosting hydrogen production potential from coal and natural gas feedstocks,” Fuel, vol. 266, p. 117111, Apr. 2020, doi: 10.1016/j.fuel.2020.117111.

[9] Z. Liang et al., “Recent progress and new developments in post-combustion carbon-capture technology with amine based solvents,” Int. J. Greenh. Gas Control, vol. 40, pp. 26–54, 2015, doi: 10.1016/j.ijggc.2015.06.017.

[10] Song C. Global challenges and strategies for control, conversion and utilization of CO2 for sustainable development involving energy, catalysis, adsorption and chemical processing. Catal Today 2006;115:2–32. https://doi.org/10.1016/j.cattod.2006.02.029.

[11] E. Kötter, L. Schneider, F. Sehnke, K. Ohnmeiss, and R. Schröer, “The future electric power system: Impact of Power-to-Gas by interacting with other renewable energy components,” J Energy Storage, vol. 5, pp. 113–119, Feb. 2016, doi: 10.1016/j.est.2015.11.012

[12] H. Allouhi, A. Allouhi, K. M. Almohammadi, A. Hamrani, and A. Jamil, "Hybrid renewable energy system for sustainable residential buildings based on Solar Dish Stirling and wind Turbine with hydrogen production," Energy Convers Manag, vol. 270, p. 116261, Oct. 2022, doi: 10.1016/j.enconman.2022.116261.

[13] D. Bessarabov et al., "South African hydrogen infrastructure (HySA infrastructure) for fuel cells and energy storage: Overview of a projects portfolio," Int J Hydrogen Energy, vol. 42, no. 19, pp. 13568–13588, May 2017, doi: 10.1016/j.ijhydene.2016.12.140

[14] G. Cipriani et al., "Perspective on hydrogen energy carrier and its automotive applications," Int J Hydrogen Energy, vol. 39, no. 16, pp. 8482–8494, May 2014, doi: 10.1016/j.ijhydene.2014.03.174.

[15] D. Çelik and M. Yıldız, "Investigation of hydrogen production methods in accordance with green chemistry principles," Int J Hydrogen Energy, vol. 42, no. 36, pp. 23395–23401, Sep. 2017, doi: 10.1016/j.ijhydene.2017.03.104.

[16] A. Sami, M. Mehrpooya, and A. Noorpoor, "Investigation of an integrated thermochemical hydrogen production and high temperature solar thermochemical energy storage and CO2 capture process," Appl Therm Eng, vol. 214, p. 118820, Sep. 2022, doi: 10.1016/j.applthermaleng.2022.118820

[17] Hydrogen Council, "Path to Hydrogen Competitiveness: A Cost Perspective", a global report published on 20 January 2020, available at https://hydrogencouncil.com/wp-content/uploads/2020/01/Path-to-Hydrogen-Competitiveness_Full-Study-1.pdf.

[18] X. Zhao et al., "Thermo-economic analysis of a novel hydrogen production system using medical waste and biogas with zero carbon emission," Energy, vol. 265, p. 126333, Feb. 2023, doi: 10.1016/j.energy.2022.126333.

[19] N. Muradov and T. Veziroglu, "'Green' path from fossil-based to hydrogen economy: An overview of carbon-neutral technologies," Int J Hydrogen Energy, vol. 33, no. 23, pp. 6804–6839, Dec. 2008, doi: 10.1016/j.ijhydene.2008.08.054.

[20] F. Safari and I. Dincer, "Development and analysis of a novel biomass-based integrated system for multigeneration with hydrogen production," Int J Hydrogen Energy, vol. 44, no. 7, pp. 3511–3526, Feb. 2019, doi: 10.1016/j.ijhydene.2018.12.101.

[21] L. Heng, R. Xiao, and H. Zhang, "Life cycle assessment of hydrogen production via iron-based chemical-looping process using non-aqueous phase bio-oil as fuel," International Journal of Greenhouse Gas Control, vol. 76, pp. 78–84, Sep. 2018, doi: 10.1016/j.ijggc.2018.06.020.

[22] P. Moriarty and D. Honnery, "Can renewable energy power the future?," Energy Policy, vol. 93, pp. 3–7, Jun. 2016, doi: 10.1016/j.enpol.2016.02.051.

[23] H. Liu and S. Liu, “Life cycle energy consumption and GHG emissions of hydrogen production from underground coal gasification in comparison with surface coal gasification,” Int J Hydrogen Energy, vol. 46, no. 14, pp. 9630–9643, Feb. 2021, doi: 10.1016/j.ijhydene.2020.12.096.

[24] A. I. Osman et al., “Hydrogen production, storage, utilisation and environmental impacts: a review,” Environ Chem Lett, vol. 20, no. 1, pp. 153–188, Feb. 2022, doi: 10.1007/s10311-021-01322-8.

[25] D. Erdemir and I. Dincer, “Development and assessment of a novel hydrogen storage unit combined with compressed air energy storage,” Appl Therm Eng, vol. 219, p. 119524, Jan. 2023, doi: 10.1016/j.applthermaleng.2022.119524.

[26] S. Cloete, O. Ruhnau, J. H. Cloete, and L. Hirth, “Blue hydrogen and industrial base products: The future of fossil fuel exporters in a net-zero world,” J Clean Prod, vol. 363, p. 132347, Aug. 2022, doi: 10.1016/j.jclepro.2022.132347.

[27] I. Staffell et al., “The role of hydrogen and fuel cells in the global energy system,” Energy Environ Sci, vol. 12, no. 2, pp. 463–491, 2019, doi: 10.1039/C8EE01157E.

[28] Nikolaidis P, Poullikkas A. A comparative overview of hydrogen production processes. Renewable and Sustainable Energy Reviews 2017;67:597–611. https://doi.org/10.1016/J.RSER.2016.09.044.

[29] R. Chaubey, S. Sahu, O. O. James, and S. Maity, “A review on development of industrial processes and emerging techniques for production of hydrogen from renewable and sustainable sources,” Renewable and Sustainable Energy Reviews, vol. 23, pp. 443–462, Jul. 2013, doi: 10.1016/j.rser.2013.02.019.

[30] Y. Lang, R. R. Arnepalli, and A. Tiwari, “A Review on Hydrogen Production: Methods, Materials and Nanotechnology,” J Nanosci Nanotechnol, vol. 11, no. 5, pp. 3719–3739, May 2011, doi: 10.1166/jnn.2011.4157.

[31] L. Barelli, G. Bidini, F. Gallorini, and S. Servili, “Hydrogen production through sorption-enhanced steam methane reforming and membrane technology: A review,” Energy, vol. 33, no. 4, pp. 554–570, Apr. 2008, doi: 10.1016/j.energy.2007.10.018.

[32] Graves C, Ebbesen SD, Mogensen M, Lackner KS. Sustainable hydrocarbon fuels by recycling CO2 and H2O with renewable or nuclear energy. Renewable and Sustainable Energy Reviews 2011;15:1–23. https://doi.org/10.1016/J.RSER.2010.07.014.

[33] J. Fan, L. Zhu, P. Jiang, L. Li, and H. Liu, “Comparative exergy analysis of chemical looping combustion thermally coupled and conventional steam methane reforming for hydrogen production,” J Clean Prod, vol. 131, pp. 247–258, Sep. 2016, doi: 10.1016/j.jclepro.2016.05.040.

[34] A. B. Hamzah, R. C. Awang, S. Haryati, and M. D. Bustan, “Exergetic evaluation and optimisation of primary methane steam reformer,” International Journal of Exergy, vol. 35, no. 4, p. 484, 2021, doi: 10.1504/IJEX.2021.117053.

[35] G. Guan, M. Kaewpanha, X. Hao, and A. Abudula, “Catalytic steam reforming of biomass tar: Prospects and challenges,” Renewable and Sustainable Energy Reviews, vol. 58, pp. 450–461, May 2016, doi: 10.1016/j.rser.2015.12.316.

[36] P. Parthasarathy and K. S. Narayanan, “Hydrogen production from steam gasification of biomass: Influence of process parameters on hydrogen yield – A review,” Renew Energy, vol. 66, pp. 570–579, Jun. 2014, doi: 10.1016/j.renene.2013.12.025.

[37] J. A. Medrano et al., “The membrane-assisted chemical looping reforming concept for efficient H2 production with inherent CO2 capture: Experimental demonstration and model validation,” Appl Energy, vol. 215, pp. 75–86, Apr. 2018, doi: 10.1016/j.apenergy.2018.01.087.

[38] J. C. Abanades et al., “Emerging CO2 capture systems,” International Journal of Greenhouse Gas Control, vol. 40, pp. 126–166, Sep. 2015, doi: 10.1016/j.ijggc.2015.04.018.

[39] Y. Zhao, B. Jin, X. Luo, and Z. Liang, “Thermodynamic evaluation and experimental investigation of CaO-assisted Fe-based chemical looping reforming process for syngas production,” Appl Energy, vol. 288, p. 116614, Apr. 2021, doi: 10.1016/j.apenergy.2021.116614.

[40] K. Anaya, A. Olufemi Oni, and A. Kumar, “Investigating the techno-economic and environmental performance of chemical looping technology for hydrogen production,” Sustainable Energy Technologies and Assessments, vol. 56, p. 103008, Mar. 2023, doi: 10.1016/j.seta.2022.103008.

[41] S. G. Gopaul, A. Dutta, and R. Clemmer, “Chemical looping gasification for hydrogen production: A comparison of two unique processes simulated using ASPEN Plus,” Int J Hydrogen Energy, vol. 39, no. 11, pp. 5804–5817, Apr. 2014, doi: 10.1016/j.ijhydene.2014.01.178.

[42] G. Wei et al., “Syngas production from lignite via chemical looping gasification with hematite oxygen carrier enhanced by exogenous metals,” Fuel, vol. 321, p. 124119, Aug. 2022, doi: 10.1016/j.fuel.2022.124119.

[43] H. Nami, A. Anvari-Moghaddam, and A. Nemati, “Modelling and analysis of a solar boosted biomass-driven combined cooling, heating and power plant for domestic applications,” Sustainable Energy Technologies and Assessments, vol. 47, p. 101326, Oct. 2021, doi: 10.1016/j.seta.2021.101326.

[44] L. Rath, V. Chou, and N. Kuehn, “Assessment of Hydrogen Production with CO₂ Capture Volume 1: Baseline State-of-the-Art Plants (Final Report),” Nov. 2011. doi: 10.2172/1767148.

[45] C.-C. Cormos, “Evaluation of iron based chemical looping for hydrogen and electricity co-production by gasification process with carbon capture and storage,” Int J Hydrogen Energy, vol. 35, no. 6, pp. 2278–2289, Mar. 2010, doi: 10.1016/j.ijhydene.2010.01.033.

[46] O. Oruc and I. Dincer, “Evaluation of hydrogen production with iron-based chemical looping fed by different biomass,” Int J Hydrogen Energy, vol. 45, no. 60, pp. 34557–34565, Dec. 2020, doi: 10.1016/j.ijhydene.2020.04.119.

[47] H. Ishaq and I. Dincer, “Design and performance evaluation of a new biomass and solar based combined system with thermochemical hydrogen production,” Energy Convers Manag, vol. 196, pp. 395–409, Sep. 2019, doi: 10.1016/j.enconman.2019.05.100.

[48] O. Siddiqui and I. Dincer, “Analysis and performance assessment of a new solar-based multigeneration system integrated with ammonia fuel cell and solid oxide fuel cell-gas turbine combined cycle,” J Power Sources, vol. 370, pp. 138–154, Dec. 2017, doi: 10.1016/j.jpowsour.2017.10.008.

[49] M. V. Kathe, A. Empfield, J. Na, E. Blair, and L.-S. Fan, “Hydrogen production from natural gas using an iron-based chemical looping technology: Thermodynamic simulations and process system analysis,” Appl Energy, vol. 165, pp. 183–201, Mar. 2016, doi: 10.1016/j.apenergy.2015.11.047.

[50] F. Kong et al., “Hydrogen Production from Natural Gas Using an Iron-Based Chemical Looping Technology: Process Modelling, Heat Integration, and Exergy Analysis,” Energy Technology, vol. 8, no. 8, p. 1900377, Aug. 2020, doi: 10.1002/ente.201900377.

[51] P. Jiang, A. S. Berrouk, and S. Dara, “Biomass Gasification Integrated with Chemical Looping System for Hydrogen and Power. Coproduction Process – Thermodynamic and Techno-Economic Assessment,” Chem Eng Technol, vol. 42, no. 5, pp. 1153–1168, May 2019, doi: 10.1002/ceat.201900130.

[52] Y. Cao et al., “Hydrogen production using solar energy and injection into a solid oxide fuel cell for CO2 emission reduction; Thermoeconomic assessment and tri-objective optimization,” Sustainable Energy Technologies and Assessments, vol. 50, p. 101767, Mar. 2022, doi: 10.1016/j.seta.2021.101767.

[53] W. L. Theo, J. S. Lim, H. Hashim, A. A. Mustaffa, and W. S. Ho, “Review of pre-combustion capture and ionic liquid in carbon capture and storage,” Applied Energy, vol. 183. Elsevier Ltd, pp. 1633–1663, Dec. 01, 2016, doi:10.1016/j.apenergy.2016.09.103.

[54] K. Goto, K. Yogo, and T. Higashii, “A review of efficiency penalty in a coal-fired power plant with post-combustion CO2 capture,” Applied Energy, vol. 111. Elsevier Ltd, pp. 710–720, Nov. 01, 2013, doi: 10.1016/j.apenergy.2013.05.020.

[55] S. Nandi et al., “A single-ligand ultra-microporous MOF for precombustion CO2 capture and hydrogen purification,” Sci. Adv., vol. 1, no. 11, p. e1500421, Dec. 2015, doi: 10.1126/sciadv.1500421.

[56] R. Stanger et al., “Oxyfuel combustion for CO2 capture in power plants,” Int. J. Greenh. Gas Control, vol. 40, pp. 55–125, Sep. 2015, doi: 10.1016/j.ijggc.2015.06.010.

[57] P. Versteeg and E. S. Rubin, “A technical and economic assessment of ammonia-based post-combustion CO2 capture at coal-fired power plants,” Int. J. Greenh. Gas Control, vol. 5, no. 6, pp. 1596–1605, Nov. 2011, doi: 10.1016/j.ijggc.2011.09.006

[58] J. Wang, L. Liu, X. Zeng, and K. Li, “Solar-Assisted CO2 Capture with Amine And Ammonia-Based Chemical Absorption: A Comparative Study,” Therm. Sci., p. 25, 2020, doi: 10.2298/tsci191222149w.

[59] L. E. Øi and S. H. P. Kvam, “Comparison of energy consumption for different CO2 absorption configurations using different simulation tools,” in Energy Procedia, 2014, vol. 63, pp. 1186–1195, doi: 10.1016/j.egypro.2014.11.128.

[60] A. Chitsaz, M. A. Haghghi, and J. Hosseinpour, “Thermodynamic and exergoeconomic analyses of a proton exchange membrane fuel cell (PEMFC) system and the feasibility evaluation of integrating with a proton exchange membrane electrolyzer (PEME),” Energy Convers. Manag., vol. 186, pp. 487–499, Apr. 2019, doi: 10.1016/j.enconman.2019.03.004.

[61] Z. Dai, L. Ansaloni, and L. Deng, “Recent advances in multi-layer composite polymeric membranes for CO2 separation: A review,” Green Energy and Environment, vol. 1, no. 2. KeAi Publishing Communications Ltd., pp. 102–128, Jul. 01, 2016, doi: 10.1016/j.gee.2016.08.001.

[62] J. Ströhle, M. Orth, and B. Epple, “Chemical looping combustion of hard coal in a 1 MWth pilot plant using ilmenite as oxygen carrier,” Appl Energy, vol. 157, pp. 288–294, Nov. 2015, doi: 10.1016/j.apenergy.2015.06.035.

[63] M. Gómez-Delgado and S. Tarantola, “GLOBAL sensitivity analysis, GIS and multi-criteria evaluation for a sustainable planning of a hazardous waste disposal site in Spain,” International Journal of Geographical Information Science, vol. 20, no. 4, pp. 449–466, Apr. 2006, doi: 10.1080/13658810600607709.

[64] Y. Huang, S. Rezvani, D. McIlveen-Wright, A. Minchener, and N. Hewitt, “Techno-economic study of CO2 capture and storage in coal fired oxygen fed entrained flow IGCC

power plants," Fuel Processing Technology, vol. 89, no. 9, pp. 916–925, Sep. 2008, doi: 10.1016/j.fuproc.2008.03.002.

[65] K. Jiang, P. Feron, A. Cousins, R. Zhai, and K. Li, "Achieving Zero/Negative-Emissions Coal-Fired Power Plants Using Amine-Based Postcombustion CO 2 Capture Technology and Biomass Cocombustion," Environ Sci Technol, vol. 54, no. 4, pp. 2429–2438, Feb. 2020, doi: 10.1021/acs.est.9b07388.

[66] S. Biswas, A. P. Kulkarni, S. Giddey, and S. Bhattacharya, "A Review on Synthesis of Methane as a Pathway for Renewable Energy Storage With a Focus on Solid Oxide Electrolytic Cell-Based Processes," Front Energy Res, vol. 8, Sep. 2020, doi: 10.3389/fenrg.2020.570112.

[67] M. Stec et al., "Demonstration of a post-combustion carbon capture pilot plant using amine-based solvents at the Łaziska Power Plant in Poland," Clean Technol Environ Policy, vol. 18, no. 1, pp. 151–160, Jan. 2016, doi: 10.1007/s10098-015-1001-2.

[68] C. Bassano, P. Deiana, L. Lietti, and C. G. Visconti, "P2G movable modular plant operation on synthetic methane production from CO2 and hydrogen from renewables sources," Fuel, vol. 253, pp. 1071–1079, Oct. 2019, doi: 10.1016/j.fuel.2019.05.074.

[69] S. Sollai, A. Porcu, V. Tola, F. Ferrara, and A. Pettinau, "Renewable methanol production from green hydrogen and captured CO2: A techno-economic assessment," Journal of CO2 Utilization, vol. 68, p. 102345, Feb. 2023, doi: 10.1016/j.jcou.2022.102345.

[70] F. Dalena, A. Senatore, A. Marino, A. Gordano, M. Basile, and A. Basile, "Methanol Production and Applications: An Overview," in Methanol, Elsevier, 2018, pp. 3–28. doi: 10.1016/B978-0-444-63903-5.00001-7.

[71] A. Al-Karaghouli and L. L. Kazmerski, "Energy consumption and water production cost of conventional and renewable-energy-powered desalination processes," Renewable and Sustainable Energy Reviews, vol. 24, pp. 343–356, Aug. 2013, doi: 10.1016/j.rser.2012.12.064.

[72] R. A. A. Nugroho, A. F. Alhikami, and W.-C. Wang, "Thermal decomposition of polypropylene plastics through vacuum pyrolysis," Energy, vol. 277, p. 127707, Aug. 2023, doi: 10.1016/j.energy.2023.127707.

[73] C. Xu, Z. Wang, X. Li, and F. Sun, "Energy and exergy analysis of solar power tower plants," Appl Therm Eng, vol. 31, no. 17–18, pp. 3904–3913, Dec. 2011, doi: 10.1016/j.applthermaleng.2011.07.038.

[74] O. Siddiqui, H. Ishaq, and I. Dincer, "A novel solar and geothermal-based trigeneration system for electricity generation, hydrogen production and cooling," Energy Convers Manag, vol. 198, 111812, 2019, doi: 10.1016/j.enconman.2019.111812.